GENERAL-PURPOSE PARALLEL UNSTEADY RANS SHIP HYDRODYNAMICS CODE: CFDSHIP-IOWA

by

Eric G. Paterson, Robert V. Wilson, and Fred Stern

IIHR Technical Report No. 432

IIHR—Hydroscience & Engineering
College of Engineering
The University of Iowa
Iowa City, Iowa 52242-1585 USA

November 2003

Report Documentation Page

Form Approved
OMB No. 0704-0188

1. REPORT DATE	2. REPORT TYPE	3. DATES COVERED
NOV 2003		**00-00-2003 to 00-00-2003**

4. TITLE AND SUBTITLE	5a. CONTRACT NUMBER
General-Purpose Parallel Unsteady Rans Ship Hydrodynamics Code: CFDSHIP-Iowa	5b. GRANT NUMBER
	5c. PROGRAM ELEMENT NUMBER
6. AUTHOR(S)	5d. PROJECT NUMBER
	5e. TASK NUMBER
	5f. WORK UNIT NUMBER
7. PERFORMING ORGANIZATION NAME(S) AND ADDRESS(ES) **The University of Iowa,College of Engineering,IIHR - Hydroscience & Engineering,Iowa City,IA,52242-1585**	8. PERFORMING ORGANIZATION REPORT NUMBER
9. SPONSORING/MONITORING AGENCY NAME(S) AND ADDRESS(ES)	10. SPONSOR/MONITOR'S ACRONYM(S)
	11. SPONSOR/MONITOR'S REPORT NUMBER(S)

12. DISTRIBUTION/AVAILABILITY STATEMENT
Approved for public release; distribution unlimited

13. SUPPLEMENTARY NOTES
The original document contains color images.

14. ABSTRACT

15. SUBJECT TERMS

16. SECURITY CLASSIFICATION OF:			17. LIMITATION OF ABSTRACT	18. NUMBER OF PAGES	19a. NAME OF RESPONSIBLE PERSON
a. REPORT	b. ABSTRACT	c. THIS PAGE			
unclassified	**unclassified**	**unclassified**		**115**	

TABLE OF CONTENTS

ABSTRACT ..... **iii**

ACKNOWLEDGEMENTS ..... **iv**

LIST OF SYMBOLS ..... **iv**

FONT CONVENTIONS ..... **vii**

1. INTRODUCTION **1**

2. CFD PROCESS **4**

3. MODELING **7**

3.1. Governing equations *8*
3.2. Turbulence *13*
3.3. Initial and Boundary Conditions *16*
3.4. Free-surface *17*
3.5. Body-force propulsor *18*

4. NUMERICAL METHODS **20**

4.1. Coordinate transformation *21*
4.2. Discretization scheme *22*
4.3. RANS solution algorithm & pressure Poisson equation *25*
4.4. Free-surface solver and adaptive gridding *26*
4.5. Initial conditions *29*
4.6 Boundary conditions *30*
4.7 Chimera overset gridding *38*
4.8 Calculation of forces and moments *40*
4.9 Algebraic equation solver *43*
4.10 Algorithm summary and flowchart *43*

5. CODE DEVELOPMENT AND HIGH-PERFORMANCE COMPUTING **46**

5.1. Code and data structures *46*
5.2 Parallel Computing *49*
5.3 Portability *52*
5.4 Code distribution, extraction, compilation and execution *53*

6. CREATING INPUT FILES AND POST-PROCESSING **55**

6.1 Input files *55*
6.2 Output files & post-processing *57*

7. RECOMMENDED VERIFICATION AND VALIDATION PROCEDURES **58**

7.1 Methodology *59*
7.2 Procedures *60*

8. EXAMPLE SIMULATION: OPEN-WATER PROPELLER P5168 62

8.1 Geometry, Benchmark Data, and Conditions 63
8.2 Computational Grids and Input Parameters 65
8.3 Computing Platforms 69
8.4 Verification and Validation Results 69

9. CONCLUDING REMARKS 75

APPENDICES 81

APPENDIX A: FILE FORMATS 81

A.1 Grid File 81
A.2 Namelist Input File 81
A.3 Boundary Condition File 86
A.4 Overset Interpolation Coefficient File 86
A.5 Global Solution File 87
A.6 Restart File 87

APPENDIX B: SAMPLE INPUT FILES 88

B.1 CFDSHIP-IOWA Namelist Input File, "cfd_ship.nml" 88
B.2 PEGASUS v5.1 Namelist Input File, "peg.in" 89
B.3 Boundary condition file 93

ABSTRACT

CFDSHIP-IOWA is a general-purpose unsteady Reynolds-averaged Navier-Stokes CFD code that has been developed, over the past 10 years, to handle a broad range of ship hydrodynamics problems. Originally designed to support both thesis and project research in the areas of resistance and propulsion, it has been successfully transitioned to Navy and university laboratories and industry, and has recently been extended to unsteady applications such as seakeeping and maneuvering. It was developed following a modern software-development philosophy, which was based upon open source, revision control, modular coding using Fortran 90/95, liberal use of comments, and an easy to understand architecture which enables model development by users.

Purpose of this report is to provide: detailed documentation of the modeling, numerical methods, and code development; user instructions on creating input files and post-processing; recommended procedures for verification and validation; and an example simulation for CFDSHIP-IOWA v3.03. As a framework for achieving successful simulations, an approach based upon formulation of an initial boundary value problem and execution of a well-defined CFD process is developed and followed throughout the report.

Example simulation and other recent applications demonstrate the capability of CFDSHIP-IOWA to simulate practical ship hydrodynamics problems. Successful use in both thesis and project research and transition to other organizations demonstrates the success of the overall design objectives. With increasing use of CFD in design process, it is expected that CFDSHIP-IOWA will serve as a platform for simulation-based design and optimization of future naval vehicles.

ACKNOWLEDGEMENTS

This work was supported by the Office of Naval Research under a number of grants, most recent being N00014-01-1-0073 and N00014-00-1-0473 monitored by Drs. Patrick Purtell and Ki-Han Kim. The authors would also like to acknowledge Dr. Edwin Rood, formerly Program Officer at ONR, for his support, Dr. Richard Leighton, Naval Research Laboratory, for his important discussions concerning CFD data structures and parallel computing, and Dr. Bob Sinkovits, San Diego Supercomputing Center, for his crucial role in MPI education and software development. Finally, Department of Defense (DOD) High-Performance Computing Modernization Office (HPCMO) provided computing resources at the Naval Oceanographic Office, Naval Research Laboratory, and the Army Research Laboratory under the auspices of the HPCMO Challenge Program (http://www.hpcmo.hpc.mil/Htdocs/Challenge/index.html).

LIST OF SYMBOLS

Alphabetical Symbols

b_i^j	geometric coefficients
C_T	(1) thrust coefficient $\left(=2T/\rho U_0^2 \pi R_p^2\right)$
	(2) total resistance $\left(=T/\frac{1}{2}\rho U_0^2 S\right)$
D_p	propeller diameter
D	benchmark data value
E	comparison error ($= D - S$)
f_{b_i}	Cartesian components of propeller body-force field
Fr	Froude number, $\left(U_0/\sqrt{gL}\right)$
g^{ij}	conjugate metric tensor
imax, jmax, kmax	size of grid in ξ,η,ζ directions
J	(1) Jacobian
	(2) Advance coefficient, $\left(=U_0/nD_p\right)$
k	turbulent kinetic energy $\left(=\frac{1}{2}q^2=\frac{1}{2}\left(\overline{uu}+\overline{vv}+\overline{ww}\right)\right)$

K_T	thrust coefficient $\left(=T/\rho n^2 D_p^4\right)$
K_Q `	torque coefficient $\left(=Q/\rho n^2 D_p^5\right)$
L	characteristic length (ship length at design waterline)
n	revolutions per second of propeller
p	non-dimensionalized static pressure, $\left(=\left(p-p_o\right)/\rho U_o^2\right)$
$\hat{p}$	piezometric pressure, $\left(=\frac{p-p_\infty}{\rho U_0^2}+\frac{z}{Fr^2}\right)$
Re	Reynolds number, $\left(=U_0 L/\nu\right)$
R_ϕ	effective Reynolds number
S	(1) wetted surface area
	(2) simulation value
S_ϕ, s_ϕ	source functions
t	time
U_i	Velocity components *(U,V,W)* in Cartesian or cylindrical coordinates
U^i	modified contravariant velocity components
$\hat{U}_i$	pseudovelocity components
U_0	reference velocity (ship speed)
U_τ	friction velocity, $\left(=\sqrt{\tau_w/\rho}\right)$
U_D	experimental uncertainty
U_{SN}	simulation numerical uncertainty
U_V	validation uncertainty
V^i	contravariant velocity components
$\overline{u_i u_j}$	Reynolds stress tensor
x_i	Cartesian *(x,y,z)* or cylindrical *(x,r,θ)* coordinates
y^+	wall coordinate $\left(=U_\tau y/\nu\right)$

Greek Symbols

ϕ	velocity components (U,V,W)
κ	von Kármán constant
ε	turbulent dissipation
ν	kinematic viscosity
ν_t	eddy viscosity
ρ	fluid density
ω	specific dissipation rate
ω_x, ω_y, ω_z	angular velocity around x-, y-, and z-axis
τ	time in computational domain
τ_w	wall-shear stress
ξ^i	curvilinear coordinates (ξ,η,ζ)
ζ	wave elevation
∇	gradient operator
∇^2	Laplacian operator

FONT CONVENTIONS

The following conventions are used in this report:

Italic

is used for variables and mathematical symbols

`Constant Width`

is used for programs and procedures, input variables, and in examples to show the contents of files or the output from commands.

`Constant Width Bold`

is used in examples to show commands or other text that should be typed literally by the user. (For example, **`mpirun -np 1 cfd_ship`** means to type "mpirun -np 1 cfd_ship" exactly as it appears in the text or the example)

`Constant Width Italic`

is used in examples to show variables for which a context-specific substitution should be made. (The variable *`filename`*, for example, would be replaced by some actual filename).

%

is the UNIX C shell prompt

1. INTRODUCTION

Reynolds-averaged Navier-Stokes (RANS) computational fluid dynamics (CFD) codes have matured for most disciplines and are rapidly being integrated into the design process such that the reality of physics-based simulation based design seems imminent. General-purpose research codes are available for many engineering applications such as aerospace (Meakin and Wissink, 1999; Bush et al., 1998), ship hydrodynamics (Hyams et al., 2000; Larsson et al., 2000), and turbomachinery (Chima, 2001; Hall et al., 1999) whereas other applications, such as automobile and industrial processes, primarily take advantage of commercial codes. Most codes, especially commercial ones, can handle more than one application. Code development has evolved from Ph.D. thesis projects to dedicated groups at academic institutes, government and industry laboratories, and commercial companies. These groups struggle to keep pace with the requirements of the design community by addressing issues of modeling, numerical methods, high performance computing (HPC), structured and unstructured grids and grid generation, and pre and post processing. Other pace setting issues include lack of trained users and consensus on quality assessment verification and validation (V&V) methodology and procedures.

Present interest is in ship hydrodynamics, which has unique features in comparison to related applications due large Reynolds number ($\mathrm{Re} \approx 10^9$; small Mach number (incompressible flow); tanker, cargo/container, and combatant geometries; ballast, motions, maneuvering, restricted water, and ambient waves operating and environmental conditions; Froude number (Fr) and free-surface effects (waves, spray, breaking, near-surface turbulence, and boundary-layer and wake and vortex interactions); and propulsor-body interactions and cavitation. Detailed physics vary considerably depending on geometry and operating and environmental conditions.

The status of ship hydrodynamics CFD for steady flow design conditions was assessed at the recent Gothenburg 2000 Workshop on CFD in Ship Hydrodynamics (Larsson et al., 2000). Twenty groups representing 16 (8 academic and 8 industrial) institutes and 1 commercial CFD code company from 11 countries submitted results for one or more of three test cases for modern tanker, container, and surface-combatant hull forms with validation focusing on, respectively, turbulence modeling and full-scale Re; free-surface effects and propeller-hull interaction; and free-surface effects. Verification was required for each group for at least one of the test cases and the V&V approach of Stern et al. (2001) was recommended. Most codes used 2 or more

equation turbulence models and had free-surface capability; finite volume or difference and 2nd- and 3rd-order accurate numerical methods; multi or single block structured grids; and either pressure Poisson-equation or artificial compressibility formulations. Few codes included capability for propulsor modeling, unstructured grids, or parallel computing. Most groups conducted verification for resistance C_T and many followed recommended procedures; however, there were some problems due to solutions far from asymptotic range and lack of experience with detailed verification procedures, especially for practical applications. Seven codes showed grid convergence for C_T with average number of grid points 1.5M and simulation numerical uncertainty U_{SN}=3.65%. Some groups showed oscillatory convergence and variability between grid studies, which indicates need for finer grids. Quantitative validation was performed for C_T. The average comparison error was E=5%, which approximately equals the validation uncertainty U_V=5% such that the codes are approximately validated at the 5% level, which interestingly is also equal to the coefficient of variation for C_T. The average experimental uncertainty was U_D=1.6%. Only qualitative validation was performed for point variables. The Reynolds stress turbulence models performed best, however 2 equation models were also surprisingly good. Both surface tracking and capturing methods showed good free surface results.

Advancements for off-design problems and unsteady flow, although warranted since previous CFD Workshop Tokyo (Kodama, 1994), are still relatively rare. For off-design yaw, steady turn, and shallow water problems, steady flow methods can still be used and have shown fairly good agreement with data, although issues remain as to resolution of steep and breaking waves and body and wave-induced vortices (Tahara et al., 1998; Alessandrini and Delhommeau, 1998; Hochbaum, 1999; Di Mascio and Campana, 1999; Ohmori et al., 2000). For unsteady flow problems, studies are very limited partly due to the fact that not all steady flow methods are easily extended to unsteady flow. Ohmori (1998) performs simulations of unsteady combined sway and yaw motions as per captive model testing in towing tanks using planar motion mechanisms; however, the free-surface is neglected, i.e., simulations are for the so-called double body zero Froude number problem. Beddhu et al. (1998), Gentaz et al. (1999), and Yeung et al. (2000) perform simulations for forced motions, and Sato et al. (1999) and Rhee and Stern (2001) perform simulations for motions in regular head waves. With capability for more practical geometries and conditions, coupled with continuing improvements in HPC resources, the

promise of CFD-based optimization will soon be realized (Tahara et al., 2000; and Dreyer, 2002).

This report provides documentation of code development of CFDSHIP-IOWA, which is a general-purpose parallel unsteady RANS ship hydrodynamics code. It is intended for use both in research and design at universities, and industrial and governmental laboratories. The approach includes 2-equation turbulence, free-surface tracking, and body-force propulsor modeling; structured overset-grid, higher-order finite-difference, and pressure-implicit split-operator (PISO), numerical methods; parallel and portable high performance computing (HPC); and open source, commented, and modular programming with revision control; and web site distribution (http://www.iihr.uiowa.edu/~cfdship). The current version of CFDSHIP-IOWA has benefited from predecessor thesis codes (Tahara and Stern, 1996; Rhee and Stern 2001), but as a complete package represents significantly improved modeling, numerical methods, HPC, and overall code development effort. Current version is primarily intended for steady and unsteady resistance and propulsion simulations, including option of with or without free surface and body force modeling or complete propulsor. Forthcoming versions will include capability for body motions enabling steady and unsteady ship motions and maneuvering simulations.

Code development was done over period of last 10 years during which time earlier versions were released (Paterson et al., 1998; Wilson et al., 1998) and used as intended for numerous applications including: turbulence modeling (Walker, 2000; Gill, 2000); two phase flow modeling (Larreteguy, et al., 1998); wave-induced separation (Kandysami, 2001); maneuvering (Simonsen and Stern, 2003); surface-ship motions (Weymouth et al., 2003; Wilson and Stern, 2002); optimization (Tahara et al., 2000); propulsor flows (Kim et al., 2003; Chen, 2000); and preliminary industrial design of DD21, i.e., 21st century US Navy destroyer, through recent ONR Accelerated Hydrodynamics program. Also, simulations for naval surface combatant were included at Gothenburg 2000 Workshop. Levels of verification and validation and overall code performance demonstrated that CFDSHIP-IOWA was among the best codes for the combatant test case (Wilson et al., 2000).

The report provides documentation of the modeling, numerical methods, and code architecture for CFDSHIP-IOWA v3.03. An example simulation is presented to demonstrate capabilities and concluding remarks are provided. This report and a suite of example problems can be found on the CFDSHIP-IOWA website http://www.iihr.uiowa.edu/~cfdship.

2. CFD PROCESS

Overall philosophy for the CFD process is given in this section as a set of procedures to guide engineers and scientists through the process of modeling fluid flow problems using a CFD code. Although some of the elements of the CFD process are relatively straightforward, development of a comprehensive process is useful for training non-expert CFD users, establishing confidence in results from CFD codes, assessing risks in the use of CFD results in a design environment, and streamlining the task of obtaining CFD solutions leading to reduced manpower requirements. As described in the following paragraphs, the CFD process is composed of two distinct parts, (*i*) selection or development of a general-purpose CFD code and (*ii*) use of the CFD code for solution of a particular flow problem of interest. In general, the former occurs only at infrequent intervals when need arises to make large shifts in technology, whereas the latter must be followed for each simulation.

Development of any general-purpose CFD code has several common elements. Specifically, formulation of the general initial and boundary value problem (IBVP) which is to be solved numerically using a CFD code, development of numerical methods for approximate solution of the IBVP, and documentation of the CFD code. Key issues in the formulation of the IBVP are in definition of the scope and level of flow description (e.g., RANS, LES, DNS), selection of governing partial differential equations (PDEs) and physical models for the fluid flow, and selection of a comprehensive set of initial and boundary conditions required to solve a wide range of applications. With regard to numerical methods, key issues include discretization of the continuous modeled PDEs, initial and boundary conditions, development of numerical algorithms for solution of the discretized modeled equations, and programming and testing the algorithm in a CFD code. Finally, documentation of the CFD code is required to assist users in running the code. Additional documentation may be required to assist other users in the development of new models or numerical methods.

The CFD process for simulation of a fluid flow application is summarized here in six distinctive phases as shown in Fig. 1. The process is initiated by clearly defining the purpose for the CFD simulation and the acceptable levels of CFD simulation error and uncertainty (e.g., prediction of vehicle drag with validation of uncertainty of 5% over a specified range of Reynolds numbers). The second step is to formulate the IBVP, which involves definition of the required governing PDEs, physical models, and initial and boundary conditions for the

application of interest. In addition, the flow geometry, domain, and coordinate system are defined in this step. As an aid in later steps, it is often useful to construct sketches, such as those shown in Figs. 2 and 3, which summarize geometry, domain, coordinate system, and boundary conditions. It is assumed that the selected CFD code meets the requirements for the

CFD Process

1. Define purpose and required levels for V&V
2. Formulate the IBVP
   - Define continuous PDEs
   - Define physical models
   - Define initial and boundary conditions
   - Define geometry, domain, coordinate system
3. Plan simulation matrix
4. Create input files
   - Generate grid(s)
   - Prescribe boundary conditions
   - Prescribe initial conditions
   - Select flow conditions
   - Select models
   - Select numerical parameters and post-processing variables
5. Execute CFD code
6. Post-process and document results

Figure 1. CFD Process

particular application as defined in this step or can be modified to do so with an acceptable level of effort. If further code development is required, issues with source code architecture and availability become important as discussed in Section 4. These issues may impact whether the user selects a commercial or research code.

The third step involves planning of the simulation matrix (i.e., number of simulations required to study desired range of flow conditions). Depending on the purpose of the CFD simulation and the environment, some or all cases may be selected to estimate simulation error and uncertainty through comparison of the simulation results with available benchmark data.

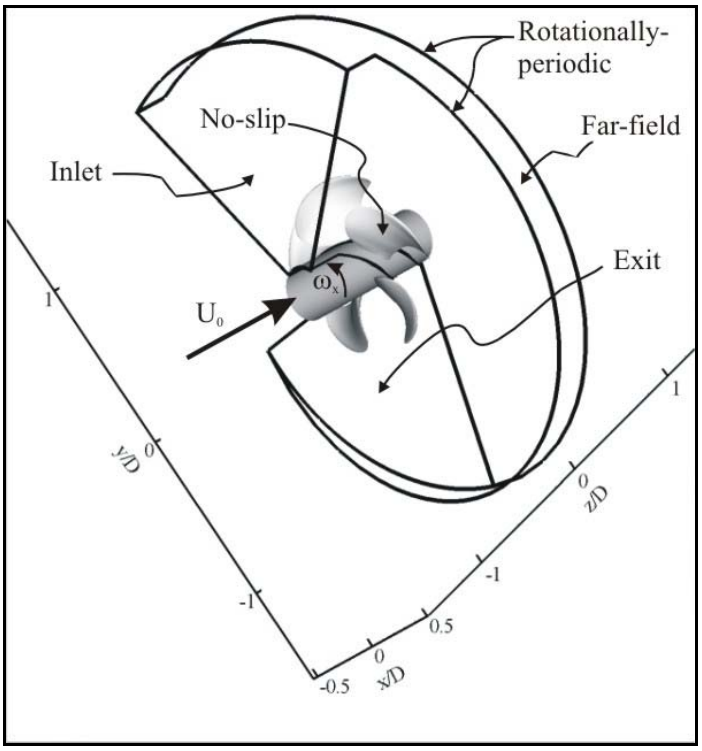

Figure 2. Open-Water Propeller Model P5168:
Computational domain and boundary conditions.

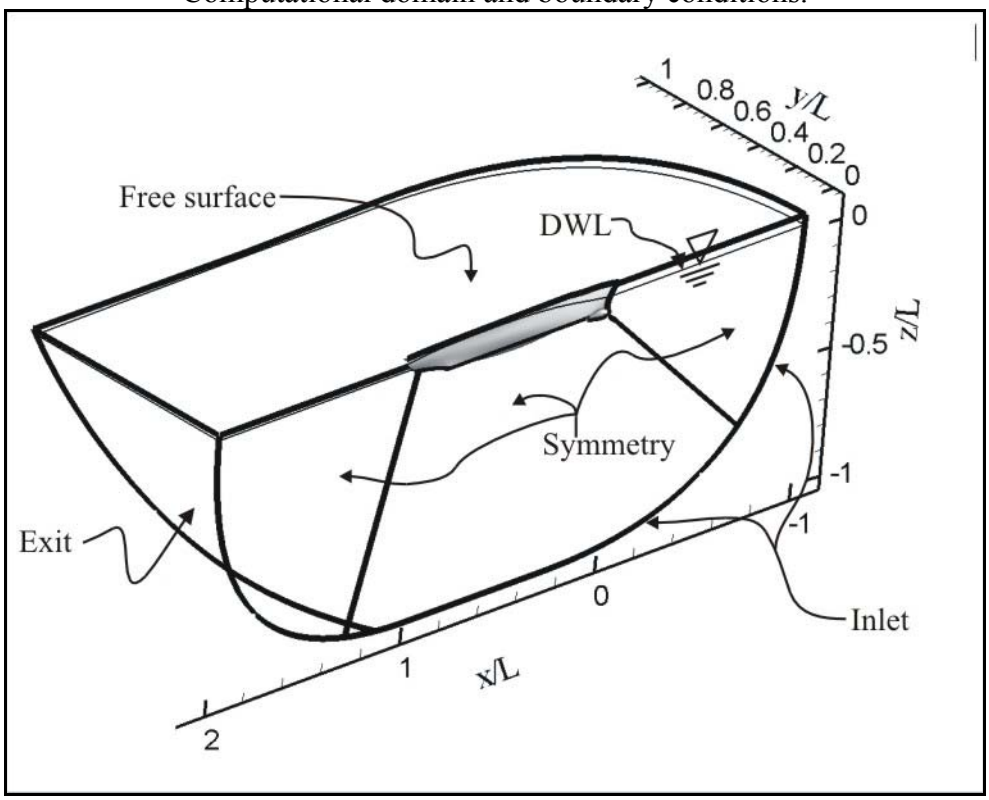

Figure 3. Surface Combatant Model 5415:
Computational domain and boundary conditions.

Recommended verification and validation procedures are summarized in Section 7 to accomplish this task and involve obtaining solutions with multiple grids and time steps with systematic refinement. As a result, the simulations used for grid and time step studies and available benchmark data are identified in this step.

The fourth step of the CFD process involves creation of the CFD code input files. For CFDSHIP-IOWA, at least three input files are required to run the code and to specify the grid coordinates (`FNAMEG`), boundary conditions (`FNAMEO.bcs`), and runtime parameters (`cfd_ship.nml`). The purpose, creation, and format of the input files are described in detail in Section 6. The fifth step is to execute the CFD code, which involves selecting a computer platform (e.g., serial or vector machine), compiling the source code to produce an executable if necessary, and running the CFD code as described in Section 5.4.

The sixth and final step is the post-processing and documentation of results. In this step, any secondary variables of interest (e.g., vorticity, turbulence energy budget) are computed from the primary results (i.e., velocity, pressure, turbulence quantities). If the results are unsteady, running statistics for computation of variable mean and variance may be collected, or a Fourier analysis may be conducted to determine the harmonic content of the results. Flow visualization of the results may be useful in interpreting the results and understanding the flow phenomena. If an assessment of simulation error and uncertainty is required, a verification and validation analysis is performed at this phase following the procedures given in Section 7. Finally, the results are documented in an appropriate format.

3. MODELING

As mentioned in the previous section, formulation of the IBVP, which is the second step of the CFD process, requires definition of the governing equations, physical models, and initial and boundary conditions. Here, this definition is provided through a detailed presentation of the unsteady RANS equations, turbulence closure and model equations, initial and boundary conditions, and free-surface and body-force-propulsor models.

3.1. Governing equations

High-fidelity resolution of a certain portion of the frequency spectrum of unsteady flow physics and resultant fluid forces and moments can be obtained using unsteady RANS. In the context of a triple decomposition, an instantaneous flow quantity $f(\mathbf{x},t)$ can be written as

$$f(\mathbf{x},t) = \overline{f}(\mathbf{x}) + f''(\mathbf{x},t) + f'(\mathbf{x},t) = F(x,t) + f'(\mathbf{x},t) \tag{1}$$

where $\overline{f}(\mathbf{x})$ is the mean, $f''(\mathbf{x},t)$ are the organized, or deterministic, fluctuations, and $f'(\mathbf{x},t)$ are the turbulent, or random, fluctuations. It is assumed that the RANS equations solve for $F(\mathbf{x},t) = f(\mathbf{x}) + f''(\mathbf{x},t)$ and that the Reynolds-averaging process is based upon a time interval large enough to average out $f'(\mathbf{x},t)$ but also small enough to capture $f''(\mathbf{x},t)$. This implies that the frequencies of $f''(\mathbf{x},t)$ lay sufficiently outside the spectrum of turbulence and the effect of turbulence upon $F(\mathbf{x},t)$ can be modeled as Reynolds stresses. This also implies that for unsteady RANS, all turbulent production and dissipation is subgrid scale.

The code has been formulated to solve the RANS equations in either Cartesian or cylindrical-polar base coordinate systems. In addition, both systems may be in either absolute (i.e., earth-fixed inertial) or relative non-inertial (i.e., fixed to a moving body) reference frames. Available options with corresponding input parameter values are listed in Table 1.

Table 1. Coordinate system options

icoord	*Description*	*Equations solved*
1	Cartesian, absolute frame	(2) - (3)
2	Cartesian, non-inertial relative frame	(13)
3	Cylindrical, absolute frame	(4) - (8)
4	Cylindrical, non-inertial relative frame	(4) - (7), (14)

For Cartesian coordinates the continuous continuity and momentum equations in nondimensional tensor form are

$$\frac{\partial U_i}{\partial x_i} = 0 \tag{2}$$

$$\frac{\partial U_i}{\partial t} + U_j \frac{\partial U_i}{\partial x_j} = -\frac{\partial \hat{p}}{\partial x_i} + \frac{1}{Re}\frac{\partial^2 U_i}{\partial x_j \partial x_j} - \frac{\partial}{\partial x_j}\overline{u_i u_j} + f_{b_i}^* \tag{3}$$

where U_i = *(U, V, W)* are the Reynolds-averaged velocity components, x_i = *(x, y, z)* are the independent coordinate directions, $\hat{p} = \left(\frac{p - p_\infty}{\rho U_0^2} + z/Fr^2 \right)$ is the piezometric pressure coefficient, $\overline{u_i u_j}$ are the Reynolds stresses which are a two-point correlation of the turbulent fluctuations u_i, $f_{b_i}^*$ is the non-dimensional body-force vector $\left(= f_{b_i} L / \rho U_0^2 \right)$ where f_{b_i} is a force per unit volume which represents the effect of the propeller, $Fr = U_0 / \sqrt{gL}$ is the Froude number, and $Re = U_O L / \nu$ is the Reynolds number. All equations are nondimensionalized by reference velocity U_O, length L, and density ρ.

For cylindrical-polar coordinates the continuity and momentum equations in nondimensional vector form are

$$\frac{\partial U}{\partial x} + \frac{1}{r}\frac{\partial (rV)}{\partial r} + \frac{1}{r}\frac{\partial W}{\partial \theta} = 0 \tag{4}$$

$$\frac{DU}{Dt} = -\frac{\partial \hat{p}}{\partial x} + \frac{1}{Re}\nabla^2 U + \left\{ -\frac{\partial}{\partial x}\overline{uu} - \frac{\partial}{\partial r}\overline{uv} - \frac{1}{r}\frac{\partial}{\partial \theta}\overline{uw} \right\} + \frac{1}{\rho} f_{b_i}^* \tag{5}$$

$$\begin{aligned} \frac{DV}{Dt} - \frac{W^2}{r} &= -\frac{\partial \hat{p}}{\partial r} + \frac{1}{Re}\left\{ \nabla^2 V - \frac{2}{r^2}\frac{\partial W}{\partial \theta} - \frac{V}{r^2} \right\} \\ &+ \left\{ -\frac{\partial}{\partial x}\overline{uv} - \frac{\partial}{\partial r}\overline{vv} - \frac{1}{r}\frac{\partial}{\partial \theta}\overline{vw} - \frac{1}{r}\left(\overline{vv} - \overline{ww} \right) \right\} + \frac{1}{\rho} f_{b_i}^* \end{aligned} \tag{6}$$

$$\begin{aligned} \frac{DW}{Dt} + \frac{VW}{r} &= -\frac{1}{r}\frac{\partial \hat{p}}{\partial \theta} + \frac{1}{Re}\left\{ \nabla^2 W + \frac{2}{r^2}\frac{\partial V}{\partial \theta} - \frac{W}{r^2} \right\} \\ &+ \left\{ -\frac{\partial}{\partial x}\overline{uw} - \frac{\partial}{\partial r}\overline{vw} - \frac{1}{r}\frac{\partial}{\partial \theta}\overline{ww} - \frac{2}{r}\left(\overline{vw} \right) \right\} + \frac{1}{\rho} f_{b_i}^* \end{aligned} \tag{7}$$

where U_i = *(U, V, W)* are the velocity components in the axial, radial, and circumferential *(x,r,θ)* directions and the operators *D/Dt* and ∇^2 are defined as

$$\begin{aligned} \frac{D}{Dt} &= \frac{\partial}{\partial t} + U\frac{\partial}{\partial x} + V\frac{\partial}{\partial r} + \frac{W}{r}\frac{\partial}{\partial \theta} \\ \nabla^2 &= \frac{\partial^2}{\partial x^2} + \frac{\partial^2}{\partial r^2} + \frac{1}{r}\frac{\partial}{\partial r} + \frac{1}{r^2}\frac{\partial^2}{\partial \theta^2} \end{aligned} \tag{8}$$

In the absolute frame, body motions are resolved by time-dependent grid motions, which, as will be explained in section 3, are accounted for in the transformation from physical to

computational coordinates. An obvious consequence of moving-body simulations in the absolute frame is that, except for the simple cases of inertial motions such as steady translation, they are inherently unsteady.

Relative frame formulations, on the other hand, provide capability for steady simulation of some simple, but important, non-inertial motions. Shown in Figure 4 are two examples: constant-speed rotating machinery with circumferentially uniform inflow, such as a propeller; and a ship in a constant radius turn.

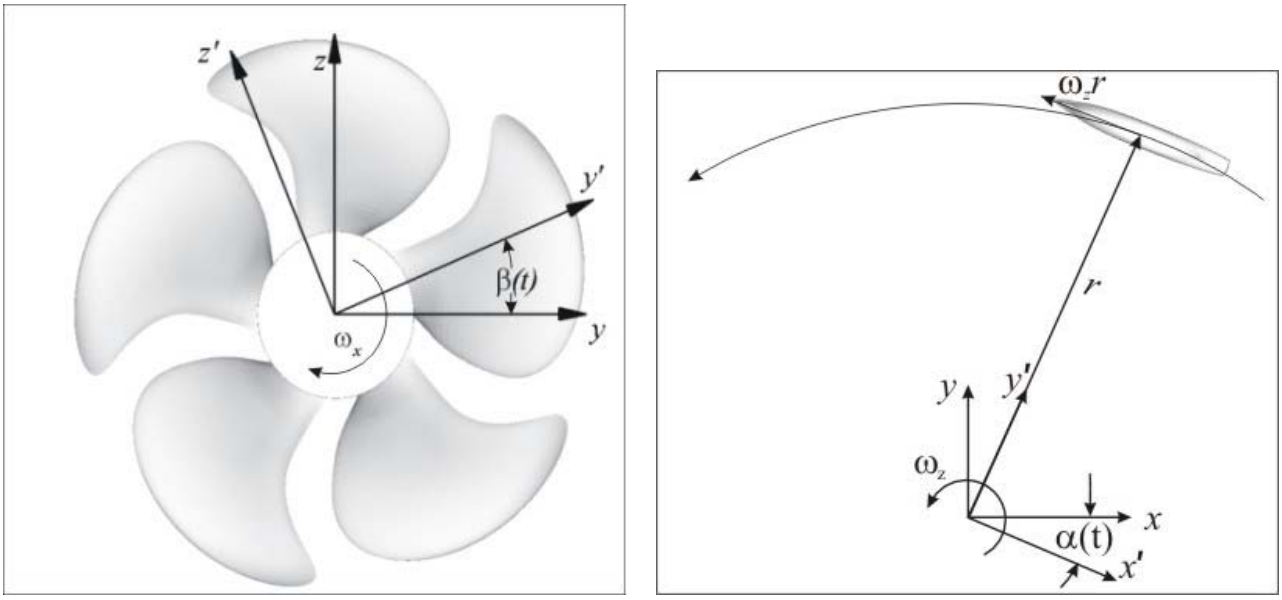

(a) Propeller rotating about x-axis (b) Ship in constant-radius-turn about z-axis

Figure 4. Example relative-frame applications.

Transformation to relative frame is straightforward. The acceleration term on the left hand side (LHS) of (3) and (5)-(7) is replaced with the following general expression

$$\frac{D\mathbf{U}}{Dt} = \frac{D\mathbf{U}'}{Dt} + \frac{d^2\mathbf{R}}{dt^2} + \frac{d\boldsymbol{\Omega}}{dt} \times \mathbf{r}' + \boldsymbol{\Omega} \times \left(\boldsymbol{\Omega} \times \mathbf{r}'\right) + 2\boldsymbol{\Omega} \times \mathbf{U}' \qquad \textbf{(9)}$$

where $\mathbf{r}$ is the displacement vector of the relative frame with respect to the absolute frame, $\boldsymbol{\Omega} = (\omega_x, \omega_y, \omega_z)$ is the angular velocity vector, and $\mathbf{r}'$ and $\mathbf{U}'$ are the coordinate and velocity vectors in the relative frame, respectively. The terms on the right-hand-side of (9) represent non-inertial, linear, tangential, centripetal, and coriolis accelerations and can accommodate general 6-degree-of-freedom motions.

Currently, however, relative-frame motion in Cartesian coordinates is restricted to steady rotation about either the *x*- or *z*-axes. For these simple cases, (9) reduces to the following

$$\frac{D\mathbf{U}}{Dt} = \frac{D\mathbf{U}'}{Dt} + \begin{pmatrix} -\omega_z^2 y' - 2\omega_z V' \\ -\omega_x^2 y' - 2\omega_x W' - \omega_z^2 x' + 2\omega_z U' \\ -\omega_x^2 z' + 2\omega_x V' \end{pmatrix} \tag{10}$$

where (x', y', z') and (U', V', W') are the coordinates and velocity components in the relative frame. As shown in Figure 4, the relationship between frames is a function of time, defined by the angle $\beta(t)$ or $\alpha(t)$. In cylindrical coordinates, motion is restricted to steady rotation about the *x*-axis, which reduces (9) to

$$\frac{D\mathbf{U}}{Dt} = \frac{D\mathbf{U}'}{Dt} + \begin{pmatrix} 0 \\ -\omega_x^2 r' - 2\omega_x W' \\ +2\omega_x V' \end{pmatrix} \tag{11}$$

In addition to modifying the acceleration terms, the initial and boundary conditions must be transformed into relative frame. This results in a large solid-body rotation of the free-stream velocity and is the usual approach to formulating relative-frame codes (e.g., Chen, 2000).

An alternative approach is used here which has the benefits of removing the solid-body rotation, moving most of the non-inertial terms from the source-term on the RHS to the convective terms on the LHS of (3) and (5)-(7), and simplifying calculation of vorticity and wall-shear stress, such that the same algorithms may be used for either reference frame. To derive such a system of equations, a new relative-frame velocity vector (U'', V'', W'') is defined with the solid-body rotation removed. In Cartesian coordinates

$$\begin{pmatrix} U'' \\ V'' \\ W'' \end{pmatrix} = \begin{pmatrix} U' \\ V' \\ W' \end{pmatrix} + \begin{pmatrix} -\omega_z y \\ -\omega_x z + \omega_z x \\ +\omega_x y \end{pmatrix} \tag{12}$$

Rearranging (12) for (U', V', W'), substituting into (2), (3), and (10), and collecting terms provides RANS equations in terms of (U'', V'', W'')

$$\frac{\partial U''}{\partial x'}+\frac{\partial V''}{\partial y'}+\frac{\partial W''}{\partial z'}=0$$

$$\begin{aligned}
&\frac{\partial U''}{\partial t}+\left(U''-\omega_z y'\right)\frac{\partial U''}{\partial x'}+\left(U''-\omega_x z'+\omega_z x'\right)\frac{\partial U''}{\partial y'}+\left(U''-\omega_x y'\right)\frac{\partial U''}{\partial z'}\\
&\quad=-\frac{\partial \hat{p}}{\partial x'}+\frac{1}{Re}\frac{\partial^2 U''}{\partial x_j \partial x_j}-\frac{\partial}{\partial x_j'}\overline{uu_j}+f_{b_i}^*-\omega_z V\\
&\frac{\partial V''}{\partial t}+\left(U''-\omega_z y'\right)\frac{\partial V''}{\partial x'}+\left(U''-\omega_x z'+\omega_z x'\right)\frac{\partial V''}{\partial y'}+\left(U''-\omega_x y'\right)\frac{\partial V''}{\partial z'}\\
&\quad=-\frac{\partial \hat{p}}{\partial y'}+\frac{1}{Re}\frac{\partial^2 V''}{\partial x_j' \partial x_j'}-\frac{\partial}{\partial x_j'}\overline{vu_j}+f_{b_i}^*-\omega_x W+\omega_z U\\
&\frac{\partial W''}{\partial t}+\left(U''-\omega_z y'\right)\frac{\partial W''}{\partial x'}+\left(U''-\omega_x z'+\omega_z x'\right)\frac{\partial W''}{\partial y'}+\left(U''-\omega_x y'\right)\frac{\partial W''}{\partial z'}\\
&\quad=-\frac{\partial \hat{p}}{\partial z'}+\frac{1}{Re}\frac{\partial^2 W''}{\partial x_j' \partial x_j'}-\frac{\partial}{\partial x_j'}\overline{wu_j}+f_{b_i}^*+\omega_x V
\end{aligned} \qquad \textbf{(13)}$$

As a result, all of the centripetal and half the Coriolis terms have been effectively moved to the LHS of (13) in the form of modified convective velocities. For cylindrical coordinates, similar transformation may be performed. However, in this case, all of the non-inertial terms are moved to the LHS such that the governing equations are exactly the same as (4)-(7) with $\left(U,V,W\right)=\left(U'',V'',W''\right)$, except for the following modification of the substantial derivative

$$\frac{D}{Dt}=\frac{\partial}{\partial t}+U''\frac{\partial}{\partial x'}+V''\frac{\partial}{\partial r'}+\frac{\left(W''-\omega_x r'\right)}{r'}\frac{\partial}{\partial \theta'} \qquad \textbf{(14)}$$

It is noted that this approach is essentially the same as the Arbitrary Lagrangian Eulerian (ALE) methods (Hirt et al., 1974) wherein the convective velocity is defined as the difference between fluid particle velocity and the mesh velocity.

Although there are numerous subroutines that have coordinate-system dependent logic (e.g., boundary condition formulation, calculation of wall-proximity functions and wall-shear stress, and coordinate transformation including grid-velocity terms), users only are required to specify consistent coordinate system `(icoord)`, flow conditions `(agvx, agvy, agvz)`, and boundary conditions, the latter of which are discussed in Section 4.6.

3.2. Turbulence

CFDSHIP-IOWA is designed to use a linear closure model where the Reynolds stresses are directly related to the mean rate-of-strain through an isotropic eddy viscosity ν_t. In Cartesian coordinates, it is written as

$$-\overline{u_i u_j} = \nu_t \left(\frac{\partial U_i}{\partial x_j} + \frac{\partial U_j}{\partial x_i} \right) - \frac{2}{3} \delta_{ij} k \tag{15}$$

where δ_{ij} is the Kronecker delta and $k = \frac{1}{2} q^2 = \frac{1}{2} \left(uu + vv + ww \right)$ is the turbulent kinetic energy. In cylindrical coordinates,

$$\begin{aligned}
-\overline{uv} &= \nu_t \left(\frac{\partial U}{\partial r} + \frac{\partial V}{\partial x} \right) - \frac{2}{3} \delta_{ij} k \\
-\overline{uw} &= \nu_t \left(\frac{1}{r} \frac{\partial U}{\partial \theta} + \frac{\partial W}{\partial x} \right) - \frac{2}{3} \delta_{ij} k \\
-\overline{vw} &= \nu_t \left(\frac{1}{r} \frac{\partial V}{\partial \theta} + \frac{\partial W}{\partial r} - \frac{W}{r} \right) - \frac{2}{3} \delta_{ij} k \\
-\overline{uu} &= \nu_t \left(2 \frac{\partial U}{\partial x} \right) \\
-\overline{vv} &= \nu_t \left(2 \frac{\partial V}{\partial r} \right) \\
-\overline{ww} &= \nu_t \left(\frac{2}{r} \frac{\partial W}{\partial \theta} + 2 \frac{V}{r} \right)
\end{aligned} \tag{16}$$

For unsteady flow, equations (15) and (16) are quasi-steady relationships where it is assumed that $-\overline{u_i u_j}$ responds instantaneously to the mean rate of strain.

Substituting (15) for the Reynolds-stress term in (3), the momentum equations in Cartesian coordinates become

$$\frac{\partial U_i}{\partial t} + U_j \frac{\partial U_i}{\partial x_j} = -\frac{\partial P}{\partial x_i} + \frac{1}{R_{U_i}} \frac{\partial^2 U_i}{\partial x_j \partial x_j} + \frac{\partial \nu_t}{\partial x_j} \left(\frac{\partial U_i}{\partial x_j} + \frac{\partial U_j}{\partial x_i} \right) + f_{b_i} \tag{17}$$

where

$$P = \hat{p} + \frac{2}{3} k \tag{18}$$

$$\frac{1}{R_{U_i}} = \frac{1}{Re} + \nu_t \tag{19}$$

The same can be done for cylindrical coordinates where (16) is substituted into (5),(6), and (7)

$$\begin{aligned}\frac{DU}{Dt} &= -\frac{\partial P}{\partial x} + \frac{1}{R_{U_i}}\nabla^2 U \\ &+ \left\{ 2\frac{\partial \nu_t}{\partial x}\frac{\partial U}{\partial x} + \frac{\partial \nu_t}{\partial r}\left(\frac{\partial U}{\partial r} + \frac{\partial V}{\partial x}\right) + \frac{1}{r}\frac{\partial \nu_t}{\partial \theta}\left(\frac{1}{r}\frac{\partial U}{\partial \theta} + \frac{\partial W}{\partial x}\right)\right\} + \frac{1}{\rho} f_{b_i}^*\end{aligned} \tag{20}$$

$$\begin{aligned}\frac{DV}{Dt} - \frac{W^2}{r} - 2\omega W - \omega^2 r &= -\frac{\partial P}{\partial r} + \frac{1}{R_{U_i}}\left\{\nabla^2 V - \frac{2}{r^2}\frac{\partial W}{\partial \theta} - \frac{V}{r^2}\right\} \\ &+ \left\{\frac{\partial \nu_t}{\partial x}\left(\frac{\partial U}{\partial r} + \frac{\partial V}{\partial x}\right) + 2\frac{\partial \nu_t}{\partial r}\frac{\partial V}{\partial r} + \frac{1}{r}\frac{\partial \nu_t}{\partial \theta}\left(\frac{1}{r}\frac{\partial V}{\partial \theta} + \frac{\partial W}{\partial r} - \frac{W}{r}\right)\right\} + \frac{1}{\rho} f_{b_i}^*\end{aligned} \tag{21}$$

$$\begin{aligned}\frac{DW}{Dt} + \frac{VW}{r} + 2\omega V &= -\frac{1}{r}\frac{\partial P}{\partial \theta} + \frac{1}{R_{U_i}}\left\{\nabla^2 W + \frac{2}{r^2}\frac{\partial V}{\partial \theta} - \frac{W}{r^2}\right\} \\ &+ \left\{\frac{\partial \nu_t}{\partial x}\left(\frac{1}{r}\frac{\partial U}{\partial \theta} + \frac{\partial W}{\partial x}\right) + \frac{\partial \nu_t}{\partial r}\left(\frac{1}{r}\frac{\partial V}{\partial \theta} + \frac{\partial W}{\partial r} - \frac{W}{r}\right) + \frac{1}{r}\frac{\partial \nu_t}{\partial \theta}\left(\frac{2}{r}\frac{\partial W}{\partial \theta} + \frac{2}{r}V\right)\right\} + \frac{1}{\rho} f_{b_i}^*\end{aligned} \tag{22}$$

In CFDSHIP-IOWA, eddy viscosity can be calculated using one of two models: Baldwin-Lomax or the blended *k-ω/k-ε* (BKW), including an option for shear-stress transport (SST) model (Menter, 1994). The turbulence model and options are selected using the input parameters `itm` and `itm_switch` as described in Section 6.

For the Baldwin Lomax model (`itm`=1), details have previously been documented in Stern et al. (1996). However, as illustrated in Paterson and Sinkovits (1999), care must be exercised when using BL for geometries with multiple no-slip surfaces and multi-block grid systems since the turbulent length scale is calculated as a weighted average based upon the wall distance y^+ to each no-slip surface in a given block. Since a search process through all blocks is not performed, the length scale may be incorrect given certain blocking topologies. Therefore, BL is not recommended for general application to complex geometries and/or grid systems.

The BKW model (`itm`=2) has proven to be robust, applicable to complex geometries and flows, and fairly accurate. In nearly all circumstances, it is superior to *k-ε* models, which require complicated near-wall models that are difficult to implement in a general fashion. The

governing equations for the eddy viscosity ν_t, turbulent kinetic energy k, and the turbulent specific dissipation rate ω are as follows,

$$\nu_t = \frac{k}{\omega} \tag{23}$$

$$\begin{aligned} &\frac{\partial k}{\partial t} + \left(U_j - \sigma_k \frac{\partial \nu_t}{\partial x_j} \right) \frac{\partial k}{\partial x_j} - \frac{1}{R_k} \nabla^2 k + s_k = 0 \\ &\frac{\partial \omega}{\partial t} + \left(U_j - \sigma_\omega \frac{\partial \nu_t}{\partial x_j} \right) \frac{\partial \omega}{\partial x_j} - \frac{1}{R_\omega} \nabla^2 \omega + s_\omega = 0 \end{aligned} \tag{24}$$

where the source terms, effective Reynolds numbers, and turbulence production are defined as

$$\begin{aligned} s_k &= R_k \left(-G + \beta^* \omega k \right) \\ s_\omega &= R_\omega \left[-\gamma \frac{\omega}{k} G + \beta \omega^2 + 2\left(1 - F_1\right) \sigma_{\omega 2} \frac{1}{\omega} \frac{\partial k}{\partial x_j} \frac{\partial \omega}{\partial x_j} \right] \end{aligned} \tag{25}$$

$$\begin{aligned} R_k &= \left(\frac{1}{1/\mathrm{Re} + \sigma_k \nu_t} \right) \\ R_\omega &= \left(\frac{1}{1/\mathrm{Re} + \sigma_\omega \nu_t} \right) \end{aligned} \tag{26}$$

$$G = \tau_{ij} \frac{\partial U_i}{\partial x_j} = \nu_t \left[\left(U_y + V_x \right)^2 + \left(U_z + W_x \right)^2 + \left(V_z + W_y \right)^2 + 2U_x^2 + 2V_y^2 + 2W_z^2 \right] \tag{27}$$

$$\begin{aligned} F_1 &= \tanh\left(\left\{ \min\left[\max\left(\frac{\sqrt{k}}{0.09\omega\delta}; \frac{500}{\mathrm{Re}\,\delta^2 \omega} \right); \frac{4\sigma_{\omega 2} k}{CD_{k\omega} \delta^2} \right] \right\}^4 \right) \\ CD_{k\omega} &= \max\left(2\sigma_{\omega 2} \frac{1}{\omega} \frac{\partial k}{\partial x_j} \frac{\partial \omega}{\partial x_j}; 10^{-20} \right) \end{aligned} \tag{28}$$

The blending function F_1 was designed to be 1 in the sublayer and logarithmic regions of boundary layers and gradually switch to zero in the wake region to take advantage of the strengths of the k-ω and k-ε models, i.e., k-ω does not require near-wall damping functions and uses simple Dirichlet boundary conditions and the k-ε does not exhibit sensitivity to the level of free-stream turbulence as does the k-ω model. The distance to the nearest no-slip surface δ is required for calculation of F_1 and the model constants are calculated locally as a weighted

average, i.e., $\phi = F_1\phi_1 + (1 - F_1)\phi_2$ where ϕ_1 are the standard k-ω model and ϕ_2 are the transformed k-ε model constants in Table 2.

Table 2. Blended k-ω/k-ε model constants.

ϕ	ϕ_1	ϕ_2	$\phi_{1,\,SST}$
σ_k	0.5	1.0	0.85
σ_ω	0.5	0.856	0.5
β	0.075	0.0828	0.075
β^*	0.09	0.09	0.09
κ	0.41	0.41	0.41
γ	0.0553	0.04403	0.0553

In addition to the standard BKW model, a SST model (Menter, 1994) is included as a user specified option. The SST model accounts for transport of the principal turbulent stresses and has shown improved results for flows with adverse pressure gradients. The SST model is identical to the standard model except for a change in σ_k as shown in Table 2 and the definition of eddy viscosity

$$\nu_t = \frac{0.31k}{\max\left(0.31\omega, \Omega F_2\right)}$$
$$F_2 = \tanh\left(\max\left(\frac{2\sqrt{k}}{0.09\omega y}, \frac{500\nu}{y^2\omega}\right)^2\right) \qquad \textbf{(29)}$$

where Ω is the absolute value of the vorticity, and y is the distance to the nearest wall. This effectively reduces eddy viscosity in regions of high off-body vorticity such as that found in separated flow or in a tip vortex.

3.3. Initial and Boundary Conditions

Formulation of an IBVP requires mathematical derivation of the initial and boundary conditions for each dependent variable and for each type of condition that is to be simulated. Complete presentation of the available palette of conditions and underlying numerics in CFDSHIP-IOWA is deferred until Sections 4.5 and 4.6. Here, a brief discussion of the initial and boundary condition modeling is provided.

Since CFDSHIP-IOWA can be run in two different modes, i.e., steady (time-asymptotic) and unsteady (time-accurate), the initial conditions serve two purposes. For steady-flow simulations, the initial conditions provide the zeroth iteration to an iterative scheme and can be fairly crude. Usually, out of convenience, free-stream conditions are used throughout the domain. For unsteady flow, on the other hand, the initial conditions serve as the solution at time=0.0 and should therefore satisfy the governing equations at this time. General specification for arbitrary geometries and conditions is nearly impossible; therefore, the available initial condition corresponds to a start from rest (i.e., $U = V = W = P = 0.0$, $k = k_{fst}$, $\omega = \omega_{fst}$) with a cubic polynomial acceleration to ship speed. Details of numerical implementation are provided in Section 4.5.

As with most CFD codes, there are numerous BC types which, for convenience, can be grouped into domain truncation boundaries, physical boundaries, and computational boundaries. Physical BC's are due to solid surfaces or water-air free surface, the latter of which is described in the next section. For external-flow hydrodynamics, an infinite unbounded fluid often represents the physical domain. This requires that the computational domain be truncated to a size that can be economically filled with grid points, but has no influence on the computed solution. Computational boundaries are due to grid topology, modeling assumptions, and multi-block domain decomposition. Available options in CFDSHIP-IOWA are listed in Table 7 and will be discussed in more complete detail in Section 4.6.

3.4. Free-surface

CFDSHIP-IOWA uses a surface tracking approach for modeling the free surface. The kinematic free-surface boundary condition (KFSBC) is used to compute the evolution of the free surface, while the dynamic free-surface boundary condition (DFSBC) provides boundary conditions for velocity and pressure. Considering the KFSBC, the requirement that the wave elevation ζ be a stream surface is satisfied by the condition

$$\frac{D(\zeta - z)}{Dt} = 0 \tag{30}$$

Expanding equation (30) gives a continuous 2D hyperbolic PDE for ζ

$$\frac{\partial \zeta}{\partial t} + U\frac{\partial \zeta}{\partial x} + V\frac{\partial \zeta}{\partial y} - W = 0 \tag{31}$$

At the intersection of free- and no-slip surfaces (i.e., the contact line), equation (31) becomes singular when the contact line is in motion but the fluid velocity is zero due to the viscous no-slip boundary condition. This problem is overcome through the use of an approximate contact line model where a small near-wall region is "blanked out" when solving equation (31) and the solution in this region is linearly extrapolated from the interior of the domain. The numerical method for solution of the KFSBC given by equation (31) is presented in Section 4.4.

The DFSBC requires that the normal and tangential stresses are continuous across the free-surface

$$\tau_{ij} n_j = \tau^*_{ij} n_j \tag{32}$$

where n_j is the unit normal vector to the free surface and τ_{ij} $\left[= -p\delta_{ij} + \mathrm{Re}^{-1}\left(\partial U_i/\partial x_j + \partial U_j/\partial x_i\right) - \overline{u_i u_j} \right]$ and τ_{ij}^* are the fluid- and external-stress tensors, respectively. Although not included in this presentation, the effects of air and surface tension can be included through the external-stress tensor τ_{ij}^*. The following approximations were used to obtain free-surface boundary conditions from equation (32): (*i*) the external stress and surface tension are assumed zero so that $\tau_{ij} n_j = 0$; and (*ii*) the gradients of the free surface and normal velocity in the tangential directions are assumed small (i.e., $\partial\zeta/\partial x \approx 0$, $\partial\zeta/\partial y \approx 0$, $\partial W/\partial x \approx 0$, and $\partial W/\partial y \approx 0$). Under these assumptions, expansion of equation (32) gives the following approximate dynamic boundary conditions for pressure and tangential velocity components

$$\hat{p} = \frac{\zeta}{Fr^2} \tag{33}$$

$$\frac{\partial (U,V)}{\partial z} = 0 \tag{34}$$

Lastly, a zero-gradient condition is used for *W*, which is consistent with the approximations employed for the dynamic condition

$$\frac{\partial W}{\partial z} = 0 \tag{35}$$

3.5. Body-force propulsor

The momentum equations (3) include a body-force term f_{b_i}, which may be used to model the effects of a propulsor without resolving the detailed blade flow. There are numerous

approaches to calculating f_{b_i} including simple prescribed distributions, which recover the total thrust and torque, to more sophisticated methods which use a propeller performance code in an interactive fashion with the RANS solver to capture propeller-hull interaction and to distribute f_{b_i} according to the actual blade loading (e.g., Stern et al., 1994). For the latter, custom interface software must be developed to extract effective wake from RANS solution and to produce f_{b_i} calculated by performance code. This is not provided with CFDSHIP-IOWA, but can be easily developed by experienced users with access to a propeller performance code.

CFDSHIP-IOWA does, however, include a prescribed axisymmetric body force with axial and tangential components (Stern et al., 1988). The radial distribution of forces is based the Hough and Ordway circulation distribution (Hough and Ordway, 1964) which has zero loading at the root and tip. Therein,

$$\begin{aligned} f_{bx} &= A_x r^* \sqrt{1-r^*} \\ f_{b\theta} &= A_\theta \frac{r^* \sqrt{1-r^*}}{(1-R_H) r^* + R_H} \end{aligned} \tag{36}$$

where

$$\begin{aligned} r^* &= \frac{r/\mathrm{RP} - \mathrm{RH}}{1-\mathrm{RH}} \\ r &= \sqrt{(y - \mathrm{Y\_PROP\_CENTER})^2 + (z - \mathrm{Z\_PROP\_CENTER})^2} \\ A_x &= \frac{C_T}{(\mathrm{DXPROP})} \frac{105}{16(4+3\mathrm{RH})(1-\mathrm{RH})} \\ A_\theta &= \frac{K_Q}{(\mathrm{DXPROP}) J^2} \frac{105}{\pi(4+3\mathrm{RH})(1-\mathrm{RH})} \end{aligned} \tag{37}$$

and where C_T and K_Q are the thrust and torque coefficients, J is the advance coefficient, `RP` is the propeller radius non-dimensionalized by ship length, `RH` is the hub radius in decimal percent of `RP`, and `DXPROP` is the mean chord length projected into the *x*-*z* plane. As derived, these forces are defined over an "actuator cylinder" with volume defined by RP, RH, and DXPROP, i.e., $\pi\left(\mathrm{RP}^2\left(1-\mathrm{RH}^2\right)\right)\mathrm{DXPROP}$. Integration of the body forces (36) over this analytical volume exactly recovers the prescribed thrust and torque,

$$T = \rho L^2 U_0^2 \int_{R_H}^{R_P} \int_0^{2\pi} \int_{x_p}^{x_s} f_{bx} r dx d\theta dr$$
$$Q = \rho L^3 U_0^2 \int_{R_H}^{R_P} \int_0^{2\pi} \int_{x_p}^{x_s} f_{b\theta} r^2 dx d\theta dr \quad \textbf{(38)}$$

Since curvilinear non-orthogonal multi-block grids are typically used, implementation of (36) requires several issues to be addressed. A vertex-based search algorithm is used to determine which grid-point control volumes are within the actuator cylinder.Figure 5 shows an example for commercial ship geometry, Esso Osaka. In this simulation, an O-grid topology is used to wrap around the stern. The search algorithm identifies 814 total cells in two blocks that lie within the cylinder and upon integration give an approximate volume of the cylinder, i.e., prescribed volume = 1.6979×10^{-6} and integrated volume = 1.6714×10^{-6}. Given this 1.6% error in volume, total thrust and torque in (38) is not recovered. Therefore, magnitude of body forces in (36) are uniformly scaled by the volume error such that the integrated total force is equal to that which is prescribed. Finally, it should be noted that all body-force algorithms are designed to only work with Cartesian coordinates (`icoord`=1 or 2).

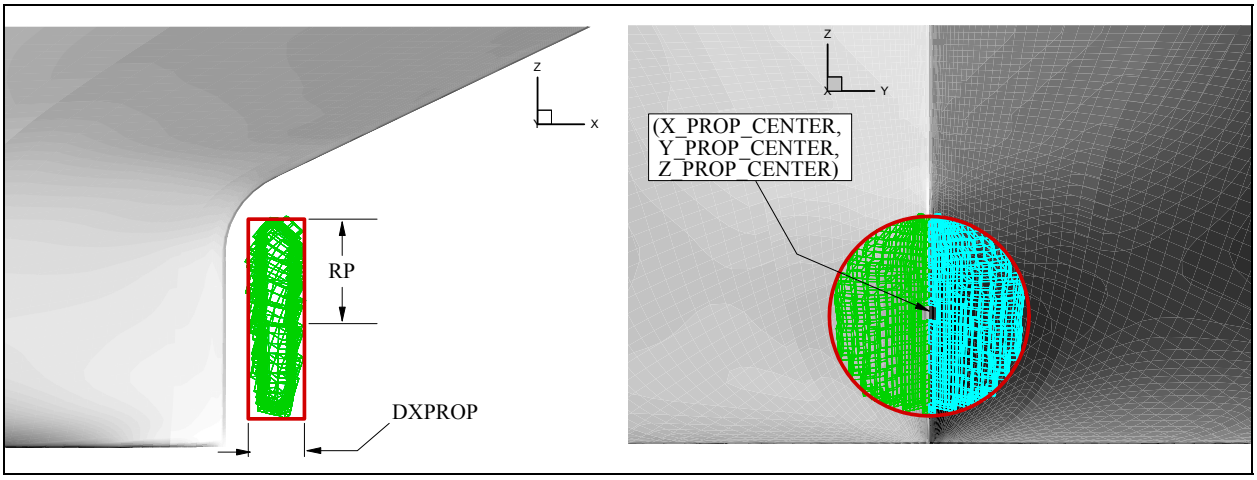

Figure 5. Grid-cells in body-force propeller "actuator cylinder."

4. NUMERICAL METHODS

This section describes the numerical methods used in CFDSHIP-IOWA and includes a discussion of the coordinate transformation, discretization scheme, free-surface solver and

adaptive gridding, RANS solution algorithm and pressure-Poisson equation, initial and boundary conditions, Chimera overset gridding, and calculation of forces and moments.

4.1. Coordinate transformation

The continuous governing equations are transformed from the physical domain in either Cartesian (x,y,z,t) or cylindrical-polar (x,r,θ,t) coordinates into the computational domain in non-orthogonal curvilinear coordinates (ξ, η, ζ, τ). A partial transformation is used in which only the independent variables are transformed, leaving the velocity components U_i in the base coordinates. The transformation relations are

$$\nabla \cdot \boldsymbol{q} = \frac{1}{J}\frac{\partial}{\partial \xi^j}\left(b_i^j q_i\right) \tag{39}$$

$$\left(\nabla \phi\right)_i = \frac{1}{J} b_i^j \frac{\partial \phi}{\partial \xi^j} \tag{40}$$

$$\nabla^2 \phi = \frac{1}{J}\frac{\partial}{\partial \xi^i}\left(J g^{ij} \frac{\partial \phi}{\partial \xi^j} \right) = g^{ij} \frac{\partial^2 \phi}{\partial \xi^i \partial \xi^j} + f^i \frac{\partial \phi}{\partial \xi^i} \tag{41}$$

$$\frac{\partial \phi}{\partial t} = \frac{\partial \phi}{\partial \tau} - \frac{1}{J} b_i^j \frac{\partial x_i}{\partial t}\frac{\partial \phi}{\partial \xi^j} \tag{42}$$

where q_i represents the components of an arbitrary vector $\boldsymbol{q}(x_i)$. The geometric coefficients b_i^j and g^{ij}, the Jacobian J, and f^i are functions of coordinates only and are defined for Cartesian grids as

$$b_l^i = \varepsilon_{lmn} \frac{\partial x^m}{\partial \xi^j}\frac{\partial x^n}{\partial \xi^k} \tag{43}$$

$$g^{ij} = \frac{1}{J^2} b_l^i b_l^j \tag{44}$$

$$J = \begin{vmatrix} x_\xi & x_\eta & x_\zeta \\ y_\xi & y_\eta & y_\zeta \\ z_\xi & z_\eta & z_\zeta \end{vmatrix} \tag{45}$$

$$f^i = \frac{1}{J}\frac{\partial}{\partial \xi^j}\left(J g^{ij}\right) \tag{46}$$

where ε_{lmn} is the permutation symbol with *lmn* cyclic. The grid-velocity terms $\frac{\partial x_i}{\partial t}$ in (42), which are used only for unsteady flows in an absolute frame of reference, are calculated directly using finite difference expressions, as given in the following section.

Using the transformation relations, the continuity (2) and momentum (17) equations are written as

$$\frac{1}{J}\frac{\partial}{\partial \xi^j}\left(b_i^j U_i\right) = 0 \tag{47}$$

$$\frac{\partial U_i}{\partial \tau} + a_{U_i}^k \frac{\partial U_i}{\partial \xi^k} = -\frac{1}{J} b_i^k \frac{\partial P}{\partial \xi^k} + \frac{1}{R_{eff}} g^{km} \frac{\partial^2 U_i}{\partial \xi^k \partial \xi^m} + \left(\frac{1}{J} b_j^k \frac{\partial \nu_t}{\partial \xi^k}\right)\left(\frac{1}{J} b_i^m \frac{\partial U_j}{\partial \xi^m}\right) + f_{bi} \tag{48}$$

where

$$a_{U_i}^k = \frac{1}{J} b_j^k \left(U_j - \frac{1}{J} b_j^m \frac{\partial \nu_t}{\partial \xi^m} - \frac{\partial x_j}{\partial \tau} \right) - \frac{f^k}{R_{eff}} \tag{49}$$

Note that the convective-term coefficient $a_{U_i}^k$ in (49) contains contributions from both the linear Reynolds-stress closure (15) and the grid velocity (42), the latter of which introduces non-inertial accelerations due to body motions.

Splitting the viscous term into normal and cross components and rearranging gives the continuous form of the momentum equations in the computational domain

$$\frac{\partial U_i}{\partial \tau} + a_{U_i}^k \frac{\partial U_i}{\partial \xi^k} - \frac{1}{R_{eff}} g^{ii} \frac{\partial^2 U_i}{\partial \xi^i \partial \xi^i} = -\frac{1}{J} b_i^k \frac{\partial P}{\partial \xi^k} + s_{U_i} \tag{50}$$

$$s_{U_i} = \frac{2}{R_{eff}}\left(g^{12} \frac{\partial^2 U_i}{\partial \xi^1 \partial \xi^2} + g^{13} \frac{\partial^2 U_i}{\partial \xi^1 \partial \xi^3} + g^{23} \frac{\partial^2 U_i}{\partial \xi^2 \partial \xi^3} \right) + \left(\frac{1}{J} b_j^k \frac{\partial \nu_t}{\partial \xi^k}\right)\left(\frac{1}{J} b_i^m \frac{\partial U_j}{\partial \xi^m}\right) + f_{bi} \tag{51}$$

4.2. Discretization scheme

For temporal discretization of equations for *k*-ω (24), KFSBC (31), and momentum (50), a general formula for an Euler backward difference is given by

$$\frac{\partial \phi}{\partial \tau} = \frac{1}{\Delta \tau}\left(wt_n \phi^n + wt_m \phi^{n-1} + wt_{mm} \phi^{n-2}\right) \tag{52}$$

where the weights, wt_n, wt_m, wt_{mm}, determine the order of the difference expression and are given in Table 3 for the first- and second-order formulations. For steady state and time-accurate solutions, first-order formulation and second-order formulations are used, respectively, and are

Table 3. Finite-difference weights for temporal discretization.

Scheme	`itemp_order`	wt_n	wt_m	wt_{mm}
1st order	1	1	-1	0
2nd order	2	3/2	-2	1/2

specified using the input variable `itemp_order`. Eq. (52) is also used to compute grid velocity terms $\frac{\partial x_i}{\partial t}$ in Eq. (42) where the general variable ϕ is replaced with the grid coordinates x_i.

For spatial discretization of equations for k-ω (24), KFSBC (31), geometric coefficients (43), Jacobian (45), and momentum (50), the convective (or first derivative) terms are discretized with the following higher-order upwind formula

$$U^k \frac{\partial \phi}{\partial \xi_k} = \frac{1}{2}\left(U^k + \left|U^k\right|\right)\delta^-_{\xi_k}\phi + \frac{1}{2}\left(U^k - \left|U^k\right|\right)\delta^+_{\xi_k}\phi \tag{53}$$

where

$$\delta^-_{\xi_i}\phi = w_{mm}\phi_{i-2} + w_m\phi_{i-1} + w_n\phi_i + w_p\phi_{i+1} + w_{pp}\phi_{i+2} \tag{54}$$

$$\delta^+_{\xi_i}\phi = -w_{pp}\phi_{i-2} - w_p\phi_{i-1} - w_n\phi_i - w_m\phi_{i+1} - w_{mm}\phi_{i+2} \tag{55}$$

Six convective schemes are available in CFDSHIP-IOWA and their weighting coefficients are supplied in Table 4.

Table 4. Finite-difference weights for spatial discretization of convective terms.

Scheme	`ispat_order`	w_{mm}	w_m	w_n	w_p	w_{pp}
1st order upwind	1	0	-1	1	0	0
2nd order central	2	0	-1/2	0	1/2	0
2nd order upwind	3	1/2	-2	3/2	0	0
2nd order upwind biased (Quick)	4	1/8	-7/8	3/8	3/8	0
3rd order upwind biased	5	1/6	-1	1/2	1/3	0
4th order central	6	1/12	-2/3	0	2/3	1/12

The user may specify the order of accuracy for the momentum equations and the KFSBC using the input variable `ispat_order`, however, 2nd-order upwind is sufficient for most simulations. For the BKW, equation (24) is discretized, by default, using the same scheme as the momentum equations. However, order-of-accuracy can be set to a lower-order scheme using namelist variable `itm_spat_order`. To maintain stability, it is occasionally necessary to set the turbulence model discretizaiton to 1st-order upwind. Evaluation of the transformation relations in equations (43) and (45) is accomplished using the 2nd-order central scheme.

The viscous terms are written as

$$\frac{\partial^2 \phi}{\partial \xi^i \partial \xi^i} = \omega 2_{mm}\phi_{i-2} + \omega 2_m \phi_{i-1} + \omega 2_n \phi_i + \omega 2_p \phi_{i+1} + \omega 2_{pp}\phi_{i+2} \qquad \textbf{(56)}$$

and the coefficients are supplied in Table 5. Although written in a general fashion, the viscous terms are preset to 2nd-order central, and selection of 4th-order scheme is not accessible by input parameter.

Table 5. Finite-difference weights for spatial discretization of viscous terms.

Scheme	*Order*	$\omega 2_{mm}$	$\omega 2_m$	$\omega 2_n$	$\omega 2_p$	$\omega 2_{pp}$
2nd order central	2nd	0	1	-2	1	0
4th order central	4th	-1/12	16/12	-30/12	16/12	-1/12

Applying the temporal and spatial discretizations given by equations (52), (53), and (56) to the continuous momentum equations (50) gives the discrete form of the momentum equations

$$A_{ijk}U_i^n + \sum_{nb} A_{nb}U_{i,nb}^n = S_{U_i} - \frac{1}{J} b_i^k \frac{\partial P^n}{\partial \xi^k} \qquad \textbf{(57)}$$

where A_{ijk} and A_{nb} denote the central and neighboring coefficients of the discretized momentum equations, respectively. The source term S_{U_i} contains velocities from the previous two time steps (n-1) and (n-2) and the mixed derivative terms (51), the latter of which are lagged to the previous iteration.

$$S_{U_i} = s_{U_i} - \frac{1}{\Delta \tau}(wt_m \phi^{n-1} + wt_{mm}\phi^{n-2}) \qquad \textbf{(58)}$$

4.3. RANS solution algorithm & pressure Poisson equation

The pressure-implicit split-operator (PISO) algorithm for solving the incompressible Navier-Stokes equations (Issa, 1985) uses a predictor-corrector approach to advance the momentum equation while enforcing the continuity equation. In the predictor step, the momentum equation (57) is advanced implicitly using the pressure field from the previous time step P^{n-1}

$$A_{ijk}U_i^* + \sum_{nb} A_{nb}U_{i,nb}^* = S_i - \frac{1}{J}b_i^k \frac{\partial P^{n-1}}{\partial \xi^k} \tag{59}$$

where superscript '*' is used to denote advancement to an intermediate time level.

In the corrector step, the velocity is updated explicitly

$$U_i^{**} = \hat{U}_i - \frac{1}{JA_{ijk}}b_i^k \frac{\partial P^*}{\partial \xi^k} \tag{60}$$

using a pressure obtained from a derived Poisson equation and where the psuedo-velocity is defined as

$$\hat{U}_i = \frac{1}{A_{ijk}}\left(S_i - \sum_{nb} A_{nb}U_{i,nb}^* \right) \tag{61}$$

A pressure-Poisson equation is derived by taking the divergence of equation (60)

$$\frac{1}{J}\frac{\partial}{\partial \xi^j}b_i^j U_i^{**} = \frac{1}{J}\frac{\partial}{\partial \xi^j}b_i^j \hat{U}_i - \frac{1}{J}\frac{\partial}{\partial \xi^j}b_i^j \left(\frac{1}{JA_{ijk}}b_i^k \frac{\partial P^*}{\partial \xi^k} \right) \tag{62}$$

and by realizing that the LHS of equation (62) goes to zero upon convergence

$$\frac{1}{J}\frac{\partial}{\partial \xi^j}\left(\frac{Jg^{jk}}{A_{ijk}}\frac{\partial P^*}{\partial \xi^k} \right) = \frac{1}{J}\frac{\partial}{\partial \xi^j}b_i^j \hat{U}_i \tag{63}$$

Because a regular, or collocated, grid approach is used, solution of equation (63) requires special treatment to avoid odd-even decoupling. Fourth-order artificial dissipation is implicitly added by taking a linear combination of full- and half-cell operators (Sotiropoulos and Abdallah, 1992)

$$(1-\gamma)LP^* + \gamma \hat{L}P^* + NP^* = \frac{1}{J}\frac{\partial}{\partial \xi^j}b_i^j \hat{U}_i \tag{64}$$

where L is the full-cell formulation, $\hat{L}$ is the half-cell formulation, and N is the operator containing mixed-derivative terms

$$L = \frac{1}{J}\left\{\delta_{\xi_1}\left(a^{11}\delta_{\xi_1}\right) + \delta_{\xi_2}\left(a^{22}\delta_{\xi_2}\right) + \delta_{\xi_3}\left(a^{33}\delta_{\xi_3}\right)\right\} \tag{65}$$

$$\hat{L} = \frac{1}{J}\left\{\tilde{\delta}_{\xi_1}\left(a^{11}\tilde{\delta}_{\xi_1}\right) + \tilde{\delta}_{\xi_2}\left(a^{22}\tilde{\delta}_{\xi_2}\right) + \tilde{\delta}_{\xi_3}\left(a^{33}\tilde{\delta}_{\xi_3}\right)\right\} \tag{66}$$

$$N = \frac{1}{J}\{\delta_{\xi_1}\left(a^{12}\delta_{\xi_2} + a^{13}\delta_{\xi_3}\right) + \delta_{\xi_2}\left(a^{21}\delta_{\xi_1} + a^{23}\delta_{\xi_3}\right) + \delta_{\xi_3}\left(a^{31}\delta_{\xi_1} + a^{32}\delta_{\xi_2}\right)\} \tag{67}$$

and where

$$\delta_{\xi_i}\phi = \frac{1}{2}\left(\phi_{i+1} - \phi_{i-1}\right) \tag{68}$$

$$\tilde{\delta}_{\xi_i}\phi = \left(\phi_{i+1/2} - \phi_{i-1/2}\right) \tag{69}$$

$$a^{ij} = \frac{Jg^{ij}}{A_{ijk}} \tag{70}$$

The weighting function γ ranges from 1 (i.e., most dissipation and smooth solutions) to 0 (i.e., no dissipation, but prone to decoupling). This parameter is set by the namelist variable `gama_pr` which has a default value of γ = 1.0. Use of the half-cell operator introduces metrics at half-cell locations which are computed from an average of the nodal values. Note that the half-cell formulation achieved with γ = 1.0 is essentially the same as the Rhie and Chow (1983) interpolation method for avoiding odd-even decoupling.

4.4. Free-surface solver and adaptive gridding

The tracking approach used in CFDSHIP-IOWA for modeling the free surface was presented in Section 3.3. Therein, the DFSBC was used to provide boundary conditions for velocity and pressure as given by equations (33)-(35), which are relatively straightforward to numerically implement. The KFSBC was developed by requiring that the free surface be a stream surface resulting in a 2D PDE for the evolution of the wave elevation ζ, as given by equation (31). The numerical method for solution of this equation will be presented in this section and closely follows the approach for solution of the RANS equations presented in Sections 4.1 and 4.2.

Equation (31) is transformed from the physical domain in Cartesian coordinates (*x,y,t*) into the computational domain in non-orthogonal curvilinear coordinates (ε,η,τ) using a reduced 3D form (i.e., two spatial and one temporal coordinate) of the general 4D transformation

presented in Section 4.1. Using the transformation relations, the continuous KFSBC in computational space is given by

$$\frac{\partial \zeta}{\partial \tau} + a_\zeta^k \frac{\partial \zeta}{\partial \xi^k} - W = 0 \tag{71}$$

where the superscript 'k' is summed for k=1,2 in equation (71) and

$$a_\zeta^k = \frac{1}{J} b_j^k \left(U_j - \frac{\partial x_j}{\partial \tau} \right) \tag{72}$$

The temporal term in equation (72) is discretized using an Euler backward difference as given by equation (52), while the convective term is discretized using the same higher-order upwind difference as for the convective term of the RANS equations and is given by equation (53). Applying the temporal and spatial discretizations to the continuous KFSBC (71) gives

$$A_{ij}^\zeta \zeta^n + \sum_{nb} A_{nb}^\zeta \zeta_{nb}^n = S_i \tag{73}$$

where A_{ij}^ζ and A_{nb}^ζ [changed 'ij' subscript to 'nb'] denotes the central and neighboring coefficients of the discretized KFSBC. The source term S_i contains the vertical velocity component W and the wave elevation at previous time steps.

A straightforward solution of equation (73) often leads to stability problems due to several factors. First, as discussed in Section 2.2, equation (73) is singular at the contact line. Secondly, a combination of highly-clustered near-wall spacing required for turbulence models (i.e., on the order of 10^{-6}), high-aspect ratio grid cells (i.e., on the order of 10^5), and lack of either physical or numerical dissipation results in an unstable numerical system. As discussed in Section 2.2, the contact-line is modeled by "blanking out" the solution in the near wall region and extrapolating the solution from the interior. The blanking distance is set by the variable `wavblank` in the \$FREE_SURFACE namelist. In addition, the solution is filtered with a variable-order high-bypass filter after each iteration

$$\hat{\zeta}_i = a\zeta_i + \frac{b}{2}\left(\zeta_{i+1} + \zeta_{i-1}\right) + \frac{c}{2}\left(\zeta_{i+2} + \zeta_{i-2}\right) + \frac{d}{2}\left(\zeta_{i+3} + \zeta_{i-3}\right) \tag{74}$$

where the coefficients *a, b, c,* and *d* are given in Table 6 for second-, fourth-, and sixth-order filters.

Table 6. Filter coefficients.

Order	*a*	*b*	*c*	*d*
2nd	½	½	0	0
4th	5/8	½	-1/8	0
6th	11/16	15/32	-3/16	1/32

By transforming the filter from physical to wave number space (Lele, 1992), it can be shown that the 4th and 6th order filters remove energy at the highest wave number ($k\Delta x = \pi$) while leaving the low wave numbers unchanged. Since the 2nd order filter is overly dissipative, its use should be avoided. The filter coefficients are specified in the boundary condition file (`ifsfilter`= 2, 4, or 6) and are default to the 4th-order filter.

The discrete KFSBC given by equation (73) is solved on all block faces identified as a free-surface boundary using the iterative solvers as described in Section 3.2. After the filtering operation, the solution is used to conform the volume grid to the new wave elevation through the use of cubic-spline interpolation in the ζ curvilinear coordinate of the original grid system. This is equivalent to a "rigid-wire" approach where the grid points slide along the ζ coordinate as shown in Figure 6.

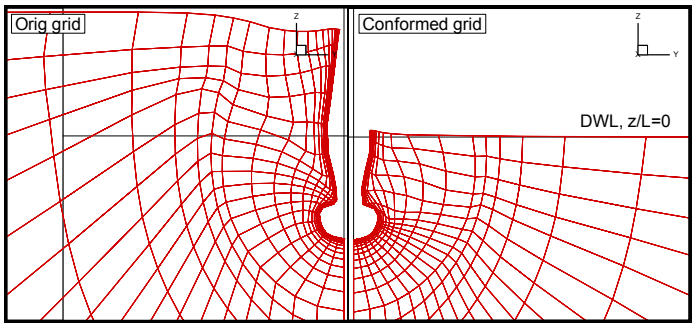

Figure 6. Dynamic Free-Surface Adaptive Grid.

In general, this approach is fairly robust, but is susceptible to poor grid quality if there is large difference between the original and conformed grid or if there is severe geometry changes in the ζ, or girthwise, direction.

4.5. Initial conditions

Solution of the IBVP requires initial conditions. For steady-flow simulations, the time-marching process serves as an iteration loop and the initial conditions provide the zeroth iteration. Usually, a fairly "poor" initial guess (e.g., free-stream at all grid points, except for no-slip boundaries) is sufficient such that the algorithm is capable of damping out any initial transients. For unsteady flow, on the other hand, the initial conditions serve as the solution at time=0 and initial conditions which do not satisfy governing equations can prevent the simulation from converging. Excluding custom and/or novel unsteady problems, most applications can be served by the two initial condition options available in the code.

The first option (`mode`=0) sets all variables to uniform free stream, i.e., the dependent variables have the following values U=`UINF`, V=`VINF`, W=`WINF`, p=0, k=k_{fst}=10^{-7}, ω=ω_{fst}=9.0, and $\nu_{t,fst}$=1.1x10^{-8} where (`UINF, VINF, WINF`) permits specification of free-stream unit vector. For steady flow, an impulsive start is used where velocity is set to no-slip values at the first time step (iteration). In contrast, for unsteady flow, the no-slip boundaries are smoothly ramped from free-stream values to no-slip values using a cubic polynomial. For `time` < `time_ramp_end`, the no-slip boundaries are set to the following

$$\begin{aligned} U &= U_{INF}\left(1-ramp\right) \\ V &= V_{INF}\left(1-ramp\right) \\ W &= W_{INF}\left(1-ramp\right) \end{aligned} \qquad \textbf{(75)}$$

$$ramp = -2\left(\frac{time}{\texttt{time\_ramp\_end}}\right)^3 + 3\left(\frac{time}{\texttt{time\_ramp\_end}}\right)^2$$

This represents a smooth acceleration of the ship from rest and provides initial conditions that satisfy continuity.

The second option (mode=1) sets initial conditions by reading a restart file. While a previous simulation typically generates this Fortran binary file, it can also be created by the user to prescribe either initial conditions or boundary conditions. For the latter, the restart file must be used in conjunction with boundary condition `ibtyp` =14 which is described below. Format of the restart file is described in Appendix A.6.

4.6 Boundary conditions

As discussed in Section 2, the CFD Process requires formulation of an IBVP where boundary conditions (BC) must be specified on all faces of the computational domain. As with most CFD codes, there are numerous BC types, which for discussion here, can be grouped into domain truncation boundaries, physical boundaries, and computational boundaries. The formulation of each BC type is described in detail and guidance provided on when and how each BC used.

Twenty-six different BC types are available in CFDSHIP-IOWA and are summarized in Table 7. Each face of each mesh must be specified and can be broken into an arbitrary number of rectangular patches over which a different boundary condition can be applied. Numerically, the 26 different conditions consist of combinations of Dirichlet and Neumann boundary conditions for the nondimensional flow variables U, V, W, $\hat{p}$, k, ω and ν_t. Note that BC for ν_t are implemented so that eddy-viscosity gradients in equation (17) can be evaluated near boundaries without changing finite-difference stencil. Dirichlet conditions are prescribed values or lagged data from donor regions (i.e., periodic or multiblock). Neumann conditions are prescribed gradients, which are evaluated using one-sided finite differences. For zero-gradient conditions, two functions are used in CFDSHIP-IOWA to evaluate first and second derivatives

$$\texttt{zero\_fd} = a + \texttt{ibcord}\frac{1}{3}(a-b) \tag{76}$$

$$\texttt{zero\_sd} = 2a - b \tag{77}$$

where a and b are the values one and two grid points inside the boundary in the `ibdir` coordinate direction, respectively. Details unique to each BC type are now described.

Table 7. Boundary Conditions

	IBTYP	*Description*	*U*	*V*	*W*	*P*	*k*	*ω*	ν_t
Domain Truncation Boundaries	10	Inlet	UINF	VINF	WINF	$\partial P/\partial\xi_i = 0$	k_{fst}=1x10^{-7}	ω_{fst}=9.0	$\nu_{t,fst}$
	11	Exit	$\partial^2 U/\partial\xi_i^2 = 0$	$\partial^2 V/\partial\xi_i^2 = 0$	$\partial^2 W/\partial\xi_i^2 = 0$	$\partial P/\partial\xi_i = 0$	$\partial k/\partial\xi_i = 0$	$\partial\omega/\partial\xi_i = 0$	$\partial\nu_t/\partial\xi_i = 0$
	12	Far-field #1	UINF	$\partial V/\partial\xi_i = 0$	$\partial W/\partial\xi_i = 0$	0	$\partial k/\partial\xi_i = 0$	$\partial\omega/\partial\xi_i = 0$	$\partial\nu_t/\partial\xi_i = 0$
	13	Far-field #2	UINF	VINF	WINF	$\partial P/\partial\xi_i = 0$	$\partial k/\partial\xi_i = 0$	$\partial\omega/\partial\xi_i = 0$	$\partial\nu_t/\partial\xi_i = 0$
	14	Prescribed	*	*	*	*	*	*	*
Physical Boundaries	20	Absolute-frame no-slip	0	0	0	$\partial P/\partial\xi_i = 0$	0	$60/\mathrm{Re}\,\beta\Delta y^2$	0
	22	Relative-frame no-slip	$\dot{x}$	$\dot{y}$	$\dot{z}$	$\partial P/\partial\xi_i = 0$	0	$60/\mathrm{Re}\,\beta\Delta y^2$	0
	27	Impermeable slip (calculate forces)	Eq. (78)	Eq. (78)	Eq. (78)	$\partial P/\partial\xi_i = 0$	$\partial k/\partial\xi_i = 0$	$\partial\omega/\partial\xi_i = 0$	$\partial\nu_t/\partial\xi_i = 0$
	28	Impermeable slip (no forces)	Eq. (78)	Eq. (78)	Eq. (78)	$\partial P/\partial\xi_i = 0$	$\partial k/\partial\xi_i = 0$	$\partial\omega/\partial\xi_i = 0$	$\partial\nu_t/\partial\xi_i = 0$
	30	Free surface	Eq. (34)	Eq. (34)	Eq. (35)	Eq. (33)	$\partial k/\partial\xi_i = 0$	$\partial\omega/\partial\xi_i = 0$	$\partial\nu_t/\partial\xi_i = 0$
Computational Boundaries	40	Zero gradient	$\partial U/\partial\xi_i = 0$	$\partial V/\partial\xi_i = 0$	$\partial W/\partial\xi_i = 0$	$\partial P/\partial\xi_i = 0$	$\partial k/\partial\xi_i = 0$	$\partial\omega/\partial\xi_i = 0$	$\partial\nu_t/\partial\xi_i = 0$
	41	Translational periodicity, w/ ghost cells	*	*	*	*	*	*	*
	42	Translational periodicity, w/o ghost cells	*	*	*	*	*	*	*
	43	Pole (I-around)	Eq. (80)	Eq. (80)	Eq. (80)	Eq. (80)	Eq. (80)	Eq. (80)	Eq. (80)
	44	Pole (j-around)	Eq. (80)	Eq. (80)	Eq. (80)	Eq. (80)	Eq. (80)	Eq. (80)	Eq. (80)
	45	Pole (k around)	Eq. (80)	Eq. (80)	Eq. (80)	Eq. (80)	Eq. (80)	Eq. (80)	Eq. (80)
	50	Cylindrical zero gradient	*	*	*	*	*	*	*
	51	Rotational periodicity, w/ ghost cells	*	*	*	*	*	*	*
	52	Rotational periodicity, w/o ghost cells	*	*	*	*	*	*	*
	60	No-slip/centerplane	*	*	*	*	*	*	*
	61	x-axis symmetry	0	$\partial V/\partial\xi_i = 0$	$\partial W/\partial\xi_i = 0$	$\partial P/\partial\xi_i = 0$	$\partial k/\partial\xi_i = 0$	$\partial\omega/\partial\xi_i = 0$	$\partial\nu_t/\partial\xi_i = 0$
	62	y-axis symmetry	$\partial U/\partial\xi_i = 0$	0	$\partial W/\partial\xi_i = 0$	$\partial P/\partial\xi_i = 0$	$\partial k/\partial\xi_i = 0$	$\partial\omega/\partial\xi_i = 0$	$\partial\nu_t/\partial\xi_i = 0$
	63	z-axis symmetry	$\partial U/\partial\xi_i = 0$	$\partial V/\partial\xi_i = 0$	0	$\partial P/\partial\xi_i = 0$	$\partial k/\partial\xi_i = 0$	$\partial\omega/\partial\xi_i = 0$	$\partial\nu_t/\partial\xi_i = 0$
	91	Multi-block w/ ghost cells	*	*	*	*	*	*	*
	92	Multi-block w/o ghost cells	*	*	*	*	*	*	*
	99	Blanked out points	0	0	0	0	0	0	0

* See text for detailed description

Domain truncation boundaries

For external-flow hydrodynamics, an infinite unbounded fluid often represents the physical domain. This requires that the computational domain be truncated to a size that can be economically filled with grid points, but has no influence on the computed solution. Actual location of boundaries and influence on solution must be evaluated as part of the verification grid studies which is discussed in Section 7. However, BC types used on truncated domain boundaries are listed in Table 7 and represent inlet, exit, far-field, and prescribed boundaries.

For the inlet boundary condition (`ibtyp`=10), the velocity field is set by the input parameters `UINF, VINF, WINF`, pressure is zero gradient, and the turbulence is set to the free stream values $k_{fst} = 1.0x10^{-7}, \omega_{fst} = 9.0$. The user specified freestream-velocity unit vector defined by `UINF, VINF, WINF` provides capability to specify the angle of attack to the vehicle.

The exit boundary condition, `ibtyp` = 11 is derived assuming that the boundary is far downstream such that streamwise viscous effects are zero, i.e., $\frac{\partial^2 U}{\partial \xi_i^2} = \frac{\partial^2 V}{\partial \xi_i^2} = \frac{\partial^2 W}{\partial \xi_i^2} = 0$. This allows velocity on boundary to be calculated using `zero_sd from` (77) and all other variables extrapolated using `zero_fd from` (76).

There are two far-field conditions, `ibtyp`=12 and 13. The latter (`ibtyp`=13) specifies that velocity field is set by the input parameters `UINF, VINF, WINF` and pressure and turbulence variables are zero gradient. This is preferred option, but requires that boundary location be sufficiently far from vehicle. The former (ibtyp=12), on the other hand, sets the axial-component of velocity to `UINF` and pressure to zero while all other variables are assumed to be zero gradient.

Prescribed boundary condition, `ibtyp`=14, must be used in combination with a user-generated restart file, format of which is documented in Appendix A.6. This condition holds all variables constant to those in the restart file except for pressure, which is calculated assuming a zero-gradient condition. Typically, this condition is used when specifying either an analytical (e.g., Blasius flat plate boundary layer) or previously computed flow. An example of the latter

may be an isolated propeller blade simulation, where the wake from upstream is computed by a previous simulation, and used to prescribe inflow boundary conditions.

Physical boundary conditions

Physical BC's are due to either solid surfaces or water-air free surface. Available options are listed in Table 7.

There are two no-slip boundary conditions. The first (`ibtyp`=20) is for surfaces which are moving with the grid and the second (`ibtyp`=22) is for surfaces which are moving in the relative-frame system provided angular velocities (`agvx` or `agvz`), which are defined in the namelist input file `cfd_ship.nml`.

Impermeable slip boundary conditions are specified using `ibtyp`=27 and 28, the only difference being whether or not the specified boundary be included (27) or not (28) in the calculation of forces and moments. This distinction is useful since impermeable slip boundaries are often used, for example, to model water-tunnel walls or stream surfaces and it may not be desired to include the forces on these boundaries in the integration process. The boundary condition is formulated using contravariant velocity components at one point off the boundary and by forcing the normal component to be zero. For example, on a `j`=1 slip surface, the velocity boundary conditions are

$$\begin{aligned} U(i,1,k) &= U_\xi x_\xi + U_\eta x_\eta + U_\zeta x_\zeta \\ V(i,1,k) &= U_\xi y_\xi + U_\eta y_\eta + U_\zeta y_\zeta \\ W(i,1,k) &= U_\xi z_\xi + U_\eta z_\eta + U_\zeta z_\zeta \end{aligned} \qquad \textbf{(78)}$$

where

$$\begin{aligned} U_\xi &= \frac{1}{J}\left(U(i,2,k)b_1^1 + V(i,2,k)b_2^1 + W(i,2,k)b_3^1\right) \\ U_\eta &= 0 \\ U_\zeta &= \frac{1}{J}\left(U(i,2,k)b_1^3 + V(i,2,k)b_2^3 + W(i,2,k)b_3^3\right) \end{aligned} \qquad \textbf{(79)}$$

and where all other variables are calculated using a zero gradient condition. Similar expressions can be dervied for `i`=constant and `k`=constant surfaces.

As indicated in Table 7, free surface (`ibtyp`=30) BC have been described earlier in Section 3.

Computational boundaries

Computational boundaries are due to grid topology, modeling assumptions, and multi-block domain decomposition. Available options in CFDSHIP-IOWA are listed in Table 7 and include zero-gradient, translational and rotational periodicity, pole singularities, symmetry, and multi-block boundaries. Each type is now described.

Zero-gradient boundaries (`ibtyp=40`) assume that all variables have zero gradient behavior. This condition is provided, but not often used because symmetry conditions, which set the normal component of velocity to zero, are typically more appropriate.

Translational periodicity, as shown in Figure 8, can be prescribed using either `ibtyp` = 41 or 42, the difference being that the former uses 2 ghost cells on each boundary to maintain solver order-of-accuracy and the latter uses a simple weighted average of the adjacent field point

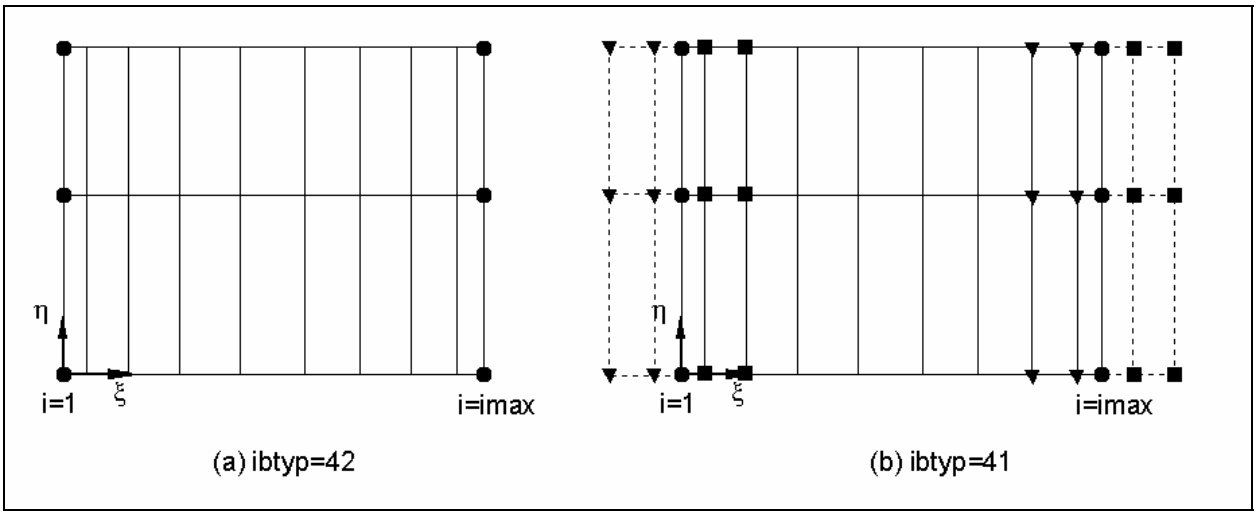

Figure 8. Translational periodic boundary conditions, `ibtyp`=41 & 42.

values. This boundary condition can be used in either Cartesian or cylindrical coordinates. Note that all flow variables are assumed periodic.

Pole boundary conditions are based upon simple average of variables one grid point off the pole in the interior of the domain with three orientations available: i-around (`ibtyp`=43), j-around (`ibtyp`=44), and k-around (`ibtyp`=45). The orientation specifies the summation index, e.g., for k-around and `ibdir`=+2, the *U* component of velocity on the pole would be

$$U(i,j,k) = \frac{1}{kbce - kbcs + 1} \sum_{k=kbcs}^{kbce} U\left(i, j+1, k\right) \tag{80}$$

Rotational periodicity about the *x*-axis, as shown in Figure 9, can be prescribed using either `ibtyp` =51 or 52. As with translational periodicity, the difference between the two is that the former uses 2 ghost cells on each boundary to maintain solver order-of-accuracy and the latter uses a simple weighted average of the adjacent field point values. However, in this case, since the radial and circumferential components are the periodic variables, *V* and *W* velocity components are calculated using the following transformation,

$$\begin{aligned} V_r &= V\cos\theta + W\sin\theta \\ V_\theta &= -V\sin\theta + W\cos\theta \\ \theta &= \tan^{-1}\left(z/y\right) \end{aligned} \tag{81}$$

Note that this boundary condition is restricted to Cartesian grids (`icoord`=1/2) and with periodicity about the *x*-axis only.

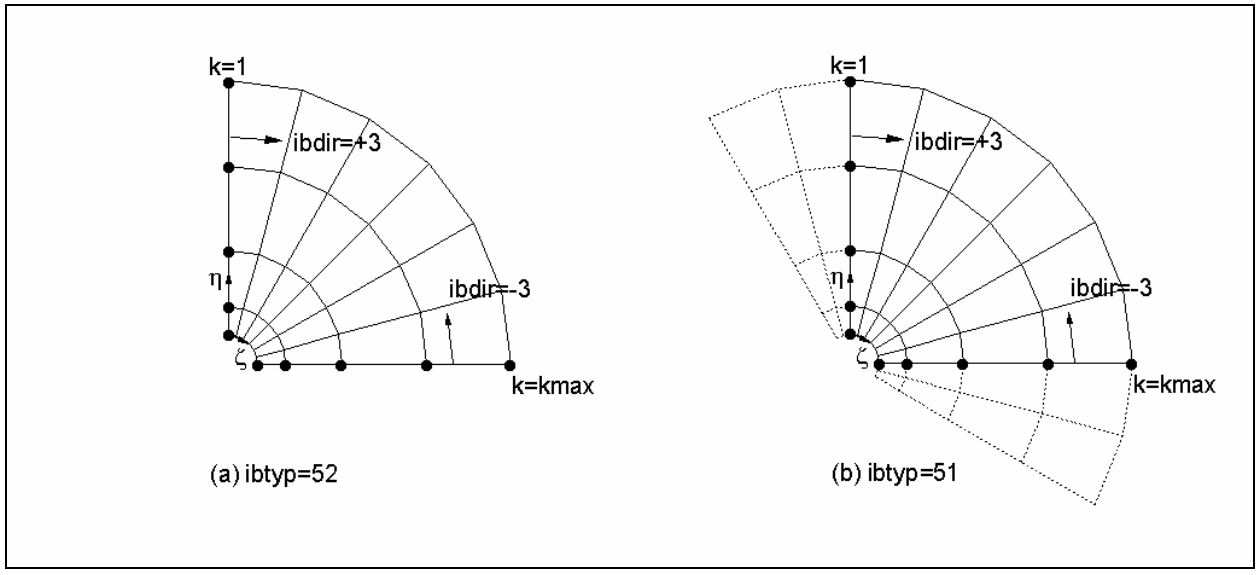

Figure 9. Rotational periodic boundary conditions, `ibtyp`=51 & 52.

Centerplane condition (`ibtyp`=60) is a boundary condition used for half-domain ship-hull simulations where part of the boundary is no-slip and part is centerplane, as shown in Figure 10. Demarcation between the no-slip/centerplane is determined by testing the *y*-coordinate, i.e., if $|y| \le 1.0x10^{-6}$ then the boundary point is assume to be centerplane, where all variables are

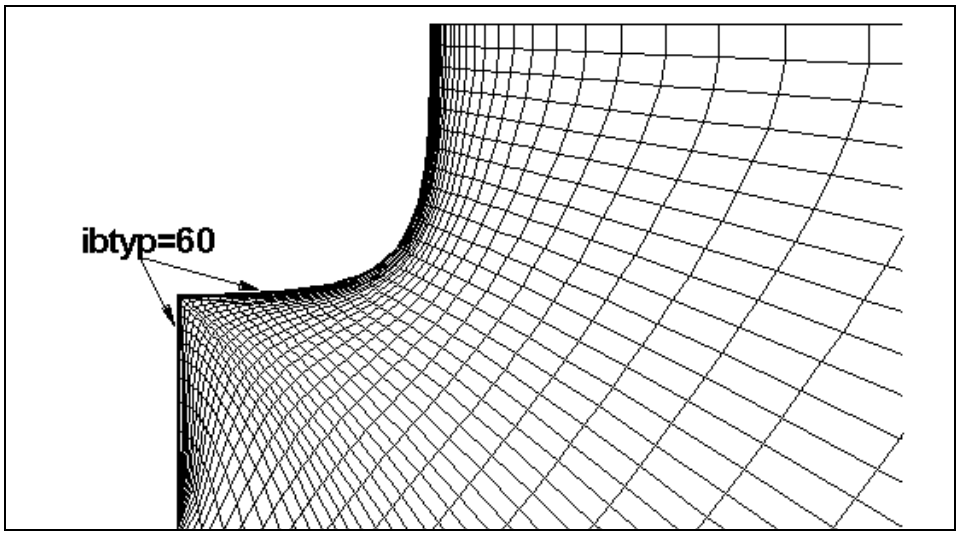

Figure 10. Centerplane/no-slip boundary condition, `ibtyp`=60.

calculated using `zero_fd`, except for the V-component of velocity which is set to zero, otherwise the point is treated as no-slip. This boundary condition is typically used to resolve bow, stern, and/or keel using a staircase resolution (e.g., Stern et al., 1996). It is restricted to Cartesian grids (`icoord`=1/2).

Symmetry conditions (ibtyp=61, 62, 63) are available for each coordinate direction. Formulation is simple: normal component of velocity is set to zero (61, U=0; 62, V=0, 63, W=0), and all other flow variables are assumed to be zero gradient.

CFDSHIP-IOWA utilizes 2 types of multi-block boundary conditions, pointwise continuous (i.e., abutted-block interface) and overset (i.e., Chimera), examples of both are shown in Figure 11.

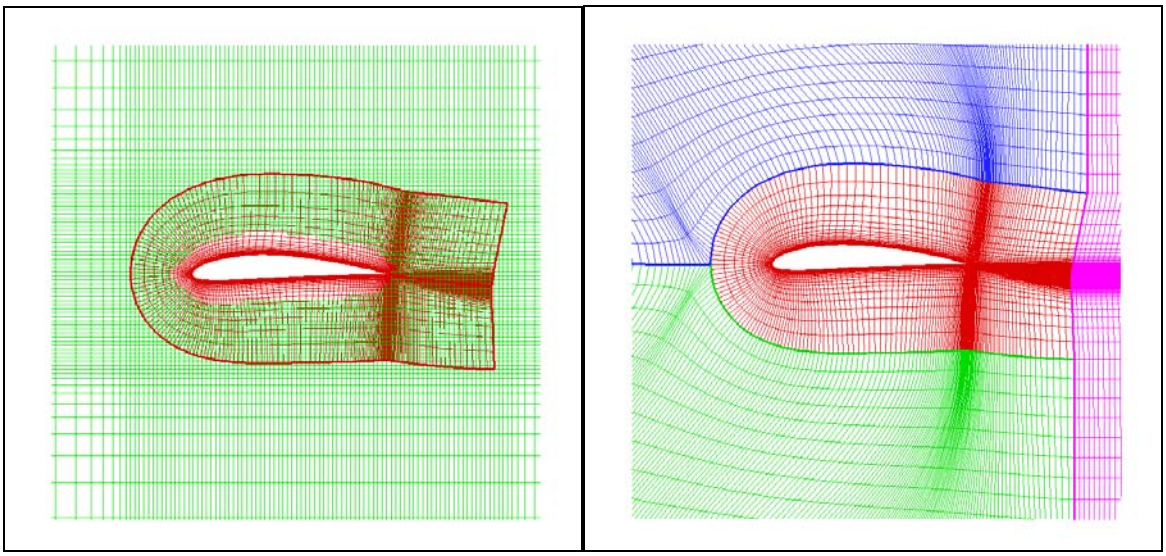

Figure 11. Overset and patched multiblock grids for airfoil.

For abutted multi-block boundary conditions, two options are available, `ibtyp`=91 and 92, where the former includes 2 rows of ghost cells, which are added after the grid is read from file. For `ibtyp`=91, all independent flow variables in the ghost cells are computed as field variables in the donor block. This conserves mass and momentum across the boundary. Furthermore, by using 2 rows of ghost cells, the 5-point stencil and therefore the solver order-of-accuracy is maintained on the boundary. In contrast, `ibtyp` =92 calculates boundary values using a weighted average, based upon distance from boundary, of the field values on each side of the interface. This condition is essentially a first order treatment across the interface and does not solve governing equations for these boundaries. It is noted that a consistent approach must be used, i.e., one or the other must be used for all abutted boundaries, mixed usage is not currently supported. Moreover, for complex grid topologies, it is possible that `ibtyp` =91 may fail to properly identify ghost cells. In those cases, `ibtyp` =92 must be used.

For overset multi-block boundary conditions, PEGASUS software from NASA Ames Research Center must be used. Interface and implementation are described in the following sub-section.

4.7 Chimera overset gridding

Capability for simulations using Chimera-style overset domain decomposition is accomplished through interface with PEGASUS version 5.1 (Suhs, et al., 2001), which is the latest version of the PEGASUS series of mesh interpolation codes, originally developed at NASA Ames Research Center. The main purpose for the development of version 5.1 was to decrease the number of user inputs required and to allow for easier operation of the code. A basic description of Chimera methodology is described in the Version 4 manual (Suhs and Tramel, 1991). It should be noted that PEGASUS is restricted to U.S. institutions and researchers due to export control regulations. Other options for computation of interpolation coefficients include CHALMESH (Petersson, 1999), OVERTURE (Quinlan et al., 2002) and PEGISUE (Denny, 2002).

CFDSHIP-IOWA is designed to use double-fringe hole and outer boundaries and level-2 interpolation. Figure 12 shows an example of an overset grid system for an airfoil to aid in defining terminology. Comparing Figures 12a and 12b, it can be seen that double-fringe blanks out 2 layers of cells around the outer and hole boundaries. Both layers are interpolated from the donor mesh. This permits use of the normal 5-point stencil for all field points and maintains order of accuracy near boundaries. Single-fringe boundaries, on the other hand, require use of 3-point stencils for the field points adjacent to hole and outer boundaries, which results in reduction of the order-of-accuracy. The downside in using a double fringe is that it requires more mesh points and makes it more difficult to obtain the required overlap between hole boundaries and outer boundaries.

Figure 12c shows the impact of enabling level-2 interpolation. This is a method where once the minimum hole has been established; the hole is enlarged to improve the communication among meshes. In addition, it can be seen that the outer boundary of the foil mesh has been moved inward. This is accomplished in PEGASUS by comparing relative grid quality between interpolation and donor meshes so as to reduce mesh disparity, which can severely impact accuracy. In addition, level-2 interpolation provides capability to create holes with refinement

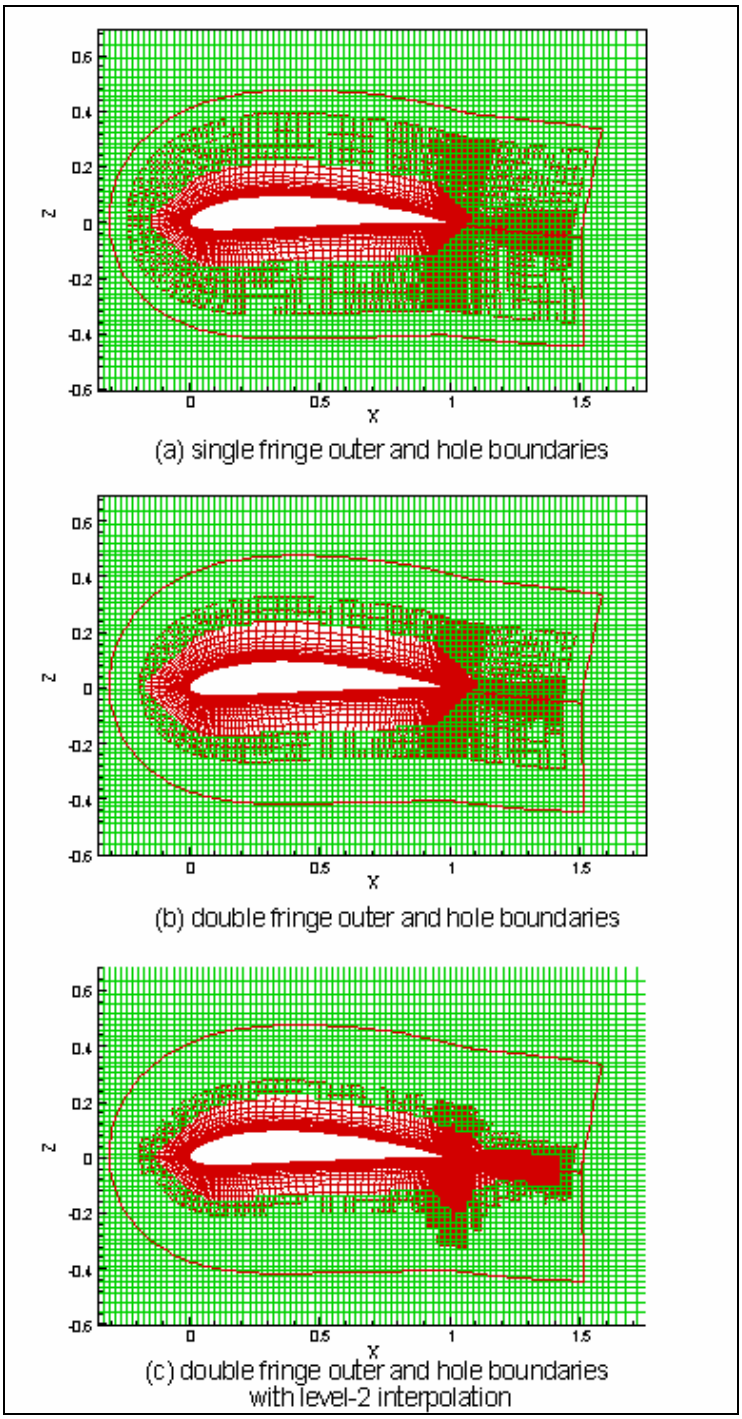

Figure 12. Illustration of PEGASUS terminology.

meshes that are added to the domain. This cannot be accomplished through the usual hole-cutting methods, since refinement meshes typically do not have solid walls that would be used for definition of hole-cutting boundaries. Refinement meshes have been used in the aerospace

community (e.g., Meakin, R., 1999) for flow adaptive refinement within context of structured flow solvers.

Given a valid PEGASUS interpolation file (i.e., in PEGASUS standard naming convention, `XINTOUT`), implementation in CFDSHIP-IOWA is straightforward. This file should be renamed ***`FNAMEI.xintout`*** since CFDSHIP-IOWA automatically looks for this file in the execution directory. If it exists, the file is read and a summary is printed in the standard output. Otherwise, the code continues and prints a notification message that ***`FNAMEI.xintout`*** does not exist. It should be emphasized that in the boundary condition input file ***`FNAMEI.bcs`*** Chimera outer boundaries remain unspecified, which for most problems, greatly simplifies and shortens this input file.

As a summary, Figure 13 provides a flowchart summarizing the overset-grid process. Further details can be found in the appropriate domain connectivity software, which in this case is PEGASUS version 5.1.

4.8 Calculation of forces and moments

The fluid forces and moments acting on all solid surfaces are obtained by integration of the normal and tangential stresses over all no-slip (`ibtyp`=20,22) and some of the user-identified slip boundaries (i.e., `ibtyp`=27). The fluid stress tensor on a no-slip surface is comprised of components due to pressure and viscous stress

$$\tau_{ij} = -p\delta_{ij} + \frac{1}{\mathrm{Re}}\left(\frac{\partial U_i}{\partial x_j} + \frac{\partial U_j}{\partial x_i}\right) \qquad \textbf{(82)}$$

On the solid surfaces, the fluid forces and moments are determined through integration of (82)

$$\underline{F} = \int_S \tau_{ij} n_i dS \qquad \textbf{(83)}$$

$$\underline{M} = \underline{r} \times \underline{F} \qquad \textbf{(84)}$$

where $\underline{n}^j$ is the unit-vector normal to a ξ^j-coordinate surface, dS^j is the local surface area element, and $\underline{r}$ is the position vector

$$\underline{n}^j = \frac{b_1^j \hat{i} + b_2^j \hat{j} + b_3^j \hat{k}}{\sqrt{\left(b_1^j\right)^2 + \left(b_2^j\right)^2 + \left(b_2^j\right)^2}} \qquad \textbf{(85)}$$

$$dS^j = \sqrt{\left(b_1^j\right)^2 + \left(b_2^j\right)^2 + \left(b_2^j\right)^2}\, d\xi^i d\xi^k$$

and where (i,j,k) are cyclic. Integration of wetted surface area S and equations (83)-(84) is accomplished using a cell-centered 2D trapezoidal rule. Calculation of the force is broken down into contributions from piezometric pressure (cppiezo), hydrostatic pressure (cphydro), which is valid only for Fr≠0, and viscous shear stress (cf). These contributions, along with the total force (ctot), are written for each base coordinate direction every iteration. The moments are treated in a similar fashion.

For overset grid-systems with overlapping surface meshes on solid surfaces, forces and moments computed by CFDSHIP-IOWA will contain errors due to multiply defined values and hole boundaries. Special tools must be used to make flow variables single-valued. Currently, the force and moment computation (FOMOCO) tools from NASA (Chan and Buning, 1996) represent the only option for performing this task. Two programs make up this toolset, MIXSUR and OVERINT where the former creates a single-valued mixed surface with triangular zipper grids and the latter performs integration over this new surface. Unlike the NASA flow solver OVERFLOW, which reads MIXSUR output as in input file and computes forces and moments on the fly by calling OVERINT as a subroutine, CFDSHIP-IOWA currently uses these tools in a stand-alone post-processing fashion. Future versions may more tightly integrate with these tools or appropriate alternatives.

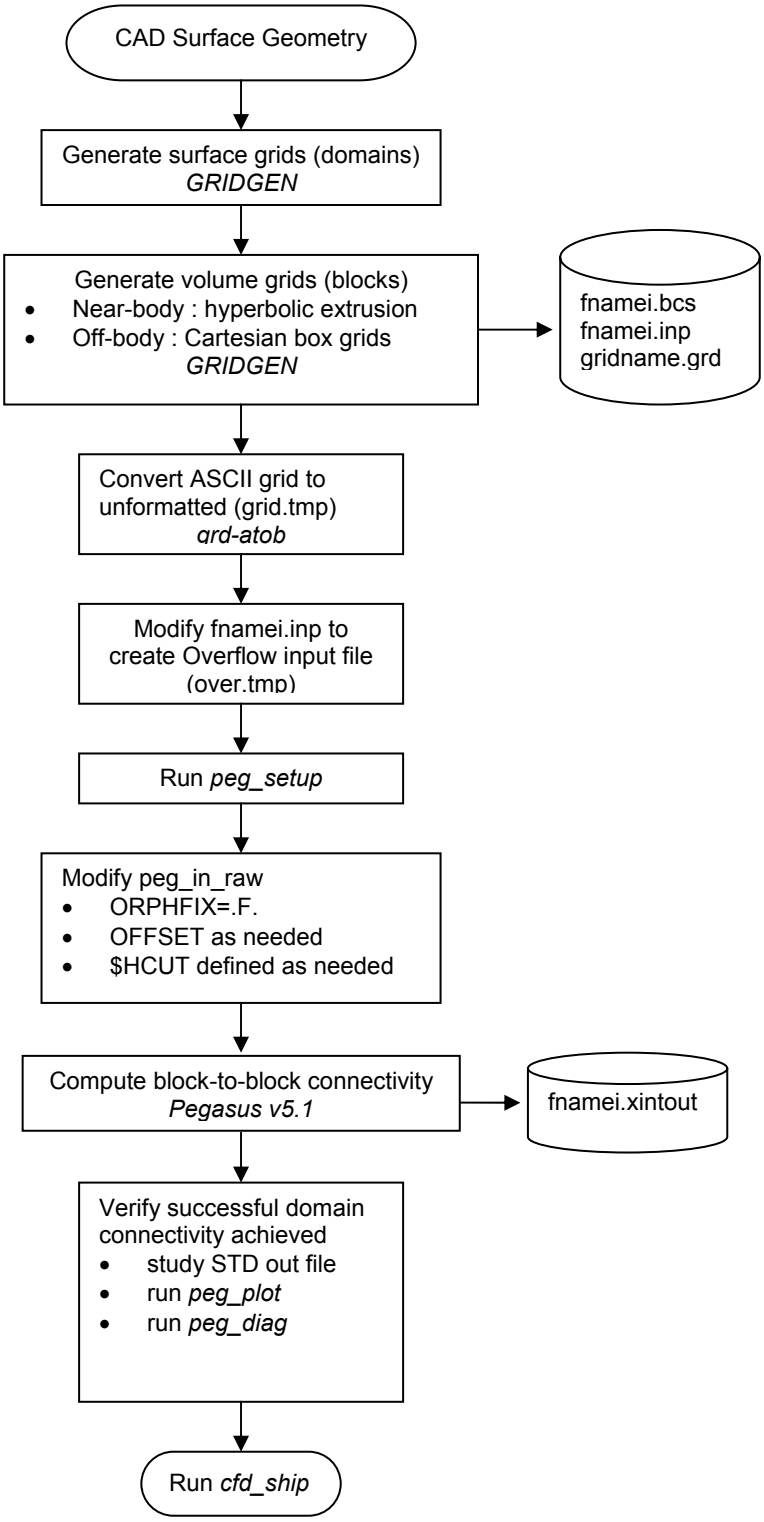

Figure 13. Flowchart of Overset Grid Process

4.9 Algebraic equation solver

The overall method is fully implicit and there are four locations in the code that require iterative solvers: momentum predictor step (59); pressure equation (64); turbulence model equations (24); and KFSBC (31). Currently, a line-ADI scheme with a pentadiagonal solver and under relaxation is used to solve the algebraic equations. The pentadiagonal solver is modified to account for hole boundaries

$$
\begin{aligned}
a_i &= a_i \square IBLANK_i \\
b_i &= b_i \square IBLANK_i \\
c_i &= c_i \square \left(1 - IBLANK_i\right) \\
d_i &= d_i \square IBLANK_i \\
e_i &= e_i \square IBLANK_i \\
f_i &= f_i \square IBLANK_i + \left(1 - IBLANK_i\right) \square \phi_i
\end{aligned}
\qquad \textbf{(86)}
$$

where IBLANK is 0 for a hole or fringe point and 1 for a field point, a_i, b_i, c_i, d_i, e_i correspond to 5 diagonals of the pentadiagnoal matrix, f_i is the right hand side, and ϕ_i corresponds to the flow variable on the hole or outer boundary fringe.

4.10 Algorithm summary and flowchart

Figures 14 and 15 summarize the algorithmic structure of CFDSHIP-IOWA in flowcharts, including pre- and post-processing functions, major time marching and iteration loops, and input and output files.

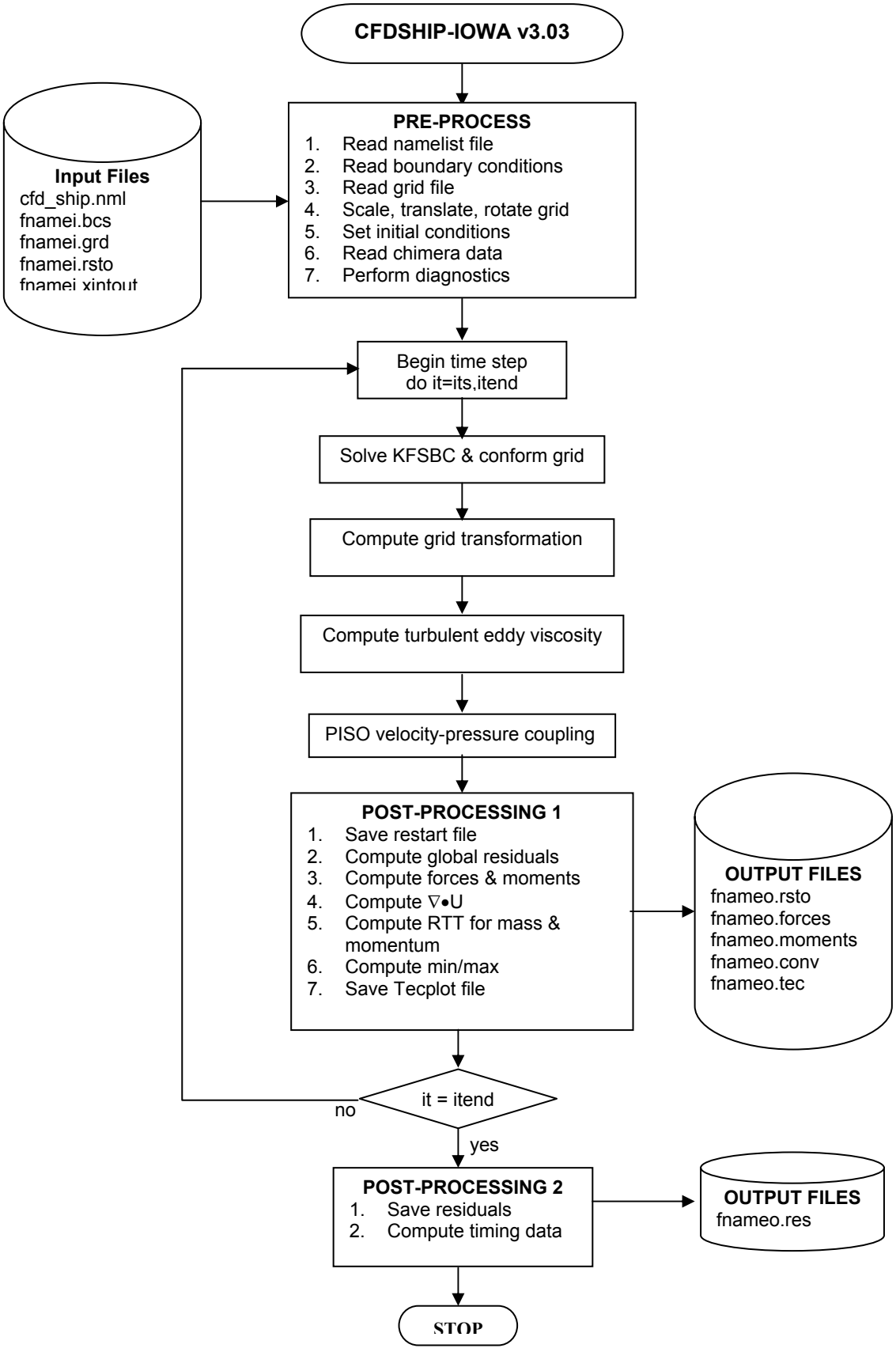

Figure 14. Algorithm flowchart.

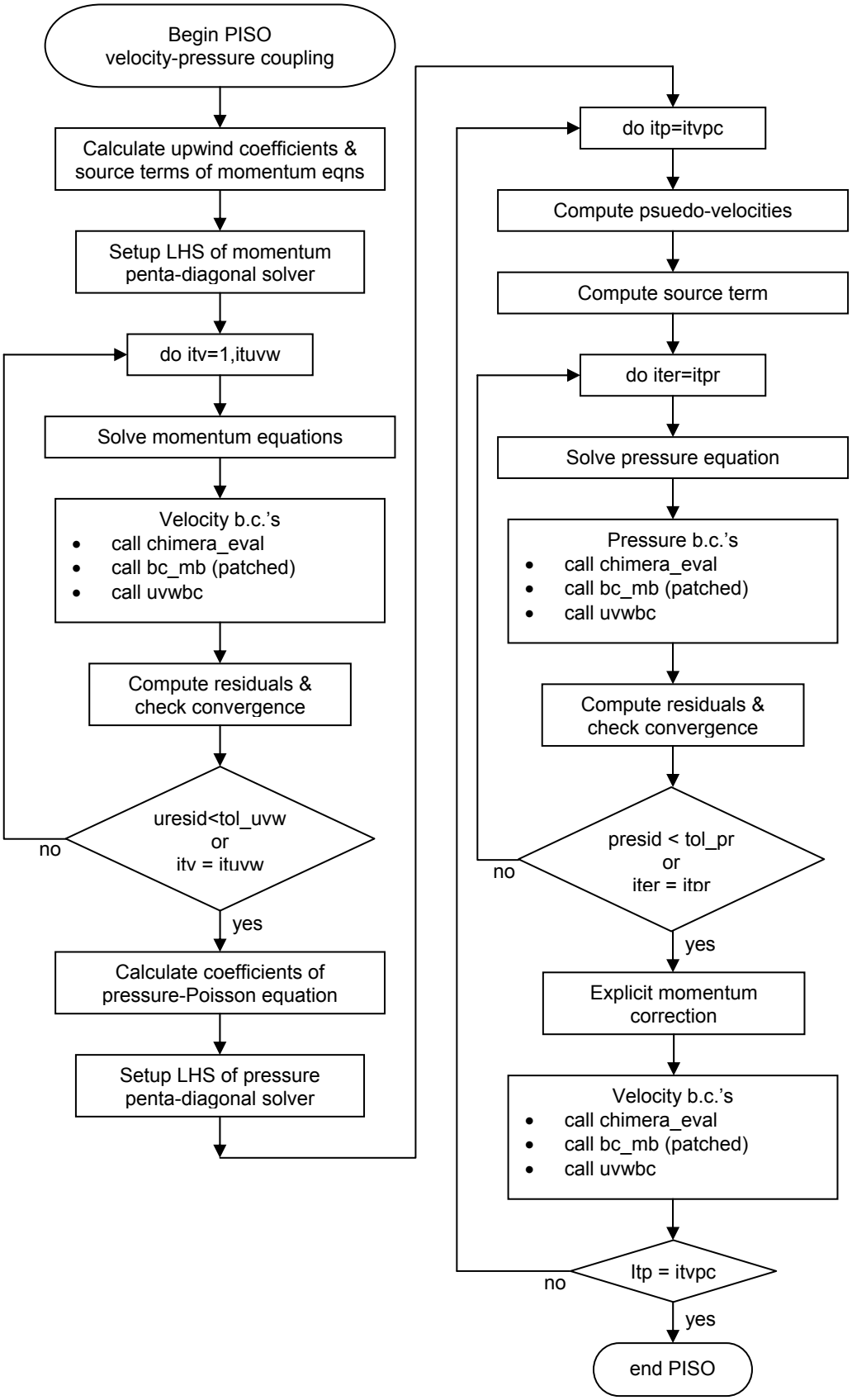

Figure 15. Detailed flowchart for PISO velocity-pressure coupling solver

5. CODE DEVELOPMENT AND HIGH-PERFORMANCE COMPUTING

Development of CFDSHIP-IOWA has taken place over the past 8 years, a period in which high-performance computing (HPC) platforms have evolved from Cray YMP vector processors to the array of architectures found today which includes commercial off-the-shelf (COTS) Beowulf clusters, SGI scalable distributed-shared non-uniform memory access (NUMA) architectures, and IBM pipelined superscalar architectures. Developing application codes which are portable and which are capable of harnessing a given platform's capability, is a challenging task. In addition, CFDSHIP-IOWA had to meet other objectives such as supporting student theses and project research, as well as vertical transition to other universities, industry, and government labs.

The approach used to meet these objectives has been based upon a flexible data structure, capability for both serial and parallel computing, adherence to standards such as MPI, modern programming using Fortran90/95, and interface with existing 3rd-party software for grid generation and boundary condition specification (GRIDGEN), Chimera overset grid methods (PEGASUS, Chimera Grid Tools, FOMOCO), and post-processing and visualization (TECPLOT). It is noted that development has taken place concurrently with several DOD HPCMO Challenge Projects from 1996 to the present (Rood, 1997; Rood, 1998; Rood, 1999; Rood, 2000; Kim, 2001). The following sections present an overview of the code and data structures, parallel computing, portability, and distribution, extraction, compilation and execution.

5.1. Code and data structures

Code and data structures are critical to successful implementation of scalable parallel computing and portability. Unfortunately, highly efficient code is often hard to understand by users. Because CFDSHIP-IOWA was designed to support research and development of new models, it is well documented with in-code comment statements and the structure at the subroutine level is based upon 3D index-ordered arrays, which are intuitively easier to understand in context of structured-grid CFD, and which lends itself naturally to distributed multi-block computing.

Top-level structure of the code, which is also shown in Figure 14, is as follows

- program cfdship_iowa

- pre_process
- free_surface
- grid_transformation
- eddyvs
- piso
- post_process1
- post_process2

In process of writing code, several guidelines were adopted. At top-level, all arrays are dynamic, 1D, and allocatable to fit current grid size. At subroutine level, computation is performed on a single block; all arrays are 3D and either explicit-shape dummy arrays (both array and dimensions are in argument list) or automatic arrays (arrays which are not in argument list and which are created/destroyed upon entry/exit of a given procedure). Index pointers are used to indicate relative location in 1D array and are defined as follows,

```
first(1)=1
length(1)=imax(1)*jmax(1)*kmax(1)
last(1)=length(1)
ntot=length(1)
do m=2,nmesh
          first(m)=last(m-1)+1
          length(m)=imax(m)*jmax(m)*kmax(m)
          last(m)=first(m)+length(m)-1
          ntot=ntot+length(m)
enddo
```

(87)

Fortran90 module procedures are used in preference over COMMON blocks to share definitions and values of data between program units due to ease of code maintenance and data-hiding capability. To reduce coding errors, IMPLICIT NONE statements are used in all routines.

By design, this approach easily permits parallel multi-block implementation via message-passing interface (MPI) and the single-program multiple data (SPMD) paradigm. As shown in the code fragment in Figure 16, serial implementation for a given function performs a `DO` loop over each block with the `locn` pointer set to `first(m)`. This passes each block to the

```
      c
      c -- calculate transformation metrics
      c
      #ifdef SERIAL
               do m = 1,nmesh
                  locn = first(m)
      #endif
      #ifdef PARALLEL
                  m = mymesh
                  locn = 1
      #endif
                  call metric(imax(m), jmax(m), kmax(m),
           .           xp(locn),yp(locn),zp(locn),
           .           xp0(locn),yp0(locn),zp0(locn),
           .           xp00(locn),yp00(locn),zp00(locn),
           .           b11(locn),b12(locn),b13(locn),
           .           b21(locn),b22(locn),b23(locn),
           .           b31(locn),b32(locn),b33(locn),
           .           a11(locn),a22(locn),a33(locn),
           .           a12(locn),a13(locn),a23(locn),aji(locn),
           .           f1(locn),f2(locn),f3(locn),
           .           agvx(m),agvy(m),agvz(m),
           .           dxdt(locn),dydt(locn),dzdt(locn))

      #ifdef SERIAL
               enddo
      #endif
```

Figure 16. Code fragment illustrating use of pointer and CPP statements.

```
      subroutine metric(imax,jmax,kmax,x,y,z,x0,y0,z0,x00,y00,z00,
     .                  b11,b12,b13,b21,b22,b23,b31,b32,b33,
     .                  a11,a22,a33,a12,a13,a23,aji,f1,f2,f3,
     .                  agvx,agvy,agvz,dxdt,dydt,dzdt)
      use global_parameters
      implicit NONE
      integer i,j,k,imax,jmax,kmax
      real (kind=double), dimension(imax,jmax,kimax):: x,y,z,x0,y0,z0,x00,y00,z00
```

Figure 17. Subroutine fragment illustrating 3D explicit-shape dummy arrays.

subroutine, as shown in Figure 17, in a sequential fashion. It is noted that grid and flow variable arrays are dimensioned at the top-level to hold the entire system, i.e., to `ntot`. In contrast, for parallel implementation, the `DO-LOOP` is eliminated and the pointer FIRST is set to 1 since each processor only has the data of a single block. As such, each processor executes its own copy of the executable. Except for input and output routines, communication between

processors occurs only at the boundary condition subroutines. Processor 0, through the use of branching statements, handles control of input and output. It should be noted that the suffix (.F or .F90) on the source code files indicates that the file contains CPP statements which in turn indicates the file contains parallel-specific programming statements.

5.2 Parallel Computing

CFDSHIP-IOWA achieves scalable parallel performance using several parallel models. Originally, it was designed as a distributed-memory coarse-grain message-passing model based upon domain decomposition and the message-passing interface (MPI). For good performance, this approach requires static load balancing, i.e., the grid system be decomposed into nearly equal sized blocks, and, in addition, requires a block for each processor. While very efficient, this process becomes tedious and makes post-processing difficult, especially when large numbers of processors (>32) are required. To alleviate this problem, a second parallel model using OpenMP threads for shared-memory fine-grain (i.e., loop-level) parallelism was introduced. This model is used in combination with MPI to achieve multi-level parallelism, which permits use of very large numbers of processors and can perform dynamic load balancing. In the following, each of these models is discussed in detail.

To demonstrate the performance of the message-passing model, a 105x61x30 single-block grid for the Wigley hull is decomposed into 2-, 4-, 8-, 12-, 16-, and 32-block grid systems and simulations timed using both `ibtyp`=91 and `ibtyp`=92 (i.e., with and without ghost cells, respectively) multi-block boundary conditions. Figure 18 shows the impact of decomposition on both the total problem and individual block sizes. Both boundary conditions impose an overhead due to replicated points, but overhead when using `ibtyp`=91 increases significantly with processors due to increasingly large number of ghost cells. This directly impacts the scalability of memory utilization. However, this tradeoff is often necessary if the improved accuracy of ibtyp=91 is required.

Figure 19 shows the parallel speedup $S_n = T_s / T_p(n)$, where T_s is the single processor wall-clock time and $T_p(n)$ is the wall-clock time for n processors, for both multi-block boundary conditions on both the CRAY T3E and the SGI Origin 2000 (O2K). For `ibtyp`=91, degradation of speedup, due to above-mentioned overhead, is obvious, especially for 16 and 32 processors. Agreement between machines for ibtyp=92 is not consistent, i.e., the O2K shows

almost linear speedup through 32 processors and the T3E shows some drop off for n = 16 and 32. Since timings were not made in dedicated mode, the reproducibility is dependent upon system load, which may explain the T3E performance. Finally, it is noted that the timings show that 99.5% of the code is parallelized.

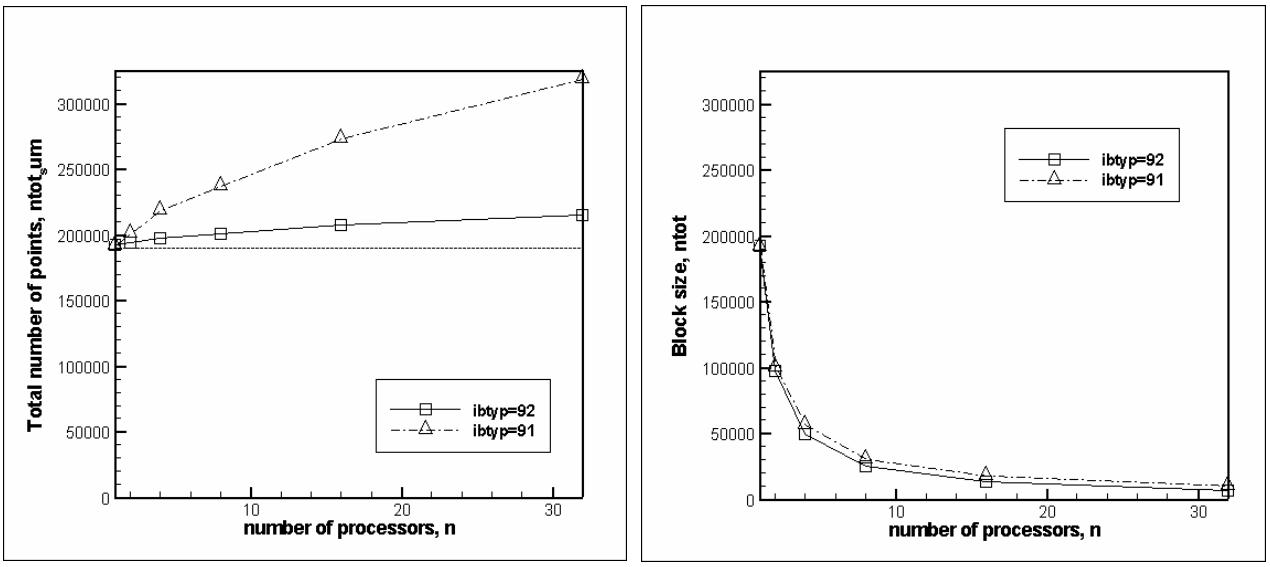

(a) total number of points (b) block size

Figure 18. Impact of domain decomposition and use of ghost cells on number of grid points.

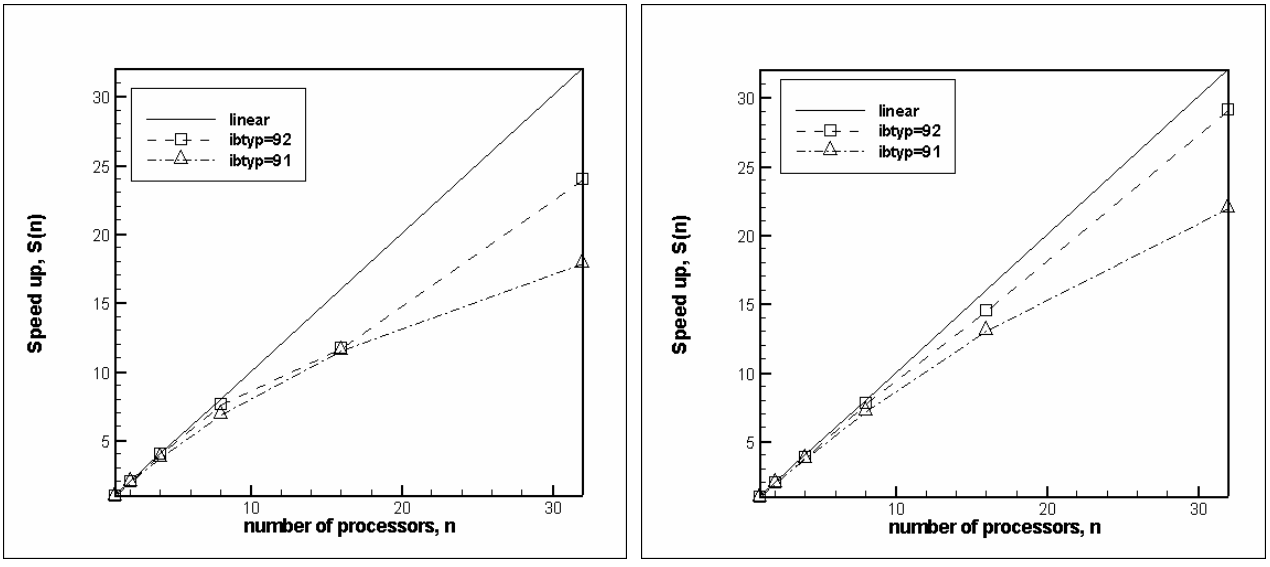

(a) CRAY T3E (b) SGI Origin 2000

Figure 19. Parallel speed-up: Wigley Hull.

Shared-memory fine-grain (i.e., loop level) parallelism is introduced using OpenMP which was designed to exploit certain characteristics of shared-memory architectures. Systems that don't fit the classic shared-memory architecture (e.g., Beowulf clusters) may use OpenMP but typical performance is very poor due to high latencies in communication. Currently, CFDSHIP-IOWA implementation of OpenMP is only supported on the SGI Origin and IBM SP machines through the use of the automatic parallelization option (-apo) in the Fortran 90 compiler. In particular, the SGI Origin uses a distributed-shared memory (DSM) architecture, which can effectively utilize the shared-memory model.

To demonstrate performance, parallel simulations were performed on the NAVO O2K using a surface-piercing flat plate (SPFP) with grid dimensions of 105x61x30 and with number of processors ranging from 1 to 32. Figure 20 shows that speedup stalls at about 4 for this problem on this machine. Analysis of cache utilization shows that the code is "non-cache friendly" for scalable shared-memory applications. While this is an area of work for the future, even a speed-up of 4 is useful for dynamic load balancing.

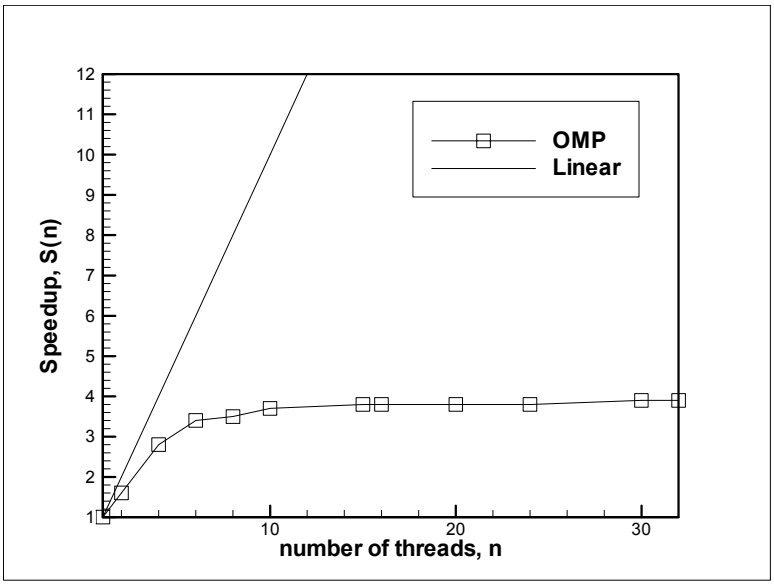

Figure 20. Parallel speedup, shared memory on NAVO O2K.

Mixed-mode, or multi-level, parallelism utilizes both MPI and OpenMP to achieve dynamic load balancing. Relative block size and the total number of processors specified by the

input variable `total_num_procs` sets the number of OpenMP threads that are used for each block,

$$num\_thrd = \max\left\{\text{int}\left(total\_num\_procs\frac{float(ntot)}{float(ntot\_sum)}\right),1\right\} \quad \textbf{(88)}$$

Table 8 shows an example for a 4-block grid system for an open-water propeller. The largest block is 8.5 times bigger than the smallest block and comprises 65% of the total number of grid points. The distribution of processors for `total_num_procs` = 16 and 32 are shown. Unfortunately, performance studies have not yet been undertaken for a simple single-block grid such as the SPFP or the Wigley Hull. However, based upon the OpenMP results, it should be expected that using 10 or 20 processors on Block 4 may be inefficient and that domain decomposition should be used to bring it's sub-blocks closer to the size of blocks 1-3.

Table 8. Dynamic load balancing for 4-block grid system.

block	*block_size (ntot)*	*num_thrd total_num_procs = 16*	*num_thrd total_num_procs = 32*
1	102951	2	4
2	102951	2	4
3	56203	1	2
4	480751	10	20
	ntot_sum = 742856	Total procs used = 15	Total procs used = 30

5.3 Portability

The code was designed to be portable across the range of machines currently available at the DOD High-Performance Computing Modernization Program (HPCMP) centers. Currently this includes the SGI Origin 2000 & Origin 3000, Cray T3E, Cray SV1, Cray T90, and IBM SP2. In addition, the code has been compiled on the DEC Alpha, HP Workstation, and Intel X86 personal computers, the latter of which uses Compaq Visual Fortran.

Portability is achieved through the use of MPI, the C preprocessor CPP, and the UNIX make utility. Vendor-optimized MPI is available on nearly all platforms. Otherwise, the generic MPICH libraries can be used. `CPP` is used to build either the parallel or serial versions from a single source code. MPI- and serial-specific code is isolated through the use of

'#IFDEF SERIAL', '#IFDEF PARALLEL', and '#ENDIF' CPP directives. Although not typically required, the source code for either version can be readily obtained by simply running CPP with the appropriate directives (i.e., -DSERIAL or –DPARALLEL). In addition, directives are used to set MPI data types to MPI_REAL for all machines except for the CRAY T3E, which requires MPI_DOUBLE_PRECISION. The code is written in FORTRAN and compiles with Fortran 90. The makefile will build platform specific versions by invoking the correct compiler options and the CPP directives. The machines and options available are shown in Table 9.

Table 9. Supported platforms and make options.

Machine	*make argument (Serial/Parallel)*
SGI Origin 2000	O2K/O2K_MPI
SGI Power Challenge Array	PCA/PCA_MPI
CRAY T3E	T3E/T3E_MPI
CRAY T90	T90/NA
DEC Alpha	DEC/DEC_MPI
HP workstation	HP/NA
Intel X86 Processor	None (Visual Fortran)
Beowulf Cluster (Portland Group Compiler)	CLUSTER/CLUSTER_MPI

5.4 Code distribution, extraction, compilation and execution

CFDSHIP-IOWA source code is distributed as a compressed tar file, which can be uncompressed and extracted using the following UNIX command,

```
%tar –xvf | uncompress cfdship.tar.Z
```

The following files are included in the distribution

filename	*Description*
readme	Description of files
makefile	UNIX makefile
cfdship_mods.F90	Definition of Fortran modules
cfdship_chimera.F90	Interface with PEGASUS
cfdship_bcs.f	Boundary conditions
cfdship_frsf.f	Free surface
cfdship_ke.F	Discretization/solution of k-ε turbulence model

cfdship_ko.F	Discretization/solution of k-ω turbulence model
cfdship_main.F	Main program
cfdship_mom.f	Discretization/solution of momentum equation
cfdship_mpsr.F	Multi-processor versions of subroutines
cfdship_pres.f	Discretization/solution of pressure equation
cfdship_ship.f	Propeller body force, forces and moments
cfdship_stio.F	Setup and input/output routines
cfdship_turb.F	Turbulence closure
cfdship_util.f	Solvers, interpolation routines,utilities
Tools/convert_chimera.F90	Converts XINTOUT file to either ASCII or unformatted format
Tools/decomp.f	Partitions grid into sub-blocks for parallel computing
Tools/grd-atob.f90	Converts grid file from ASCII to unformatted format
Tools/grid-btoa.f90	Converts grid file from unformatted to ASCII format
Tools/grid-restrict.f	Creates coarse and medium grids given fine grid
Tools/inlet-rst.f	Creates restart file given inlet profile
Tools/prolong.f	Interpolates coarse-grid solution onto medium and fine grids and creates restart files
Tools/redist.f90	Changes distribution of grid points
Tools/slicer.f90	Extracts subset of data from restart file
Tools/xyz-to-xrt.f	Convert grid from Cartesian to cylindrical coordinates

The file extension indicates the presence of CPP statements (i.e., .F or .F90) and whether the code is written in fixed (i.e., .f or .F) or free-formats (i.e., .f90 or .F90).

After uncompressing and extracting all files, the flow code is compiled using the makefile along with machine specific option listed in Table 9. For example, to compile the flow code on the SGI Origin 2000 with MPI parallelism, the following should be typed

%make O2K_MPI

Execution is platform dependent and requires site-specific preparation of job scripts and queue submission. However, serial jobs are executed with the following command,

%cfd_ship >standard_output_file

whereas parallel jobs are executed using the mpirun command

%mpirun –np 12 cfd_ship >standard_output_file

In either mode, the code automatically looks for the NAMELIST input file `cfd_ship.nml`, preparation and contents of which are described in the next section.

6. CREATING INPUT FILES AND POST-PROCESSING

The fourth and sixth steps of the CFD Process, as defined in Section 2, are focused on creating input files and post-processing of simulation results, respectively. While these steps are common to all CFD codes, the mechanics of undertaking these tasks are usually unique and can potentially represent a significant amount of time in the overall CFD Process. Because of this, an overall framework and graphical user interface, most notably in commercial codes, is often utilized to simplify the process and hide low-level details from user. Another approach is to use scripting languages to automate repetitive tasks like grid generation and setting of parameters. In recognition of the challenge this presents to small groups developing research codes, there are current efforts sponsored by HPCMP CHSSI to develop extensible frameworks for managing input file creation, file formats, and communication between tools. Unfortunately, until such software is available to the CFD community, users of CFDSHIP-IOWA will be required to have first hand knowledge of how to create and manipulate data files.

6.1 Input files

CFDSHIP-IOWA reads 5 different input files to provide data for computational grid, initial conditions, boundary conditions, flow conditions, selection of models, and specification of numerical parameters and post-processing variables. Table 10 summarizes the filenames, Fortran unit numbers, and descriptions of the input files. Detailed presentation of the file format is provided in Appendix A. Here, the purpose of, and the method for creating, each file is described.

Table 10. Input files

Filename	*Unit Number*	*Description*
cfd_ship.nml (fixed filename)	8	Namelist input for runtime variables
grid file (no filename restrictions)	15	Grid file in ASCII Plot3D format
FNAMEO.bcs	25	Boundary condition data
FNAMEO.xintout	45	Chimera interpolation coefficients
FNAMEI.rsto	35	Restart file from previous simulation

The master control file for CFDSHIP-IOWA is named `cfd_ship.nml`. Its purpose is to specify initial conditions, flow conditions, selection of models, and specification of numerical parameters and post-processing variables. All input parameters belong to one of nine namelists (`control, flow_parameters, grid parameters, iteration, solver, turbulence, free_surface, propeller, filenames`). A namelist is a list of variable names that are always read or written as a group. Namelist input provides a convenient interface for a research CFD code since default values can be set for most variables, and new variables can be added in future versions without making previous input files obsolete. In general, `cfd_ship.nml` is created by copying an existing file and modifying variables using a text editor as required. Detailed description of the namelists, variables, and default values are included in Appendix A.2 and an example can be found in Appendix B.1.

The grid file contains *(x, y, z)* or *(x, r, θ)* coordinates of the structured-grid multi-block system. Note that for Cartesian and cylindrical-polar grids, the `icoord` variable in namelist CONTROL must be set to (1/2) or (3/4), respectively. The grid file format is ASCII Plot3D, the details of which are specified in Appendix A.1. Method for generating grid file is at the discretion of the user.

The boundary condition file specifies boundary condition types on all faces, which may be arbitrarily broken into rectangular sub-patches, of the computational domain, including multi-block interfaces. For each patch, the following information must be specified in the ***FNAMEI.bcs*** input file: `ibtyp` is the boundary condition type, `ibdir` is the inward pointing normal direction in computation coordinate direction (+1/-1, +2/-2, or +3/-3), `ibcs, ibce, jbcs, jbce, kbcs, kbce` are the starting and ending indices in the (ξ,η,ζ) coordinates directions, `ibcord` is a flag used to set the discretization order-of-accuracy for Neumann boundary conditions, i.e., `ibcord`=0 for first order and 1 for second order, and `ifsfilter` is

a flag which is only used for free-surface boundaries and sets the filter type as described in Section 4.4. For multi-block and periodic conditions, the following additional information is required: `ndmesh` is the donor block number, `idbdir` is the inward-pointing normal in the donor block, and `idcs, idce, jdcs, jdce, kdcs, kdce` are the starting and ending indices for the donor block. Detailed description of the file format is provided in Appendix A.3 and an example is provided in Appendix B.3. The recommended procedure for setting boundary conditions and creating ***`FNAMEI.bcs`*** is to use GRIDGEN software from Pointwise, Inc. wherein CFDSHIP-IOWA is one of the supported analysis software options (AS/W). This allows use of the GRIDGEN graphical user interface which greatly reduces time and errors.

The final two input files are optional. Restart files are only required if initial conditions, or prescribed boundary conditions (`ibtyp=14`), are set by previous simulations. If a restart file is to be read, the variable `mode` in NAMELIST CONTROL must be set to 1. Restart file is typically created by previous simulation, however, users can write custom software similar to the provided tool `inlet-rst.f` which can write a restart file for specifying an inlet profile. The file containing Chimera overset grid interpolation coefficients is required only when using overset grids. This file is created following flowchart depicted in Figure 13.

6.2 Output files & post-processing

Output files provide access to the simulation results and can be used to assess iterative convergence, determine forces and moments, and analyze details of the flow field. As shown in Table 11, there are 8 output files that contain simulation results, however, the restart file is typically not used for post-processing. Four of the files are used for assessing iterative convergence. `FNAMEO.res` contains residuals, average divergence, and evaluation of mass and momentum balance over the computational domain, using the Reynolds-transport theorem, at each time step (or global iteration). `FNAMEO.forces` and `FNAMEO.moments` provide forces and moments acting on the no-slip surfaces at each time step and are useful for assessing iterative convergence of integral variables. Forces and moments are broken down into 9 components with contributions due to skin friction, piezometric pressure, and hydrostatic pressure in each of the 3 coordinate directions. `FNAMEO.conv` and `FNAMEO.fsconv` contain iterative convergence history of the point variables (U, P, U_τ) and free-surface wave

elevation ζ, respectively. Writing frequency is specified by the namelist variable `it_save_conv`, which is otherwise set to a default value of 500 time steps (or global iterations).

The remaining output file is the global solution file, which contains all independent and dependent flow variables. By default, the solution is written only on the last time step for steady flows or every 500 time steps for unsteady flows. If solutions are required more frequently, for example to construct animations, the namelist variable `it_save_tec` can be used to specify desired time-step frequency. This file is formatted as an ASCII Tecplot file and therefore is directly readable by the commercial visualization software Tecplot.

Table 11. Output files

Filename	*Unit Number*	*Description*
FNAMEO.rsto	16	Restart file
FNAMEO.tec	26	Global solution file in TECPLOT format
FNAMEO.res	36	Solution residuals
FNAMEO.conv	46	Iterative history of pressure, friction velocity, and velocity along no-slip surfaces
FNAMEO.forces	56	Iterative history of forces
FNAMEO.moments	57	Iterative history of moments
FNAMEO.fsconv	66	Iterative history of free surface
FNAMEO_bodyforces.tec	86	Grid, blanking variable indicating whether point is in/out of propeller disk, and body-force components.

7. RECOMMENDED VERIFICATION AND VALIDATION PROCEDURES

CFD is fast becoming an integral tool in the engineering design process as it is applied to increasing complex geometry and physics. As with use of experimental fluid dynamics (EFD) in making design decisions, assessment of quality of results is imperative, which has accelerated progress on development of verification and validation (V&V) methodology and procedures for estimating numerical and modeling errors and uncertainties in CFD simulations. However, in spite of the progress, the various viewpoints have not yet fully converged and current methodology and procedures are not yet standardized.

Here, however, the recommended V&V procedures are those provided by Stern et al. (2001) and for which Wilson et al. (2001) presented a detailed case study for a RANS simulation of an established benchmark for ship hydrodynamics. The methodology and procedures

presented therein provides a pragmatic approach for estimating simulation errors and uncertainties. The philosophy is strongly influenced by EFD uncertainty analysis. The approach allows for treatment of simulation errors as either stochastic or deterministic and properly takes into account uncertainties in both the simulation and the data in assessing the level of validation. A brief summary of the methodology and procedures is provided in the following.

7.1 Methodology

The simulation error δ_S is defined as the difference between a simulation result *S* and the truth *T* and is composed of modeling δ_{SM} and numerical δ_{SN} errors ($\delta_S = S - T = \delta_{SM} + \delta_{SN}$) with corresponding simulation uncertainty given by $U_S^2 = U_{SM}^2 + U_{SN}^2$. For certain conditions, both the sign and magnitude of the numerical error can be estimated as $\delta_{SN} = \delta_{SN}^* + \varepsilon_{SN}$ where δ_{SN}^* is an estimate of the sign and magnitude of δ_{SN} and ε_{SN} is the error in that estimate. The simulation value is corrected to provide a numerical benchmark S_C, which is defined by

$$S_C = S - \delta_{SN}^* \tag{89}$$

with error equation $\delta_{S_C} = S_C - T = \delta_{SM} + \varepsilon_{SN}$ and corresponding uncertainty equation $U_{S_C}^2 = U_{SM}^2 + U_{S_CN}^2$ where U_{S_C} is the uncertainty in the corrected simulation and U_{S_CN} is the uncertainty estimate for ε_{SN}.

Verification is defined as a process for assessing simulation numerical uncertainty U_{SN} and, when conditions permit, estimating the sign and magnitude δ_{SN}^* of the simulation numerical error itself and the uncertainty in that error estimate U_{S_CN}. Numerical error is decomposed into contributions from iteration number δ_I, grid size δ_G, time step δ_T, and other parameters δ_P, which gives the following expression for the simulation numerical uncertainty

$$U_{SN}^2 = U_I^2 + U_G^2 + U_T^2 + U_P^2 \tag{90}$$

For situations when the solution is corrected to produce a numerical benchmark S_C, the estimated simulation numerical error δ_{SN}^* and corrected uncertainty U_{S_CN} are given by

$$\delta_{SN}^* = \delta_I^* + \delta_G^* + \delta_T^* + \delta_P^* \tag{91}$$

$$U_{S_CN}^2 = U_{I_C}^2 + U_{G_C}^2 + U_{T_C}^2 + U_{P_C}^2 \tag{92}$$

Validation is defined as a process for assessing simulation modeling uncertainty U_{SM} by using benchmark experimental data and, when conditions permit, estimating the sign and magnitude of the modeling error δ_{SM} itself. The comparison error E is given by the difference in the data D and simulation S values

$$E = D - S = \delta_D - \left(\delta_{SMA} + \delta_{SPD} + \delta_{SN}\right) \tag{93}$$

where δ_{SM} has been decomposed into the sum of δ_{SPD}, error from the use of previous data such as fluid properties, and δ_{SMA}, error from modeling assumptions. To determine if validation has been achieved, E is compared to the validation uncertainty U_V given by

$$U_V^2 = U_D^2 + U_{SN}^2 + U_{SPD}^2 \tag{94}$$

If $|E| < U_V$, the combination of all the errors in D and S is smaller than U_V and validation is achieved at the U_V level. If $U_V << |E|$, the sign and magnitude of $E=\delta_{SMA}$ can be used to make modeling improvements. For the corrected approach, the equations equivalent to equations (93) and (94) are

$$E_C = D - S_C = \delta_D - (\delta_{SMA} + \delta_{SPD} + \varepsilon_{SN}) \tag{95}$$

$$U_{V_C}^2 = U_{E_C}^2 - U_{SMA}^2 = U_D^2 + U_{SPD}^2 + U_{S_C N}^2 \tag{96}$$

7.2 Procedures

The overall CFD V&V procedures can be conveniently grouped into four consecutive steps: preparation, verification, validation, and documentation.

Verification is accomplished through parameter convergence studies using multiple solutions (at least 3) with systematic parameter refinement by varying the k^{th} input parameter Δx_k while holding all other parameters constant. Iterative errors must be accurately estimated or negligible in comparison to errors due to input parameters before accurate convergence studies can be conducted. Changes between medium-fine $\varepsilon_{21_k} = \hat{S}_{k_2} - \hat{S}_{k_1}$ and coarse-medium $\varepsilon_{32_k} = \hat{S}_{k_3} - \hat{S}_{k_2}$ solutions are used to define the convergence ratio

$$R_k = \varepsilon_{21_k} / \varepsilon_{32_k} \tag{97}$$

and to determine convergence condition where $\hat{S}_{k_1}$, $\hat{S}_{k_2}$, $\hat{S}_{k_3}$ correspond to solutions with fine, medium, and coarse input parameter, respectively, corrected for iterative errors. Three convergence conditions are possible:

(*i*) Monotonic convergence: $0 < R_k < 1$

(*ii*) Oscillatory convergence: $R_k < 0$ **(98)**

(*iii*) Divergence: $R_k > 1$

For condition (*i*), generalized RE is used to estimate U_k or δ_k^* and U_{k_C}. For condition (*ii*), uncertainties are estimated simply by attempting to bound the error based on oscillation maximums S_U and minimums S_L, i.e., $U_k = \frac{1}{2}\left(S_U - S_L\right)$. For condition (*iii*), errors and uncertainties cannot be estimated.

For convergence condition (*i*), generalized RE is used to estimate the error $\delta^*_{RE_{k_1}}$ due to selection of the *kth* input parameter and order-of-accuracy p_k

$$\delta^*_{RE_{k_1}} = \frac{\varepsilon_{21_k}}{r_k^{p_k} - 1} \tag{99}$$

$$p_k = \frac{ln(\varepsilon_{32_k} / \varepsilon_{21_k})}{ln(r_k)} \tag{100}$$

Correction of equation (99) through a multiplication factor C_k accounts for effects of higher-order terms and provides a quantitative metric to determine proximity of the solutions to the asymptotic range

$$\delta^*_{k_1} = C_k \delta^*_{RE_{k_1}} = C_k \left(\frac{\varepsilon_{21_k}}{r_k^{p_k} - 1} \right) \tag{101}$$

where the correction factor is given by

$$C_k = \frac{r_k^{p_k} - 1}{r_k^{p_{k\,est}} - 1} \tag{102}$$

and $p_{k_{est}}$ is an estimate for the limiting order of accuracy as spacing size goes to zero and the asymptotic range is reached so that $C_k \to 1$. When solutions are far from the asymptotic range,

C_k is sufficiently less than or greater than 1, only the magnitude of the error is estimated through the uncertainty U_k

$$U_k = \left| C_k \delta^*_{RE_{k_1}} \right| + \left| (1 - C_k) \delta^*_{RE_{k_1}} \right| \tag{103}$$

When solutions are close to the asymptotic range, C_k is close to 1 so that δ^*_k is estimated using equation (101) and U_{k_C} is estimated by

$$U_{k_C} = \left| (1 - C_k) \delta^*_{RE_{k_1}} \right| \tag{104}$$

Alternatively, a factor of safety approach proposed in Roach (1998) can be used to define U_k and U_{k_C}.

Validation is accomplished through comparisons with benchmark EFD data, including experimental uncertainty estimates U_D. If the three variables U_V, $|E|$, and U_{reqd} (programmatic validation requirement) are considered, there are six combinations. For three cases, $|E|<U_V$ and validation is achieved at the U_V level, but for only one of these $U_V < U_{reqd}$ so that validation is also achieved at U_{reqd}. In these cases, attempting to estimate modeling errors δ_{SMA} is not feasible from an uncertainty standpoint. For the three other cases, $U_V < |E|$ and using the sign and magnitude of E to estimate δ_{SMA} is feasible from an uncertainty standpoint. In one of these cases, $U_V < |E| < U_{reqd}$ so that validation is successful at the $|E|$ level from a programmatic standpoint. Similar conclusions can be reached using the corrected comparison error and corrected validation uncertainty.

8. EXAMPLE SIMULATION: OPEN-WATER PROPELLER P5168

In this section, an example simulation for DTMB open-water propeller P5168 is presented and discussed. The intention is to demonstrate some of the capabilities of the code including overset gridding, non-inertial relative frames, and detailed high-fidelity resolution of both geometry and physics. Discussion follows the CFD process defined in Figure 1. Input files for both the example and other training problems, including some with free-surface effects, may be downloaded from the CFDSHIP-IOWA website, http://www.iihr.uiowa.edu/~cfdship.

8.1 Geometry, Benchmark Data, and Conditions

DTMB propeller model P5168, shown in Figure 22, is a five-bladed, controllable pitch propeller with a design advance ratio of J=1.27. Chesnakas and Jessup (2000) presented detailed velocity field LDV measurements, which were made in the NSWC-CD 36-inch water tunnel. Their study was undertaken as part of a joint project with the Royal Netherlands Navy and Marine Research Institute to develop propeller blade tip geometries that display improved tip-vortex cavitation characteristics. Due to the well-documented experiment, which includes data uncertainties, P5168 has become an international benchmark that has been extensively used for CFD validation. Relevant example is the work of Chen (2000) and Hsiao and Pauley (1999), both of whom used P5168 to undertake detailed study of propeller tip vortices and impact of grid resolution and non-linear turbulence closures. In this report, P5168 is used to demonstrate capability of CFDSHIP-IOWA v3.03 in simulating propulsor hydrodynamics including relative-frame formulation, near-wall turbulence models, and chimera-overset gridding.

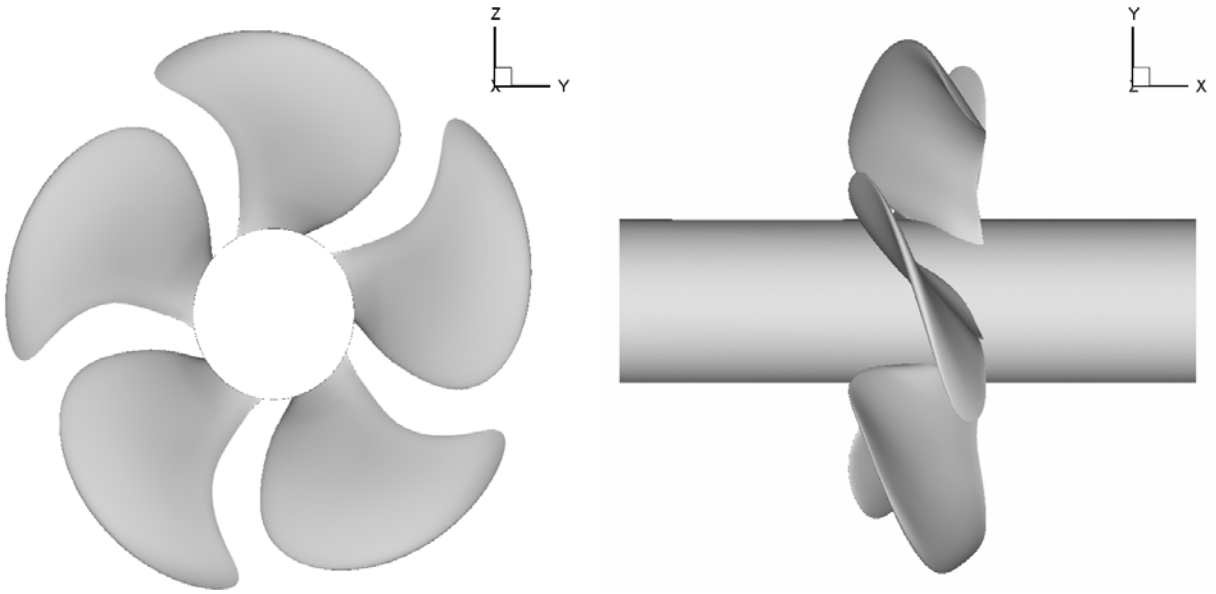

(a) View looking upstream (b) Side view

Figure 22. P5168 Geometry.

P5168 geometry is shown in Figure 22. It was obtained from NSWC-CD in the form of an IGES file. The simulated geometry uses an infinite shaft of constant radius whereas the

experimental geometry included a cylindrical fairwater that extended 96.8mm downstream of the hub. In addition, the tested geometry, as shown in Figure 1 of Chesnakas and Jessup (2000), had a small increase in hub radius near the propeller, a feature which is not included in the CFD model. Since the focus here is simulation at near-design operating conditions, it is assumed that the inflow is uniform in the circumferential direction and that the flow is steady. This allows the computational domain to be reduced to a single blade passage through the use of rotationally periodic boundary conditions. The overall domain, which was shown in Figure 2, extends 0.65D upstream, 1.5D downstream, and 1.5D outward in the radial direction.

The flow conditions and fluid properties are based upon the experimental conditions at J=1.1, which is slightly off the design point and is used since it results in a stronger tip vortex than J=1.27. This condition also corresponds to n=1450 rpm, U=10.70m/s, T=4715N, Q=481N-m. Non-dimensional parameters used in CFDSHIP-IOWA are Re=3.0x10^6 and ω_x=-2π/J=-5.712. Flow conditions are specified in the namelist input file, `cfd_ship.nml`. The file used for P5168 is included in the Appendix B.1 as an example.

For detailed propulsor simulations (as opposed to using a propeller body force), the only model choice is that of turbulence model. For the simulations here, the standard blended k-ω/k-ε turbulence model was used, i.e., `itm`=2, `itm_switch`=0.

Steady flow simulations use free-stream initial conditions where all flow variables are set to `UINF`=1 and `VINF=WINF`=0. This is achieved by setting `mode`=0 in the `cfd_ship.nml` file. As shown in Figure 2, the following boundary conditions were used for a single-blade propeller simulation: relative-frame no-slip (ibtyp=22) on the blade and hub surfaces, prescribed velocity (ibtyp=14) on the upstream inlet plane, exit (ibtyp=12) on the downstream exit plane, far-field (ibtyp=13) on the outer boundaries, and rotationally-periodic (ibtyp=52) on the periodic faces. The prescribed velocity profile is

$$U(r) = \sqrt{1 - \left[1 - \frac{r - r_h}{r_\delta - r_h}\right]^2} \qquad \textbf{(105)}$$

where r_h = 0.122199 is the hub radius and r_δ = 0.185 is the boundary layer thickness at the inlet plane. Inlet profile in equation (105) was determined by Chen (2000) to give proper loading at the blade root. Remaining block boundaries are either patched multi-block (ibtyp=92) or Chimera outer boundaries, the latter of which requires use of PEGASUS v5.1 from NASA Ames

and which will be further discussed in the next paragraph. An example boundary condition file is included in the Appendix B.3.

8.2 Computational Grids and Input Parameters

Generating high-quality patched-multi-block grids for open-water propellers is challenging due radial pitch distribution, especially beyond the tip, requirements for rotational periodicity, and need for boundary-layer resolution near blade and hub surfaces. Together, these issues make it difficult to control both skewness and expansion ratios. CFDSHIP-IOWA v3.03 is fairly sensitive to grid quality such that grids used in earlier versions (especially those based upon the Finite Analytic method) often result in unstable simulations.

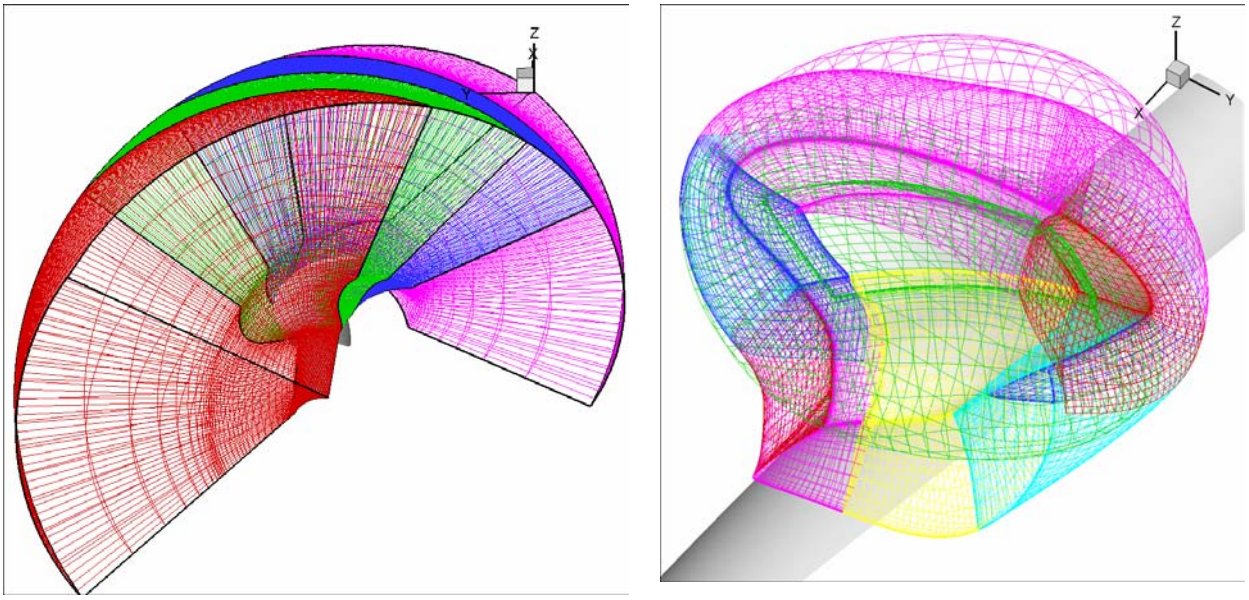

(a) Passage blocks (b) Blade blocks

Figure 23. P5168 Overset Grid System.

Although a best practices document for CFDSHIP-IOWA does not yet exist (e.g., a document similar to Chan et al., 2002), the following guidelines can be provided. As a rule of thumb, CFDSHIP-IOWA gives most accurate results using expansion ratios less than 1.5 and, in general, values greater than 3 should be avoided since simulation stability is sensitive to this parameter. At multi-block interfaces, spacing on each side of the interface should be similar. For boundary-layer resolution, near-wall spacing should be set such that the non-dimensional

wall coordinate $y^+ = u_\tau y/\nu$ is less than 2.5 and ideally near 1.0. Overset gridding provides an approach to achieve these metrics and obtain high-quality grids, especially for complex geometries.

The overset grid system used for P5168 is shown in Figure 23. This system is based upon a series of H-type "passage" blocks, which are generated without regard for the blade geometry, and O-type "blade" blocks, which are generated without regard for the periodic surfaces.

Table 11. P5168 Grid Parameters

		fine				**medium**				**coarse**			
Block #	**Name**	**imax**	**jmax**	**kmax**	**total**	**imax**	**jmax**	**kmax**	**total**	**imax**	**jmax**	**kmax**	**total**
1	passage1	61	81	81	400,221	43	58	58	144,652	31	41	41	52,111
2	passage2	61	81	81	400,221	43	58	58	144,652	31	41	41	52,111
3	passage3	61	81	81	400,221	43	58	58	144,652	31	41	41	52,111
4	passage4	61	81	81	400,221	43	58	58	144,652	31	41	41	52,111
5	inner_p	41	61	31	77,531	29	43	22	27,434	21	31	16	10,416
6	inner_s	41	61	31	77,531	29	43	22	27,434	21	31	16	10,416
7	tip_p1	45	61	31	85,095	32	43	22	30,272	23	31	16	11,408
8	tip_s1	45	61	31	85,095	32	43	22	30,272	23	31	16	11,408
9	tip_p2	45	61	31	85,095	32	43	22	30,272	23	31	16	11,408
10	tip_s2	45	61	31	85,095	32	43	22	30,272	23	31	16	11,408
11	tip_p3	41	61	45	112,545	29	43	32	39,904	21	31	23	14,973
12	tip_s3	41	61	45	112,545	29	43	32	39,904	21	31	23	14,973
13	root_p1	45	61	65	178,425	32	43	46	63,296	23	31	33	23,529
14	root_p2	41	61	65	162,565	29	43	46	57,362	21	31	33	21,483
15	root_p3	45	61	65	178,425	32	43	46	63,296	23	31	33	23,529
16	root_s1	45	61	65	178,425	32	43	46	63,296	23	31	33	23,529
17	root_s2	41	61	65	162,565	29	43	46	57,362	21	31	33	21,483
18	root_s3	45	61	65	178,425	32	43	46	63,296	23	31	33	23,529
19	*phantom*	*121*	*51*	*11*	*67,881*	*121*	*51*	*11*	*67,881*	*121*	*51*	*11*	*67,881*
				Total	3,360,246			Total	1,202,280			Total	441,936

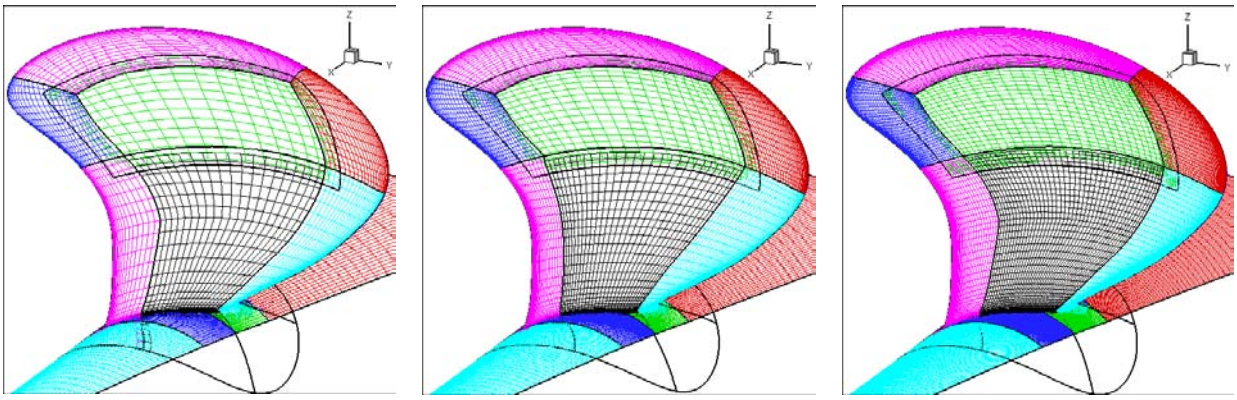

(a) coarse (b) medium (c) fine

Figure 24. Systematic grid refinement, surface meshes.

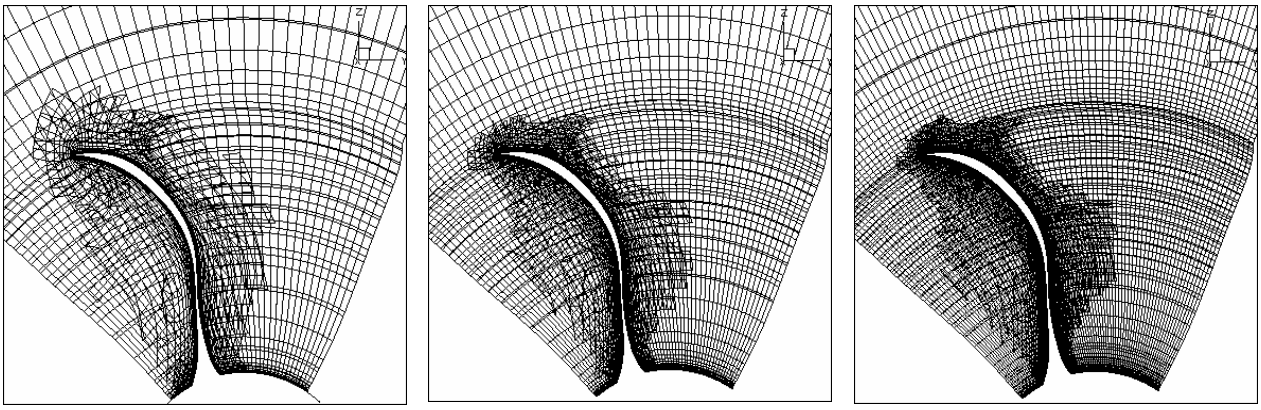

(a) coarse (b) medium (c) fine

Figure 25. Systematic grid refinement, cut at x/D=0.07.

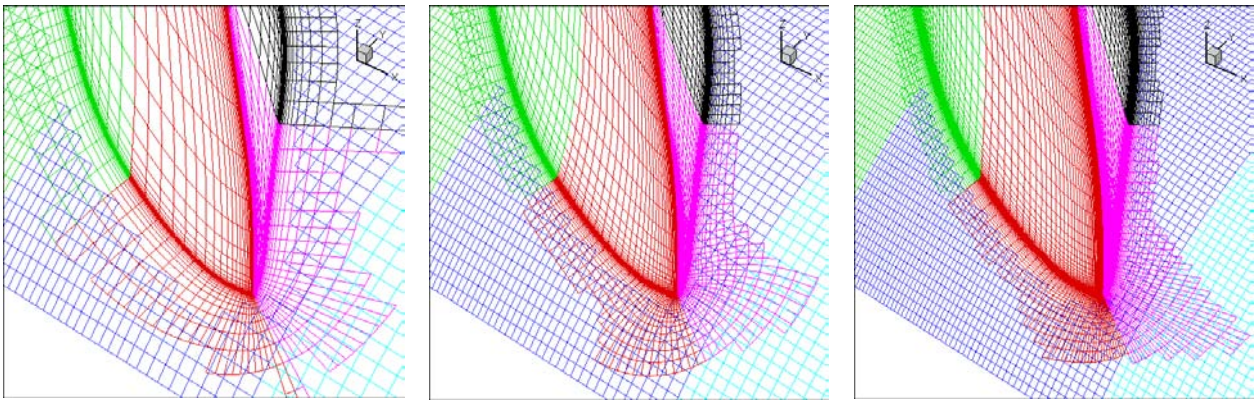

(a) coarse (b) medium (c) fine

Figure 26. Systematic grid refinement, overset-grid system at trailing-edge root.

This approach improves grid quality, as measured by orthogonality and expansion ratios, accelerates grid-generation process, and permits the use of overset refinement meshes (e.g., Kim et al., 2003). The grid system is generated using GRIDGEN from Pointwise, Inc. and was designed for a 3-grid verification study as shown in Table 11 and with near-wall spacing less than $5x10^{-6}$ on all grids. The fine grid was generated using GRIDGEN. The medium and coarse grids were obtained from the fine grid using a $\sqrt{2}$ refinement ratio in each coordinate direction. A grid-sequencing tool based upon linear interpolation in computational space is used. This results in a coarse grid, which is systematically similar to the fine grid due to the fact it is created through grid halving. In contrast, the medium grid is not exactly systematically similar to the fine grid due to handwork in GRIDGEN required to correct geometry errors introduced in using linear interpolation. Figure 24 shows the surface grids for each grid system. Total number of grid points range from 3.36 to 0.44 million points for the fine and coarse grids, respectively.

Before running CFDSHIP-IOWA, overset-grid interpolation coefficients must be computed using overset-grid communication software. Execution of PEGASUS version 5.1 is accomplished following the instructions in Section 4.7 of this report and using the sample input file found in Appendix B.2. Therein, it can be seen that a novel approach has been taken where two separate hole cutters ($HCUT NAME) have been defined. The first one is a traditional external-type HCUT named "blade_cutter." This HCUT creates a hole in the passage blocks due to the blade surfaces and uses a phantom mesh at the root of the blade so as to create the required "leak-free" surface. The second one is an internal-type hole cutter named "passage_cutter" whose purpose is to trim away points in the blade blocks that extend past the periodic surfaces. Figures 25 and 26 show the composite grid system for coarse, medium, and fine grids. Note that the fringe boundaries are a function of grid resolution. This is due to Level-2 interpolation. Impact on verification grid studies is unknown.

Numerical parameters are specified in the *cfd_ship.nml* file of which an example for P5168 can be found in the Appendix B.1. Therein, it can be seen that the following numerical parameters were specified: 2^{nd}-order upwind spatial accuracy (`ispat_order`=3); 1^{st}-order backward temporal accuracy, or steady flow (`itemp_order`=1); Cartesian relative-frame coordinate system (`icoord`=2); time step of `delt`=0.01, free stream velocities components of `uinf`=1 and `vinf=winf`=0; starting and ending iterations of `its`=1 and `itend`=10000;

iterative frequency of writing convergence history (`it_save_conv`), restart file (`it_save_rst`), and tecplot file (`it_save_tec`) of 50, 500, and 5000, respectively; number of momentum (`ituvw`), velocity-pressure coupling (`itvpc`), pressure (`itpr`), and turbulence (`itturb`) sub-iterations of 5, 3, 5, and 5, respectively; relaxation factors of `rfv`=0.2, `rfvb`=0.2, `rfp`=0.1, and `rfpb`=0.05; fully half-cell formulation of the pressure equation (`gama_pr`=1.0); line-solvers are turned on for each coordinate direction `iswp1`=1, `iswp2`=1, `iswp3`=1; pressure reference coordinate location is specified to be `mref`=1, `iref`=1, `jref`=41, `kref`=21; and convective discretization of the k and ω equations is set to 1st-order upwind (`ispat_order_tm`=1).

8.3 Computing Platforms

Simulations were undertaken using two computer systems, the 512-processor SGI Origin 3800 at the Army Research Laboratory Major-Shared Resource Center (ARL-MSRC, http://www.arl.hpc.mil/) and the 72-processor Linux Beowulf cluster at the Penn State Applied Research Laboratory. The former is a distributed-shared parallel computer, which is capable of using mixed-mode parallelism (i.e., code is compiled as `make O2K_MPI_OMP`) and the latter is a distributed parallel computer, which is capable of MPI parallelism only (i.e., code is compiled as `make CLUSTER_MPI`). As shown in Table 11, block-size distribution is not uniform, i.e., passage blocks are a factor of 5 larger than the smallest block. Therefore, on the SGI, some degree of load balancing was achieved through the use of OMP threads, which is an automatic process if `total_num_proc` is specified in the *`cfd_ship.nml`* file. Setting `total_num_proc` = 38, 4 OpenMP threads were used on the passage blocks, 1 thread on blocks 5-10, and 2 threads on the remaining blocks. The computational rate was 5.5×10^{-5} processor-secs/grid-point/iteration. For comparison, on the Linux cluster, where OMP threads cannot be used for load balancing, computational rate was 6.9×10^{-4} processor-secs/grid-point/iteration.

8.4 Verification and Validation Results

Typically, iterative convergence is assessed using both force and moment histories and residuals based upon the change in variable between iterations. However, in simulations with

overlapping surface grids, iterative history of forces and moments are not currently available due to the lack of a run-time interface with FOMOCO. As discussed in Section 4.8, FOMOCO, which is a part of the suite of Chimera Grid Tools, computes forces and moments on overlapping grids only as a post-processing step. Therefore, iterative convergence is demonstrated through the use of residuals. Coarse grid simulation was run for 15,000 iterations and shows 4 orders magnitude drop for all variables. A grid sequencing approach was used wherein coarse- and medium-grid solutions were used as medium- and fine-grid simulation initial conditions, respectively. Medium simulation was run 5000 iterations and fine simulation was run 1000 iterations. Based upon previous experience, it is assumed that U_I is approximately zero for all grids.

Table 12. P5168 Thrust and Torque Coefficients and Comparison to Data.

	EFD Data	Coarse	Medium	Fine
K_T	0.313	0.310	0.318	0.322
E%=(D-S)/D*100		1.0%	-1.6%	-2.9%
ε			0.008	0.004
$10K_Q$	0.783	0.765	0.793	0.805
E%=(D-S)/D*100		2.3%	-1.3%	-2.8%
ε			0.028	0.012

Comparing thrust and torque coefficients to EFD data and calculating changes between grids ε, as done in Table 12, it is shown that near-blade integral quantities display monotonic grid convergence as indicated by the convergence ratios of $R_G = 0.5$ and $R_G = 0.42$ for thrust and torque, respectively. Based upon the rules of Equation (99), grid uncertainty can be estimated using RE and is shown in Table 13. Since U_D is not available for K_T and K_Q, validation uncertainty U_V is not calculated.

Table 13. Verification of P5168 Thrust and Torque Coefficients.

	p_G	δ^*_{RE}	C_G	U_{GC}	U_I	U_{SN}
K_T	2.0	0.004	1.0	0.0	0.0	0.004
K_Q	2.4	0.015	1.29	0.0043	0.0	0.015

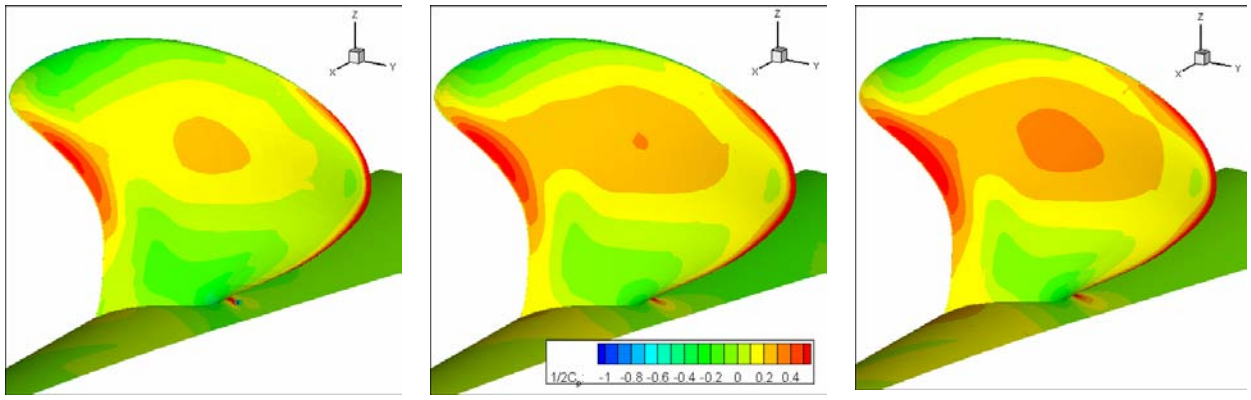

(a) coarse (b) medium (c) fine

Figure 27. Surface pressure on pressure side of blade.

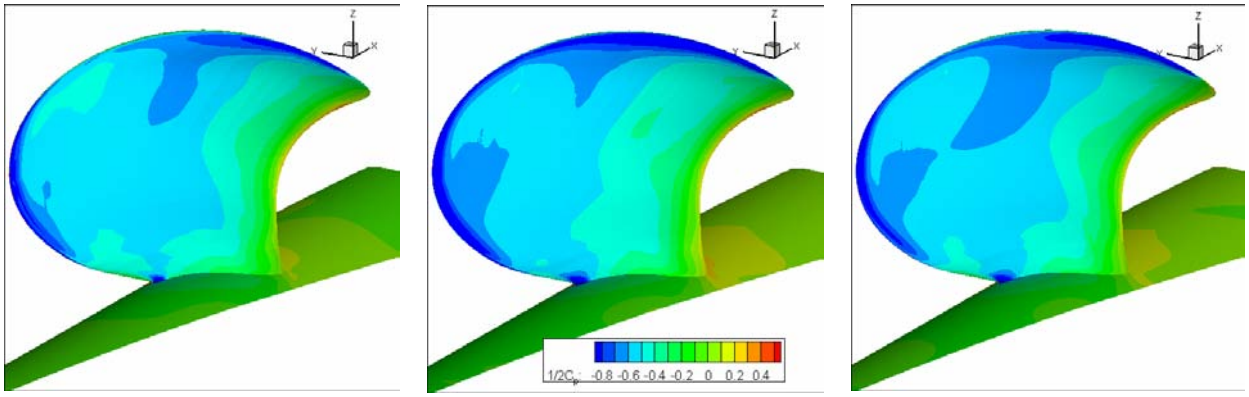

(a) coarse (b) medium (c) fine

Figure 28. Surface pressure on suction side of blade.

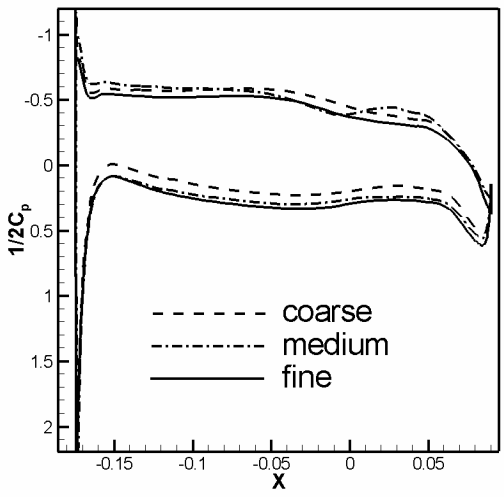

Figure 29. Comparison of surface pressure at r/R_p=0.716.

Surface pressure contours are shown, for each grid system, in Figures 27 and 28. In general, typical blade pressure distributions are shown with maximum loading at approximately ¾ span, high magnitude on the pressure-side leading- and trailing-edges, and low magnitude on the suction-side tip. Contours also display monotonic grid convergence with fine grid displaying highest resolution of detail. Figure 29 shows a comparison of surface pressure at r/R_p=0.716. Pressure-side of blade displays monotonic grid convergence whereas suction side displays more oscillatory behavior along the chord.

Figure 30 highlights the grid convergence of the tip and root vortices using iso-surfaces of intrinsic swirl parameter (Berdahl and Thompson, 1993) at level τ = 8.0 colored by normalized helicity $\bar{H} = \bar{\omega} \times \bar{U}$, the latter of which indicates direction of rotation. Counter-rotating root vortices display increasing strength, as indicated by increased persistence and organization in the downstream direction, with increasing grid resolution. Similar observation can be made for tip vortex, i.e., fine grid shows tip vortex with longest persistence, however, the very short persistence of the coarse grid suggests grid in tip-vortex region is not in the asymptotic range.

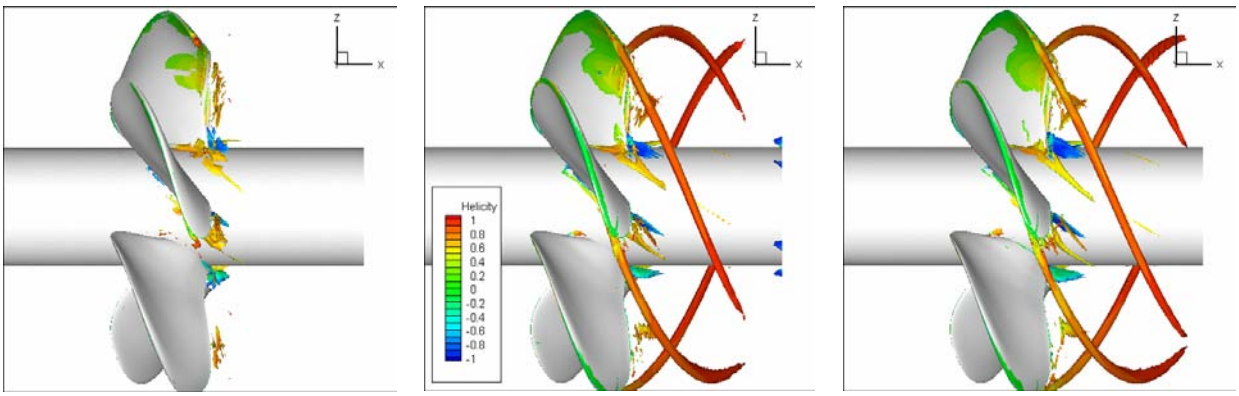

(a) coarse (b) medium (c) fine

Figure 30. Tip- and root-vortex visualization using iso-surface of intrinsic swirl parameter (τ = 8.0) colored by normalized helicity.

Figure 31 shows a comparison of simulation to data for axial-velocity contours at x/D=0.1193. In general, all three solutions show resolution of the global trends, i.e., thin blade wakes with increasing wake thickness near hub, maximum velocity on the suction side, and

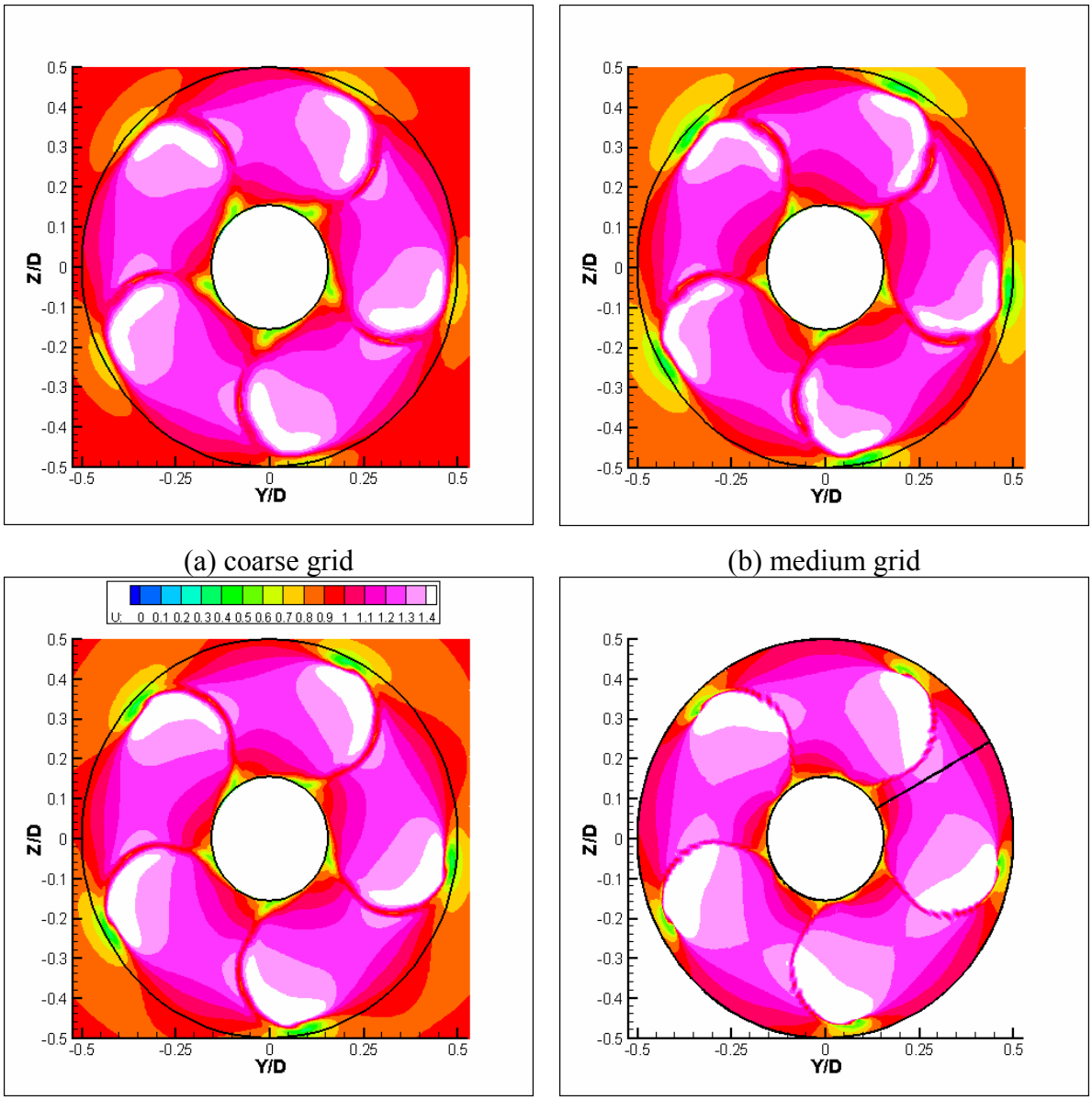

(a) coarse grid (b) medium grid

(c) fine grid (d) EFD data

Figure 31. Axial velocity contours at x/D=0.1193.

contours typical of a tip vortex at r/D=0.5. Moreover, resolution of blade wakes and tip-vortex show grid convergence in that a general trend of improved resolution with grid can be observed. However, detailed comparison of certain contour levels between the 3 solutions indicates some degree of oscillatory grid convergence. This is more clearly shown in Figure 32 which shows the axial velocity as a function of circumferential position at a constant radius of r/D = 0.465. This figure shows the blade-to-blade variability of the data. Overall, the 3 solutions display a non-monotonic divergent condition, which may be due to both a coarse grid solution outside of

the asymptotic range and grids which are not exactly systematically similar; observations supported by Figure 30 and previously discussed in section 8.2, respectively. However, medium and fine grids appear to be converging towards the data which suggests that a finer grid 4th solution at approximately 9.5 million grid points, which would be a very large grid for a single-blade simulation, would provide 3 solutions in the asymptotic range. This represents the principal challenge of RE based error estimation and points to the need for continued research and development in automatic generation of geometrically similar overset grids and interpolation coefficients, and single-grid error estimation techniques (e.g., Celik et al., 2003).

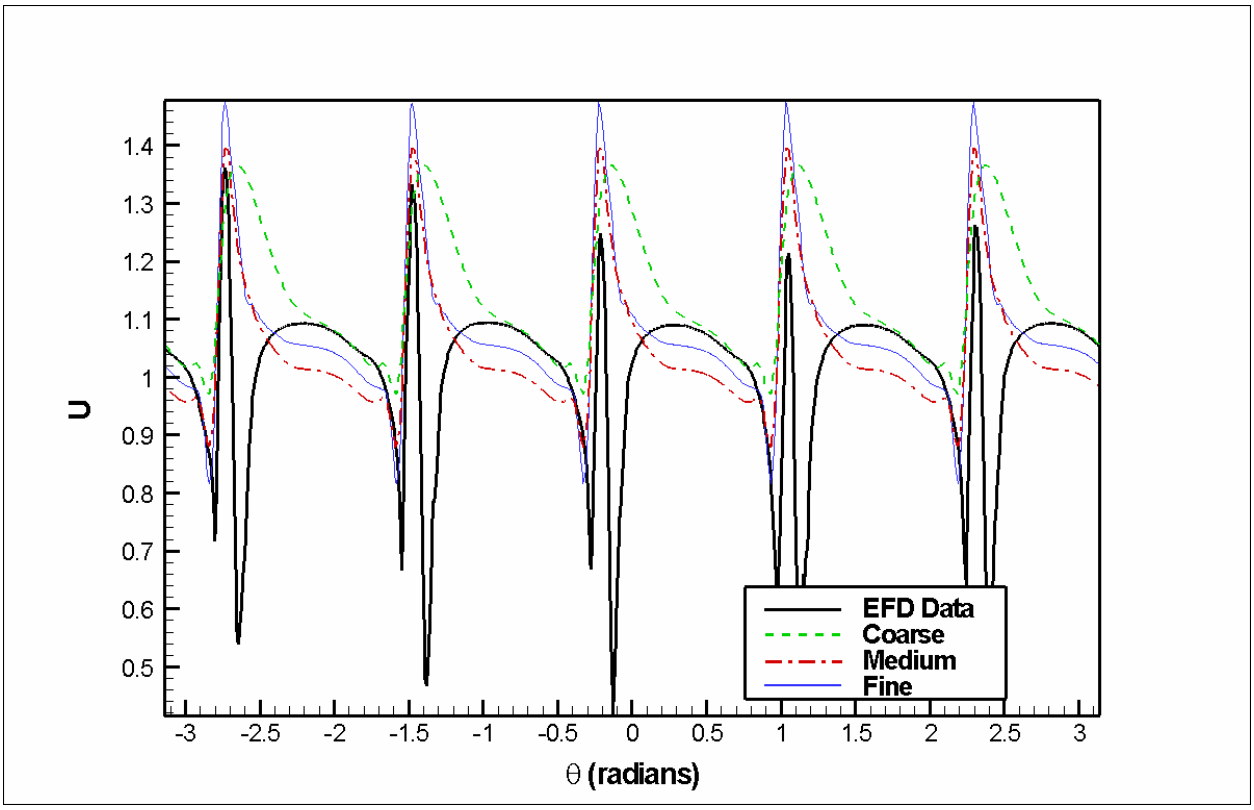

Figure 32. Comparison of circumferential distribution of axial velocity at r/D=0.465 and x/D=0.1193.

9. CONCLUDING REMARKS

CFDSHIP-IOWA is a general-purpose unsteady Reynolds-averaged Navier-Stokes CFD code that has been developed to handle a broad range of ship hydrodynamics problems. Purpose of this report was to provide: detailed documentation of the modeling, numerical methods, and code development; user instructions on creating input files and post-processing; recommended verification and validation procedures; and an example simulation. As a framework for achieving successful simulations, an approach based upon formulation of an initial boundary value problem and execution of a well-defined CFD process was developed and followed throughout the report. An example simulation, and other recent applications, demonstrates the capability of CFDSHIP-IOWA v3.03 to simulate practical ship hydrodynamics problems. Successful use in both thesis and project research and transition to other organizations demonstrates the success of the overall design objectives.

Largely due to successes such as those shown and referred to herein, role of CFD in analysis and design of future marine vehicles continues to expand. Beyond higher-fidelity simulation of resistance and propulsion problems, albeit including new applications and off-design conditions, it is anticipated that future simulations will move towards including environmental effects (e.g., seaway, stratification, shallow water), simulation-based design and optimization, resolving complex maneuvering scenarios of multiple-body configurations (e.g., submarine or surface-ship launch of adjunct vehicles), and supporting improved modeling of acoustic and non-acoustic signatures. However, in spite of continued advancements in HPC hardware, the magnitude of these problems are expected to be on the order of 20-50 million grid points and therefore require continued development of more accurate numerics and faster computing algorithms. Areas of future development include improved algebraic solvers, adaptive gridding, ideally using a single-grid error-estimation equation, implementation of geometry manipulation protocols for specification of vehicle configurations and maneuvering/seakeeping scenarios, multi-phase level-set methods for robust free-surface simulations, and hybrid RANS-LES models for numerous applications.

REFERENCES

Alessandrini B, Delhommeau G, Viscous Free Surface Flow past a Ship in Drift and in Rotating Motion, Proc. 22nd Sympo. on Naval Hydro., Washington, DC, 1998.

Beddhu, M., Jiang, M.Y., Taylor LK, and Whitfield DL, Computation of Steady and Unsteady Flows with a Free Surface Around the Wigley Hull, Applied Mathematics and Computation, Vol. 89, 1998, pp. 67-84.

Berdahl, C.H., and Thompson, D.S., "Eduction of Swirling Structure Using the Velocity Gradient Tensor," AIAA Journal, Vol. 31, No. 1, 1993.

Bush, R.H., Power, G.D., and Towne, C.E., "WIND: The Production Flow Solver of the NPARC Alliance," AIAA-98-0835, 36th Aerospace Sciences Meeting & Exhibit, Reno, NV, January 1998.

Celik, I., Hu, G., and Badeau, A., "Further Refinement and Benchmarking of a Single-Grid Error Estimation Technique," AIAA Paper 2003-0628, Reno, NV, 2003.

Chan, W.M., Gomez, R.J., Rogers, S.E., and Buning, P.G., "Best Practices in Overset Grid Generation," AIAA Paper 2002-3191, Proceedings 32nd AIAA Fluid Dynamics Conference, St. Louis, MO, 2002.

Chan, W. M. and Buning, P. G., User's Manual for FOMOCO Utilities - Force and Moment Computation Tools for Overset Grids, NASA TM 110408, July, 1996

Chen, B., "RANS Simulations of Tip Vortex Flows for a Finite-Span Hydrofoil and a Marine Propulsor," Ph.D. Thesis, The University of Iowa, 2000.

Chesnakas, C., and Jessup, J., "Experimental Characterization of Propeller Tip Flow," Proceedings 22nd Symposium on Naval Hydrodynamics, 2000.

Chima, R. V., "Swift - Multiblock Analysis Code for Turbomachinery, User's Manual and Documentation," Version 110, http://www.grc.nasa.gov/WWW/5810/webpage/rvc.htm June. 2001.

Di Mascio A, Campana EF, The Numerical Simulation of the Yaw Flow of a Free-Surface Ship, Proc. 7th International Conf. on Num. Ship Hydro., Nantes, France, 1999.

Dreyer, J.J., "Hydrodynamic Shape Optimization of Propulsor Configurations Using a Continuous Adjoint Formulation," Ph.D. Thesis, Department of Mechanical Engineering, The Pennsylvania State University, February 2002.

Gentaz, L, Guillerm, PE, Alessandrini, B, Delhommeau, G, Three-Dimensional Free Surface Viscous Flow around a Ship in Forced Motion, Proc. 7th International Conf. on Num. Ship Hydro., Nantes, France, 1999.

Gill, “Performance of the SST & BSL k-w Turbulence Models in the Prediction of the Flow Around a Surface Piercing Flat Plate with Stokes’ Waves External Flow,” Master Thesis, The University of Iowa, 2000.

Hall, E.J., Heidegger, N.J., and Delaney, R.A.: *ADPAC v1.0 - User's Manual*, NASA Contract NAS3-27394, CR-206600, February 1999.

Hirt, C.W., A.A. Amsden, and J.L. Cook, "An Arbitrary Lagrangian-Eulerian Computing Method for All Flow Speeds," J. Comp. Phys., Vol. 14, p. 227, 1974.

Hochbaum A.C. and Schumann, C., “Free-Surface Viscous Flow Around Ship Models,” Proc. 7th International Conf. on Num. Ship Hydro., Nantes, France, 1999.

Hough, G. and Ordway, D., “The generalized actuator disk,” Technical Report TAR-TR 6401, Therm Advanced Research, Inc., 1964.

Hyams, D.G., Sreenivas, K., Sheng, C., Nichols, S., Taylor, L.K., Briley, W.R., and Whitfield, D.L., "An Unstructured Multielement Solution Algorithm for Complex Geometry Hydrodynamic Simulations," *23rd Symposium on Naval Hydrodynamic*s, Val de Reuil, France, September 2000.

Hsiao, C. and Pauley, L.L., 1999, “Numerical Computation of Tip Vortex Flow Generated by a Marine Propeller,” ASME Journal of Fluids Engineering, Vol. 121, pp. 638-645.

Issa, R.I., 1985, “Solution of the Implicitly Discretized Fluid Flow Equations by Operator-Splitting,” J. Comp. Phys., Vol. 62, pp. 40-65.

Judge, C.Q., Oweis, G.F., Ceccio, S.L., Jessup, S.D., Chesnakas, C.J., and Fry, D.J., “Tip-Leakage Vortex Inception on a Ducted Rotor,” Cavitation 2001.

Kandysamy, M., “RANS Simulations of Free-Surface Wave-Induced Separation Around a Surface-Piercing NACA 0024 Hydrofoil,” Master Thesis, The University of Iowa, 2001.

Kim, K.H., “Unsteady RANS Simulation For Surface Ship Dynamics,” DoD High Performance Computing Modernization Program 2001 Users Group Conference, 18-21 June 2001, Biloxi, MS

Kim, J., Paterson, E., and Stern, F., "Sub-Visual Caviation and Acoustic Modeling for Ducted Marine Propulsor," 8th International Conference on Numerical Ship Hydrodynamics, Busan, Korea, September 2003.

Kodama, Y., Takeshi, H., Hinatsu, M., Hino, T., Uto, S., Hirata, N. Murashige, S., “Proceedings CFD Workshop Tokyo, Ship Research Institute, 1994.

Larreteguy, A.; Drew, D; Carrica, P.,and Bonetto, F.; “A Numerical Model for Three Dimensional Polydisperse Bubbly Flows around Surface Ships,” IV World Congress on Computational Mechanics, Buenos Aires, Argentina, June1998.

Larsson, L., Stern, F., Bertram, V. (eds.), Proceedings of Gothenburg 2000: A Workshop on Numerical Ship Hydrodynamics, Gothenburg, Sweden, 2000..

Lele, S.K., 1992, "Compact Finite Difference Schemes with Spectral-Like Resolution," *J. Comp. Phys.,* Vol. 103, pp. 16-42.

Meakin, R., "Adaptive Spatial Partitioning and Refinement for Overset Structured Grids," in Adaptive Methods for Compressible CFD, Special Issue of Computer Methods in Applied Mechanics and Engineering, North-Holland, 1999.

Menter, F.R., "Two-Equation Eddy Viscosity Turbulence Models for Engineering Applications," AIAA Journal, Vol. 32, No. 8., August 1994.

Ohmori T, Finite-Volume Simulation of Flows about a Ship in Maneuvering Motion, J. Marine Sci. and Technol., 1998; **3**(3)

Paterson, E.G., Kim, J., and Stern, F., "Unsteady RANS Simulation of an Integrated Marine Propulsor," Proceedings of the 7th International Conference on Numerical Ship Hydrodynamic, Nantes, France, July 1999.

Paterson, E.G., and Sinkovits, R.S., "Performance, Scalability, and Portability of a MPI-based version of CFDSHIP-IOWA: Results of a NAVO PET Tiger-Team Collaboration," Proceedings of the 9th Department of Defense High-Performance Computing Modernization Program Users Group Meeting, Monterey, CA, July 1999.

Paterson, E., Wilson, R., Stern, F., "CFDSHIP-IOWA and Steady Flow RANS Simulation of DTMB Model 5415," Proceedings of the 1st Marine CFD Applications Symposium, McClean, VA, May 1998.

Paterson, E.G., Hyman, M., Stern, F., Carrica, P., Bonetto, F., and Drew, D.,"Near- and Far-Field CFD for a Naval Combatant Including Thermal Stratification and Two-Fluid Modeling," Proceedings of the 21st Symposium on Naval Hydrodynamics, Trondheim, Norway, June, 1996.

Petersson, N.A., "An Algorithm for Assembling Overlapping Grid Systems," SIAM J. Sci. Comp., Vol. 20, No. 6, pp. 1995-2022, 1999.

Rhee, S.H., and Stern, F., "Unsteady RANS Method For Surface Ship Boundary Layer and Wake and Wave Field," Int. J. Num. Fluids, Vol. 37, pp. 445-478, 2001.

Rhie C.M. and Chow, W.L., 1983, "A Numerical Study of the Turbulent Flow Past an Isolated Airfoil with Trailing Edge Separation," *AIAA J.*, Vol. 21, pp. 1525-1532.

Rood, E.P., "Complementary RANS and LES Computations for DDG-51 and Transition to DD-21 Acquisition," Proceedings of the 9th Department of Defense High-Performance Computing Modernization Program Users Group Meeting, Monterey, CA, July 1999.

Rood, E.P., "Time-Domain Computational Ship Hydrodynamics: Features of the Flow Around the DDG-51", Proceedings of the DoD HPCMP Users' Group Meeting, Houston, 1998.

Rood, E.P., "Time-Domain Computational Ship Hydrodynamics", Proceedings of the DoD HPCMP Users' Group Meeting, San Diego, CA 1997.

Sato Y, Miyata H, Sato T, CFD Simulation of Three-Dimensional Motion of a Ship in Waves: Application to an Advancing Ship in Regular Heading Waves, J. Marine Sci. and Technol., 1999; **4**(4)

Simonsen, C. And Stern, F., "Flow Structure Around An Appended Tanker Hull Form In Simple Maneuvering Conditions," 8th International Conference On Numerical Ship Hydrodynamics, September 22-25, 2003, Busan, Korea.

Sotiropoulos, F. and Abdallah, S., "A Primitive Variable Method for the Solution of Three-Dimensional Incompressible Viscous Flows," J. Comp. Phys., Vol. 103, p.336, 1992.

Stern, F., Wilson, R.V., Coleman, H., and Paterson, E.G., "Comprehensive Approach to Verification and Validation of CFD Simulations," ASME Journal of Fluids Engineering, December 2001.

Stern, F., Paterson, E.G., and Tahara, Y., "CFDSHIP-IOWA: Computational Fluid Dynamics Method for Surface-Ship Boundary Layers, Wakes, and Wave Fields," IIHR Report #381, September 1996.

Suhs, N.E., Dietz, W.E., Rogers, S.E., Nash, S.M., and Onufer, J., T., "PEGASUS User's Guide, Version 5.1e," November 2000, http://www.nas.nasa.gov/~rogers/pegasus/uguide.html.

Suhs, N.E. and Tramel, R.W., "PEGSUS 4.0 User's Manual", AEDC-TR-91-8, November 1991.

Tahara Y, Longo J, Stern F, Himeno Y, Comparison of CFD and EFD for the Series 60 C_B=0.6 in Steady Yaw Motion, Proc. 22nd Sympo. on Naval Hydro., Washington, DC, 1998..

Tahara, Y., Paterson, E.G., Stern, F., and Himeno, Y., "Wave-Field Minimization of Surface Combatants using CFD-Based Optimization Methods," 23rd Symposium on Naval Hydrodynamics, Val de Reuil, France, September 2000.

Weymouth G., Wilson, R., And Stern, F., "RANS CFD Prediction of Pitch and Heave Ship Motions in Head Seas," 8th International Conference On Numerical Ship Hydrodynamics, September 22-25, 2003, Busan, Korea.

Wilson, R., Paterson, E., and Stern, F., "Unsteady RANS Simulation of Model 5415 in Waves," Proceedings of the 22nd Symposium on Naval Hydrodynamics, Washington D.C., August 1998.

Wilson, R., Paterson, E.G., and Stern, F., "Verification and Validation for Model 5415 Flow and Wave Fields," Gothenburg 2000 Workshop on CFD in Ship Hydrodynamics, Gothenburg, Sweden, September 2000.

Wilson, R.V., Stern, F., Coleman, H., and Paterson, E.G., "Results of Verification and Validation of a RANS Code Simulation for a Cargo/Container Ship," ASME Journal of Fluids Engineering, December 2001.

Wilson, R. And Stern, F., "Verification And Validation For RANS Simulation Of A Naval Surface Combatant," Standards For CFD In The Aerospace Industry, AIAA 2002-0904, Aerospace Sciences Meeting, Reno, Nevada, 14-17 January 2002.

Wilson, R.V. and F. Stern, "Unsteady RANS Simulation of a Surface Combatant With Roll Motion", Proceedings Of 24th Symposium On Naval Hydrodynamics, Fukuoka, Japan, July 8-13, 2002.

Yeung, R.W., Roddier, D., Alessandrini, B., Gentaz, L, and Liao, S.-W., "On Roll Hydrodynamics of Cylinders Fitted with Bilge Keels," Proceedings, 23rd Symposium on Naval Hydrodynamics, Val de Reuil, France, September 2000.

APPENDICES

APPENDIX A: FILE FORMATS

Detailed format description of input and output files are described in this appendix.

A.1 Grid File

The grid data is read by `subroutine get_grid` which is located in the `cfdship_stio.F` file. The file format is as follows.

```
read(15,*) nmesh
do m=1,nmesh
      read(15,*) imax(m), jmax(m), kmax(m)
enddo
do m=1,nmesh
      read(15,*) (((x(I,j,k),I=1,imax(m)),j=1,jmax(m),k=1,kmax(m)),  &
                 (((y(I,j,k),I=1,imax(m)),j=1,jmax(m),k=1,kmax(m)),  &
                 (((z(I,j,k),I=1,imax(m)),j=1,jmax(m),k=1,kmax(m))
enddo
```

A.2 Namelist Input File

There are 9 NAMELISTS in the code and each must appear in the input file, `cfd_ship.nml`. The file is opened and read in `subroutine input_runtime` and `subroutine input_grid_variables`, both of which are in the file `cfdship_mods.F90`

```
open(unit=8,file='cfd_ship.nml',status='old',action='read',iostat=ierror)
read(8,nml=control)
read(8,nml=flow_parameters)
read(8,nml=grid_parameters)
read(8,nml=iteration)
read(8,nml=solver)
read(8,nml=turbulence)
read(8,nml=free_surface)
read(8,nml=propeller)
read(8,nml=filenames)
close(8)
```

File format is shown in Appendix B.1, however, each NAMELIST, including function and variable name, description and default values, is described in the following.

`$CONTROL`

This input sets global values

Variable	*Description*	*Default*
`MODE`	Flag to set initial conditions (=0 for start from free-stream, =1 for start from restart file)	0
`TOTAL_NUM_PROCS`	Total number of processors used (only used for mixed-mode parallelism)	1
`ISPAT_ORDER`	Sets spatial order-of-accuracy of convective terms (see Table 4 for options)	3
`ITEMP_ORDER`	Sets temporal order of accuracy (see Table 3 for options)	1
`ICOORD`	Coordinate system flag • Cartesian, absolute frame, ICOORD=1 • Cartesian, relative frame, ICOORD=2 • Cylindrical, absolute frame, ICOORD=3 • Cylindrical, relative frame, ICOORD=4	1

`$FLOW_PARAMETERS`

This input sets flow parameters.

Variable	*Description*	*Default*
`RE`	Reynolds number	none
`FNUM`	Froude number	0.0
`DELT`	Time step	none
`TIME_RAMP_END`	Cubic polynomial ramp-up time of unsteady flow	2.0
`UINF`	Free-stream velocity component in x-direction	1.0
`VINF`	Free-stream velocity component in y (or r) direction	0.0
`WINF`	Free-stream velocity component in z (or θ) direction	0.0

`$GRID_PARAMETERS`

This input sets grid modification parameters. All variables, except for the ones that set the point about which moments are calculated, are arrays that can have a unique value for each block in the grid system.

Variable	*Description*	*Default*
`X_TRANSLATE`	Distance x-coordinate is translated. Value subtracted from initial grid	0.0
`Y_TRANSLATE`	Distance y-coordinate is translated. Value subtracted from initial grid	0.0
`Z_TRANSLATE`	Distance z-coordinate is translated. Value subtracted from initial grid	0.0

ALPHA	Rotation about z-axis	0.0
GAMA	Rotation about y-axis	0.0
BETA	Rotation about x-axis	0.0
SCALE_MESH	Multiplicative factor to scale grid	1.0
X_ROT_CENT	x-coordinate of rotation center	0.0
Y_ROT_CENT	y-coordinate of rotation center	0.0
Z_ROT_CENT	z-coordinate of rotation center	0.0
X_MOM_CENT	x-coordinate of point about which moments calculated	0.0
Y_MOM_CENT	y-coordinate of point about which moments calculated	0.0
Z_MOM_CENT	z-coordinate of point about which moments calculated	0.0
AGVX	Angular velocity about x-axis	0.0
AGVY	Angular velocity about y-axis	0.0
AGVZ	Angular velocity about z-axis	0.0

Note that the order of grid manipulation is 1) scale, 2) translate, and 3) rotate.

$ITERATION

This input controls iterative solvers, starting and ending time step, and convergence tolerances.

Variable	*Description*	*Default*
ITS	Starting time step (or global iteration)	1
ITEND	Ending time step (or global iteration)	None
IT_SAVE_TEC	Frequency for writing tecplot file	500
IT_SAVE_CONV	Frequency for saving convergence history	500
IT_SAVE_RST	Frequency for writing restart file	500
ITUVW	Number of sub-iterations for solution of momentum equation	5
ITVPC	Number of velocity-pressure coupling loops (i.e., PISO pressure correction steps)	2
ITPR	Number of sub-iterations for solution of pressure equation	5
ITTURB	Number of sub-iterations for solution of 2-equation turbulence model equations	5
TOL_UVW	Convergence tolerance for momentum equations (used only for unsteady flow)	1.0e-04
TOL_PR	Convergence tolerance for pressure equation (used only for unsteady flow)	1.0e-04

`$SOLVER`

This input sets the relaxation parameters, solver sweep directions, and the pressure-reference location for Fr=0 simulations.

Variable	*Description*	*Default*
`RFV`	Velocity relaxation factor, solver level	0.2
`RFVB`	Velocity relaxation factor, global level (=1.0 for unsteady flows)	0.2
`RFP`	Pressure relaxation factor, solver level	0.1
`RFPB`	Pressure relaxation factor, global level (=1.0 for unsteady flows)	0.1
`ISWP1,ISWP2,ISWP3`	Flag to set active directions (ξ,η,ζ coordinates) for line solver	0, 1, 0
`MREF,IREF,JREF,KREF`	Block # and (i,j,k) index for setting reference pressure location. For Fr=0, pressure at this point is 0.0	1, 1, 1, 1

`$TURBULENCE`

This input selects turbulence model and options.

Variable	*Description*	*Default*
`ITM`	Sets turbulence model. • Laminar flow, ITM=0 • Baldwin-Lomax model, ITM=1 • Blended *k-ω* model, ITM=2	0
`ITM_SWITCH`	Flag to set model options for Blended k-ω model • Standard model, ITM_SWITCH=0 • SST model, ITM_SWITCH=1 • Wilcox low-*Re* model, ITM_SWITCH=2	0
`ITM_SPAT_ORDER_TM`	Sets order-of-accuracy of 2-eqn turbulence model	`ISPAT_ORDER`

$FREE_SURFACE

This input sets parameters for free-surface solver and dynamic grid conforming process.

Variable	*Description*	*Default*
ITFSMAX	Number of free-surface iterations	5
TOL_FS	Convergence tolerance for free-surface solution (only used for unsteady simulations)	1.0e-04
WAVBLANK	Blanking distance for near-wall region of free-surface	0.0
IFS	Frequency, in global time steps, of free-surface solution	5
ICFM	Flag indicating whether grid is conformed to free surface or design waterline (z/L=0.0). ICFM=0, no conform; ICFM =1, conform turned on.	0

$PROPELLER

This input controls the prescribed body-force described in Section 2.5.

Variable	*Description*	*Default*
IPROP	number of propellers	0
CT	Thrust coefficient	0.0
CKQ	Torque coefficient	0.0
ADVANCE_COEF	Propeller advance coefficient	0.0
DXPROP	Propeller disk thickness	0.0
RP	Propeller radius	0.0
X_PROP_CENTER	*x*-coordinate of propeller center	0.0
Y_PROP_CENTER	*y*-coordinate of propeller center	0.0
Z_PROP_CENTER	*z*-coordinate of propeller center	0.0
RH	Propeller hub radius (in decimal % of RP)	0.0
SHAFTALPHA	Angle of propeller shaft with *x*-coordinate	0.0

$FILENAMES

This input sets the filename extensions.

Variable	*Description*	*Default*
FGRID	Variable which sets filename for grid file	None
FNAMEI	Variable which sets “previous_simulation” filename prefix	None
FNAMEO	Variable which sets “current_simulation” filename prefix	None

A.3 Boundary Condition File

The boundary condition data is read by `subroutine input_bcs` which is located in the `cfdship_stio.F` file. The detailed file format is as follows.

```
do i=1,nmesh
   read (iunit,*) nbc(i)
   do n=1,nbc(i)
      read (iunit,*) ibtyp(n,i)
      read (iunit,*) ibdir(n,i)
      read (iunit,*) ibcs(n,i),ibce(n,i)
      read (iunit,*) jbcs(n,i),jbce(n,i)
      read (iunit,*) kbcs(n,i),kbce(n,i)
      read (iunit,*) ibcord(n,i)
      if(ibtyp(n,i).eq.30) read (iunit,*) ifsfilter(n,i)
      if(ibtyp(n,i).eq.91.or.ibtyp(n,i).eq.92.or.   &
         ibtyp(n,i).eq.41.or.ibtyp(n,i).eq.42.or.   &
         ibtyp(n,i).eq.51.or.ibtyp(n,I).eq.52) then
         read (iunit,*) ndmesh(n,i)
         read (iunit,*) idbdir(n,i)
         read (iunit,*) idcs(n,i),idce(n,i)
         read (iunit,*) jdcs(n,i),jdce(n,i)
         read (iunit,*) kdcs(n,i),kdce(n,i)
      endif
   enddo
enddo
```

A.4 Overset Interpolation Coefficient File

The boundary condition data is read by `subroutine get_chimera` which is located in the `cfdship_chimera.F90` file. The detailed file format is as follows.

```
do m=1,nmesh
   read(199) ibpnts(m),iipnts(m),iieptr(m),iisptr(m), &
      imax_peg(m),jmax_peg(m),kmax_peg(m)
   read(199) (ii(i),i=iisptr(m),iieptr(m)), &
      (ji(i),i=iisptr(m),iieptr(m)), &
      (ki(i),i=iisptr(m),iieptr(m)), &
      (dxint_peg(i),i=iisptr(m),iieptr(m)), &
      (dyint_peg(i),i=iisptr(m),iieptr(m)), &
      (dzint_peg(i),i=iisptr(m),iieptr(m))
   read(199) (ib(i),i=ibsptr(m),ibeptr(m)), &
      (jb(i),i=ibsptr(m),ibeptr(m)), &
      (kb(i),i=ibsptr(m),ibeptr(m)), &
      (ibc(i),i=ibsptr(m),ibeptr(m))
   read(199) (iblank_peg(i),i=first(m),last(m))
enddo
```

A.5 Global Solution File

The global solution file is written by `subroutine save_tec` which is located in the `cfdship_stio.F` file. The detailed file format is as follows.

```
    write(26,10)
    write(26,20)
    do m=1,nmesh
       write(26,30) imax(m),jmax(m),kmax(m)
       write(26,40) (((x(i,j,k,m),i=1,imax(m)),j=1,jmax(m)),k=1,kmax(m))
       write(26,40) (((y(i,j,k,m),i=1,imax(m)),j=1,jmax(m)),k=1,kmax(m))
       write(26,40) (((z(i,j,k,m),i=1,imax(m)),j=1,jmax(m)),k=1,kmax(m))
       write(26,40) (((u(i,j,k,m),i=1,imax(m)),j=1,jmax(m)),k=1,kmax(m))
       write(26,40) (((v(i,j,k,m),i=1,imax(m)),j=1,jmax(m)),k=1,kmax(m))
       write(26,40) (((w(i,j,k,m),i=1,imax(m)),j=1,jmax(m)),k=1,kmax(m))
       write(26,40) (((pr(i,j,k,m),i=1,imax(m)),j=1,jmax(m)),k=1,kmax(m))
       write(26,40) (((zut(i,j,k,m),i=1,imax(m)),j=1,jmax(m)),k=1,kmax(m))
       write(26,40) (((yplus(i,j,k,m),i=1,imax(m)),j=1,jmax(m)),k=1,kmax(m))
       write(26,40) (((uplus(i,j,k,m),i=1,imax(m)),j=1,jmax(m)),k=1,kmax(m))
       write(26,41) (((iblank(i,j,k,m),i=1,imax(m)),j=1,jmax(m)),k=1,kmax(m))
       write(26,40) (((ak(i,j,k,m),i=1,imax(m)),j=1,jmax(m)),k=1,kmax(m))
       write(26,40) (((ao(i,j,k,m),i=1,imax(m)),j=1,jmax(m)),k=1,kmax(m))
    enddo

    10 format('TITLE = "TITLE STRING"')
    20 format('VARIABLES = X, Y, Z, U, V, W, P, ZUT, YPLUS, UPLUS, IBLANK',',
K, OMEGA')
    30 format('ZONE I =',I3,', J=',I3,', K=',I3,', F=BLOCK')
    40 format(6e14.6)
    41 format(30i4)
```

A.6 Restart File

The restart file is read by `subroutine get_restart` and is written by `subroutine save_restart`, both of which are located in the `cfdship_stio.F` file. The detailed file format is as follows.

```
    read(35) ntot_orig, nmesh
    do m=1,nmesh
       read(35) first_orig(m), last_orig(m), length_orig(m)
       read(35) imax_orig(m), jmax_orig(m), kmax_orig(m)
    enddo
    read(35) ((((x0(i,j,k,m),i=1,imax(m)),j=1,jmax(m)),k=1,kmax(m)),m=1,nmesh)
    read(35) ((((y0(i,j,k,m),i=1,imax(m)),j=1,jmax(m)),k=1,kmax(m)),m=1,nmesh)
    read(35) ((((z0(i,j,k,m),i=1,imax(m)),j=1,jmax(m)),k=1,kmax(m)),m=1,nmesh)
    read(35) ((((u0(i,j,k,m),i=1,imax(m)),j=1,jmax(m)),k=1,kmax(m)),m=1,nmesh)
    read(35) ((((v0(i,j,k,m),i=1,imax(m)),j=1,jmax(m)),k=1,kmax(m)),m=1,nmesh)
    read(35) ((((w0(i,j,k,m),i=1,imax(m)),j=1,jmax(m)),k=1,kmax(m)),m=1,nmesh)
    read(35) ((((pr0(i,j,k,m),i=1,imax(m)),j=1,jmax(m)),k=1,kmax(m)),m=1,nmesh)
    read(35) ((((zut0(i,j,k,m),i=1,imax(m)),j=1,jmax(m)),k=1,kmax(m)),m=1,nmesh)
```

```
    read(35) ((((ak0(i,j,k,m),i=1,imax(m)),j=1,jmax(m)),k=1,kmax(m)),m=1,nmesh)
    read(35) ((((ao0(i,j,k,m),i=1,imax(m)),j=1,jmax(m)),k=1,kmax(m)),m=1,nmesh)
    if(itemp_order.eq.2) then
       read(35) ((((x00(i,j,k,m),i=1,imax(m)),j=1,jmax(m)),k=1,kmax(m)),m=1,nmesh)
       read(35) ((((y00(i,j,k,m),i=1,imax(m)),j=1,jmax(m)),k=1,kmax(m)),m=1,nmesh)
       read(35) ((((z00(i,j,k,m),i=1,imax(m)),j=1,jmax(m)),k=1,kmax(m)),m=1,nmesh)
       read(35) ((((u00(i,j,k,m),i=1,imax(m)),j=1,jmax(m)),k=1,kmax(m)),m=1,nmesh)
       read(35) ((((v00(i,j,k,m),i=1,imax(m)),j=1,jmax(m)),k=1,kmax(m)),m=1,nmesh)
       read(35) ((((w00(i,j,k,m),i=1,imax(m)),j=1,jmax(m)),k=1,kmax(m)),m=1,nmesh)
       read(35) ((((ak00(i,j,k,m),i=1,imax(m)),j=1,jmax(m)),k=1,kmax(m)),m=1,nmesh)
       read(35) ((((ao00(i,j,k,m),i=1,imax(m)),j=1,jmax(m)),k=1,kmax(m)),m=1,nmesh)
    endif
```

APPENDIX B: SAMPLE INPUT FILES

B.1 CFDSHIP-IOWA Namelist Input File, "cfd_ship.nml"

```
$control
  mode            = 0
  total_num_procs = 24
  ispat_order     = 3
  itemp_order     = 1
  icoord          = 2
 $end

 $grid_parameters
  agvx = -5.712, -5.712, -5.712, -5.712, -5.712, -5.712,
            -5.712, -5.712, -5.712, -5.712, -5.712, -5.712,
            -5.712, -5.712, -5.712, -5.712, -5.712, -5.712,
            -5.712, -5.712, -5.712, -5.712, -5.712, -5.712,
 $end

 $flow_parameters
  re              = 3.0e6
  delt            = 0.01
  uinf            = 1.0
  vinf            = 0.0
  winf            = 0.0
 $end

 $iteration
  its             = 00001
  itend           = 10000
  it_save_conv    =   050
  it_save_rst     = 00500
  it_save_tec     = 05000
  ituvw           = 5
  itvpc           = 3
  itpr            = 5
  itturb          = 5
  tol_uvw         = 1.0e-4
  tol_pr          = 1.0e-4
 $end

 $solver
  rfv             = 0.2
  rfvb            = 0.2
  rfp             = 0.10
  rfpb            = 0.05
  gama_pr         = 1.0
  iswp1           = 1
  iswp2           = 1
```

```
 iswp3           = 1
 mref            = 1
 iref            = 1
 jref            = 41
 kref            = 21
$end

$turbulence
 itm             = 2
 itm_switch      = 0
 ispat_order_tm  = 1
$end

$free_surface
$end

$propeller
$end

$filenames
 fgrid           = "p5168_14b_c1.grd"
 fnamei          = "p5168_14b_c1"
 fnameo          = "p5168_14b_c1"
$end
```

B.2 PEGASUS v5.1 Namelist Input File, "peg.in"

```
$GLOBAL
   FRINGE  = 2,
   PROJECT =.T.,
   $END

 $MESH NAME =   'BLK-1', KINCLUDE=  2, -1, OFFSET=1, $END

 $MESH NAME =   'BLK-2', KINCLUDE=  2, -1, OFFSET=1,$END

 $MESH NAME =   'BLK-3', KINCLUDE=  2, -1, OFFSET=1,$END

 $MESH NAME =   'BLK-4', KINCLUDE=  2, -1, OFFSET=1,$END

 $MESH NAME =   'BLK-5', KINCLUDE=  2, -1, OFFSET=1,$END

 $MESH NAME =   'BLK-6', KINCLUDE=  2, -1, OFFSET=1,$END

 $MESH NAME =   'BLK-7', KINCLUDE=  2, -1, OFFSET=1,$END

 $MESH NAME =   'BLK-8', KINCLUDE=  2, -1, OFFSET=1,$END

 $MESH NAME =   'BLK-9', KINCLUDE=  2, -1, OFFSET=1,$END

 $MESH NAME =  'BLK-10', KINCLUDE=  2, -1, OFFSET=1,$END

 $MESH NAME =  'BLK-11', KINCLUDE=  2, -1, OFFSET=1,$END

 $MESH NAME =  'BLK-12', KINCLUDE=  2, -1, OFFSET=1,$END

 $MESH NAME =  'BLK-13', KINCLUDE=  2, -1, LINCLUDE=  2, -1, $END

 $MESH NAME =  'BLK-14', KINCLUDE=  2, -1, LINCLUDE=  2, -1, $END

 $MESH NAME =  'BLK-15', KINCLUDE=  2, -1, LINCLUDE=  2, -1, $END

 $MESH NAME =  'BLK-16', KINCLUDE=  2, -1, LINCLUDE=  2, -1, $END
```

```
$MESH NAME =  'BLK-17', KINCLUDE=  2, -1, LINCLUDE=  2, -1, $END

$MESH NAME =  'BLK-18', KINCLUDE=  2, -1, LINCLUDE=  2, -1, $END

$MESH NAME =  'BLK-19', KINCLUDE=  2, -1, PHANTOM=.T.,$END

$HCUT NAME = 'blade_cutter',
    INTERNAL=.F.,
    MEMBER = 'BLK-19',
             'BLK-5','BLK-6','BLK-7','BLK-8','BLK-9','BLK-10','BLK-11',
             'BLK-12','BLK-13','BLK-14','BLK-15','BLK-16','BLK-17','BLK-18',
    INCLUDE = 'BLK-1','BLK-2','BLK-3','BLK-4',
    CARTX=-81.6, 81.6,
    $END

$HCUT NAME = 'passage_cutter',
    INTERNAL=.T.,
    MEMBER = 'BLK-1','BLK-2','BLK-3','BLK-4',
    INCLUDE = 'BLK-5','BLK-6','BLK-7','BLK-8','BLK-9','BLK-10','BLK-11',
              'BLK-12','BLK-13','BLK-14','BLK-15','BLK-16','BLK-17','BLK-18',
    $END

$LEVEL2 EXCLUDE='BLK-1','BLK-2','BLK-3','BLK-4',
    $END

$BCINP ISPARTOF =   'BLK-1',
   IBTYP =     5,   40,    5,    5,    5,    5,
   IBDIR =     3,   -1,   -3,    2,    1,   -2,
   JBCS  =     1,   61,    1,    1,    1,    1,
   JBCE  =    61,   61,   61,   61,    1,   61,
   KBCS  =     1,    1,    1,    1,    1,   81,
   KBCE  =    81,   81,   81,    1,   81,   81,
   LBCS  =     1,    1,   81,    1,    1,    1,
   LBCE  =     1,   81,   81,   81,   81,   81,
   $END

$BCINP ISPARTOF =   'BLK-2',
   IBTYP =     5,    5,   40,    5,   40,    5,
   IBDIR =     2,    3,   -1,   -3,    1,   -2,
   JBCS  =     1,    1,   61,    1,    1,    1,
   JBCE  =    61,   61,   61,   61,    1,   61,
   KBCS  =     1,    1,    1,    1,    1,   81,
   KBCE  =     1,   81,   81,   81,   81,   81,
   LBCS  =     1,    1,    1,   81,    1,    1,
   LBCE  =    81,    1,   81,   81,   81,   81,
   $END

$BCINP ISPARTOF =   'BLK-3',
   IBTYP =     5,    5,    5,   40,   40,    5,
   IBDIR =     2,    3,   -3,   -1,    1,   -2,
   JBCS  =     1,    1,    1,   61,    1,    1,
   JBCE  =    61,   61,   61,   61,    1,   61,
   KBCS  =     1,    1,    1,    1,    1,   81,
   KBCE  =     1,   81,   81,   81,   81,   81,
   LBCS  =     1,    1,   81,    1,    1,    1,
   LBCE  =    81,    1,   81,   81,   81,   81,
   $END

$BCINP ISPARTOF =   'BLK-4',
   IBTYP =     5,    5,    5,   40,    5,    5,
   IBDIR =     2,   -1,    3,    1,   -3,   -2,
   JBCS  =     1,   61,    1,    1,    1,    1,
   JBCE  =    61,   61,   61,    1,   61,   61,
```

```
   KBCS  =     1,    1,    1,    1,    1,   81,
   KBCE  =     1,   81,   81,   81,   81,   81,
   LBCS  =     1,    1,    1,    1,   81,    1,
   LBCE  =    81,   81,    1,   81,   81,   81,
   $END

$BCINP ISPARTOF =   'BLK-5',
   IBTYP =     5,
   IBDIR =     2,
   JBCS  =     1,
   JBCE  =    41,
   KBCS  =     1,
   KBCE  =     1,
   LBCS  =     1,
   LBCE  =    31,
   $END

$BCINP ISPARTOF =   'BLK-6',
   IBTYP =     5,
   IBDIR =     2,
   JBCS  =     1,
   JBCE  =    41,
   KBCS  =     1,
   KBCE  =     1,
   LBCS  =     1,
   LBCE  =    31,
   $END

$BCINP ISPARTOF =   'BLK-7',
   IBTYP =     5,   40,   40,   40,
   IBDIR =     2,    1,    3,   -3,
   JBCS  =     1,    1,    1,    1,
   JBCE  =    45,    1,   45,   45,
   KBCS  =     1,    1,    1,    1,
   KBCE  =     1,   61,   61,   61,
   LBCS  =     1,    1,    1,   31,
   LBCE  =    31,   31,    1,   31,
   $END

$BCINP ISPARTOF =   'BLK-8',
   IBTYP =     5,   40,   40,   40,
   IBDIR =     2,   -1,    3,   -3,
   JBCS  =     1,   45,    1,    1,
   JBCE  =    45,   45,   45,   45,
   KBCS  =     1,    1,    1,    1,
   KBCE  =     1,   61,   61,   61,
   LBCS  =     1,    1,    1,   31,
   LBCE  =    31,   31,    1,   31,
   $END

$BCINP ISPARTOF =   'BLK-9',
   IBTYP =     5,   40,   40,   40,
   IBDIR =     2,   -1,   -3,    3,
   JBCS  =     1,   45,    1,    1,
   JBCE  =    45,   45,   45,   45,
   KBCS  =     1,    1,    1,    1,
   KBCE  =     1,   61,   61,   61,
   LBCS  =     1,    1,   31,    1,
   LBCE  =    31,   31,   31,    1,
   $END

$BCINP ISPARTOF =  'BLK-10',
   IBTYP =     5,   40,   40,   40,
   IBDIR =     2,    1,   -3,    3,
```

```
   JBCS  =     1,    1,    1,    1,
   JBCE  =    45,    1,   45,   45,
   KBCS  =     1,    1,    1,    1,
   KBCE  =     1,   61,   61,   61,
   LBCS  =     1,    1,   31,    1,
   LBCE  =    31,   31,   31,    1,
   $END

$BCINP ISPARTOF =  'BLK-11',
   IBTYP =     5,   40,   40,   40,   40,
   IBDIR =     2,   -3,   -3,    1,   -1,
   JBCS  =     1,    1,   25,    1,   41,
   JBCE  =    41,   25,   41,    1,   41,
   KBCS  =     1,    1,    1,    1,    1,
   KBCE  =     1,   61,   61,   61,   61,
   LBCS  =     1,   45,   45,    1,    1,
   LBCE  =    45,   45,   45,   45,   45,
   $END

$BCINP ISPARTOF =  'BLK-12',
   IBTYP =     5,   40,   40,   40,   40,
   IBDIR =     2,   -3,   -3,   -1,    1,
   JBCS  =     1,   17,    1,   41,    1,
   JBCE  =    41,   41,   17,   41,    1,
   KBCS  =     1,    1,    1,    1,    1,
   KBCE  =     1,   61,   61,   61,   61,
   LBCS  =     1,   45,   45,    1,    1,
   LBCE  =    45,   45,   45,   45,   45,
   $END

$BCINP ISPARTOF =  'BLK-13',
   IBTYP =     5,    5,   40,   40,   40,   40,
   IBDIR =     2,    2,   -1,   -3,    1,    3,
   JBCS  =     1,    1,   45,    1,    1,    1,
   JBCE  =    45,   45,   45,   45,    1,   45,
   KBCS  =     1,    1,    1,    1,    1,    1,
   KBCE  =     1,    1,   61,   61,   61,   61,
   LBCS  =    51,    1,    1,   65,    1,    1,
   LBCE  =    65,   51,   65,   65,   65,    1,
   $END

$BCINP ISPARTOF =  'BLK-14',
   IBTYP =     5,    5,   40,   40,   40,
   IBDIR =     2,    2,   -1,    1,    3,
   JBCS  =     1,    1,   41,    1,    1,
   JBCE  =    41,   41,   41,    1,   41,
   KBCS  =     1,    1,    1,    1,    1,
   KBCE  =     1,    1,   61,   61,   61,
   LBCS  =    51,    1,    1,    1,    1,
   LBCE  =    65,   51,   65,   65,    1,
   $END

$BCINP ISPARTOF =  'BLK-15',
   IBTYP =     5,    5,   40,   40,   40,   40,
   IBDIR =     2,    2,   -1,   -3,    1,    3,
   JBCS  =     1,    1,   45,    1,    1,    1,
   JBCE  =    45,   45,   45,   45,    1,   45,
   KBCS  =     1,    1,    1,    1,    1,    1,
   KBCE  =     1,    1,   61,   61,   61,   61,
   LBCS  =    51,    1,    1,   65,    1,    1,
   LBCE  =    65,   51,   65,   65,   65,    1,
   $END

$BCINP ISPARTOF =  'BLK-16',
```

```
   IBTYP =    40,    5,    5,   40,   40,   40,
   IBDIR =     3,    2,    2,    1,   -1,   -3,
   JBCS  =     1,    1,    1,    1,   45,    1,
   JBCE  =    45,   45,   45,    1,   45,   45,
   KBCS  =     1,    1,    1,    1,    1,    1,
   KBCE  =    61,    1,    1,   61,   61,   61,
   LBCS  =     1,   51,    1,    1,    1,   65,
   LBCE  =     1,   65,   51,   65,   65,   65,
   $END

$BCINP ISPARTOF =  'BLK-17',
   IBTYP =    40,    5,    5,   40,   40,
   IBDIR =     3,    2,    2,    1,   -1,
   JBCS  =     1,    1,    1,    1,   41,
   JBCE  =    41,   41,   41,    1,   41,
   KBCS  =     1,    1,    1,    1,    1,
   KBCE  =    61,    1,    1,   61,   61,
   LBCS  =     1,    1,   51,    1,    1,
   LBCE  =     1,   51,   65,   65,   65,
   $END

$BCINP ISPARTOF =  'BLK-18',
   IBTYP =    40,    5,    5,   40,   40,   40,
   IBDIR =     3,    2,    2,    1,   -1,   -3,
   JBCS  =     1,    1,    1,    1,   45,    1,
   JBCE  =    45,   45,   45,    1,   45,   45,
   KBCS  =     1,    1,    1,    1,    1,    1,
   KBCE  =    61,    1,    1,   61,   61,   61,
   LBCS  =     1,    1,   51,    1,    1,   65,
   LBCE  =     1,   51,   65,   65,   65,   65,
   $END

$BCINP ISPARTOF =  'BLK-19',
   IBTYP =     5,
   IBDIR =     2,
   JBCS  =     1,
   JBCE  =    -1,
   KBCS  =     1,
   KBCE  =     1,
   LBCS  =     1,
   LBCE  =    -1,
   $END
```

B.3 Boundary condition file

```
   6                ! number of boundary surfaces ===> BLK#-1
     52               !*** periodic MB #1= type #52
      3               ! coordinate direction normal to surface
      1   61          ! start, end in i-direction
      1   81          ! start, end in j-direction
      1    1          ! start, end in k-direction
      1               ! flag for order of first derivative bc
      1               ! donor mesh
     -3               ! coordinate direction normal to surface
      1   61          ! donor mesh start, end in i-direction
      1   81          ! donor mesh start, end in j-direction
     81   81          ! donor mesh start, end in k-direction
     92               !*** patched MB #2= type #92
     -1               ! coordinate direction normal to surface
     61   61          ! start, end in i-direction
      1   81          ! start, end in j-direction
      1   81          ! start, end in k-direction
      1               ! flag for order of first derivative bc
      2               ! donor mesh
```

```
 1              ! coordinate direction normal to surface
 1    1         ! donor mesh start, end in i-direction
 1   81         ! donor mesh start, end in j-direction
 1   81         ! donor mesh start, end in k-direction
52              !*** periodic MB #1= type #52
-3              ! coordinate direction normal to surface
 1   61         ! start, end in i-direction
 1   81         ! start, end in j-direction
81   81         ! start, end in k-direction
 1              ! flag for order of first derivative bc
 1              ! donor mesh
 3              ! coordinate direction normal to surface
 1   61         ! donor mesh start, end in i-direction
 1   81         ! donor mesh start, end in j-direction
 1    1         ! donor mesh start, end in k-direction
22              !*** Rel. Frame No-slip   = type #22
 2              ! coordinate direction normal to surface
 1   61         ! start, end in i-direction
 1    1         ! start, end in j-direction
 1   81         ! start, end in k-direction
 0              ! flag for order of first derivative bc
14              !*** Prescribed   = type #14
 1              ! coordinate direction normal to surface
 1    1         ! start, end in i-direction
 1   81         ! start, end in j-direction
 1   81         ! start, end in k-direction
 0              ! flag for order of first derivative bc
13              !*** Farfield (dp/dn=0)   = type #13
-2              ! coordinate direction normal to surface
 1   61         ! start, end in i-direction
81   81         ! start, end in j-direction
 1   81         ! start, end in k-direction
 0              ! flag for order of first derivative bc
 6              ! number of boundary surfaces ===> BLK#-2
22              !*** Rel. Frame No-slip   = type #22
 2              ! coordinate direction normal to surface
 1   61         ! start, end in i-direction
 1    1         ! start, end in j-direction
 1   81         ! start, end in k-direction
 0              ! flag for order of first derivative bc
41              !*** Periodic   = type #41
 3              ! coordinate direction normal to surface
 1   61         ! start, end in i-direction
 1   81         ! start, end in j-direction
 1    1         ! start, end in k-direction
 0              ! flag for order of first derivative bc
92              !*** patched MB #3= type #92
-1              ! coordinate direction normal to surface
61   61         ! start, end in i-direction
 1   81         ! start, end in j-direction
 1   81         ! start, end in k-direction
 1              ! flag for order of first derivative bc
 3              ! donor mesh
 1              ! coordinate direction normal to surface
 1    1         ! donor mesh start, end in i-direction
 1   81         ! donor mesh start, end in j-direction
 1   81         ! donor mesh start, end in k-direction
41              !*** Periodic   = type #41
-3              ! coordinate direction normal to surface
 1   61         ! start, end in i-direction
 1   81         ! start, end in j-direction
81   81         ! start, end in k-direction
 0              ! flag for order of first derivative bc
92              !*** patched MB #1= type #92
```

```
 1              ! coordinate direction normal to surface
 1    1         ! start, end in i-direction
 1   81         ! start, end in j-direction
 1   81         ! start, end in k-direction
 1              ! flag for order of first derivative bc
 1              ! donor mesh
-1              ! coordinate direction normal to surface
61   61         ! donor mesh start, end in i-direction
 1   81         ! donor mesh start, end in j-direction
 1   81         ! donor mesh start, end in k-direction
13              !*** Farfield (dp/dn=0)   = type #13
-2              ! coordinate direction normal to surface
 1   61         ! start, end in i-direction
81   81         ! start, end in j-direction
 1   81         ! start, end in k-direction
 0              ! flag for order of first derivative bc
 6              ! number of boundary surfaces ===> BLK#-3
22              !*** Rel. Frame No-slip   = type #22
 2              ! coordinate direction normal to surface
 1   61         ! start, end in i-direction
 1    1         ! start, end in j-direction
 1   81         ! start, end in k-direction
 0              ! flag for order of first derivative bc
52              !*** periodic MB #3= type #52
 3              ! coordinate direction normal to surface
 1   61         ! start, end in i-direction
 1   81         ! start, end in j-direction
 1    1         ! start, end in k-direction
 1              ! flag for order of first derivative bc
 3              ! donor mesh
-3              ! coordinate direction normal to surface
 1   61         ! donor mesh start, end in i-direction
 1   81         ! donor mesh start, end in j-direction
81   81         ! donor mesh start, end in k-direction
52              !*** periodic MB #3= type #52
-3              ! coordinate direction normal to surface
 1   61         ! start, end in i-direction
 1   81         ! start, end in j-direction
81   81         ! start, end in k-direction
 1              ! flag for order of first derivative bc
 3              ! donor mesh
 3              ! coordinate direction normal to surface
 1   61         ! donor mesh start, end in i-direction
 1   81         ! donor mesh start, end in j-direction
 1    1         ! donor mesh start, end in k-direction
92              !*** patched MB #4= type #92
-1              ! coordinate direction normal to surface
61   61         ! start, end in i-direction
 1   81         ! start, end in j-direction
 1   81         ! start, end in k-direction
 1              ! flag for order of first derivative bc
 4              ! donor mesh
 1              ! coordinate direction normal to surface
 1    1         ! donor mesh start, end in i-direction
 1   81         ! donor mesh start, end in j-direction
 1   81         ! donor mesh start, end in k-direction
92              !*** patched MB #2= type #92
 1              ! coordinate direction normal to surface
 1    1         ! start, end in i-direction
 1   81         ! start, end in j-direction
 1   81         ! start, end in k-direction
 1              ! flag for order of first derivative bc
 2              ! donor mesh
-1              ! coordinate direction normal to surface
```

```
61   61          ! donor mesh start, end in i-direction
 1   81          ! donor mesh start, end in j-direction
 1   81          ! donor mesh start, end in k-direction
13               !*** Farfield (dp/dn=0)   = type #13
-2               ! coordinate direction normal to surface
 1   61          ! start, end in i-direction
81   81          ! start, end in j-direction
 1   81          ! start, end in k-direction
 0               ! flag for order of first derivative bc
 6               ! number of boundary surfaces ===> BLK#-4
22               !*** Rel. Frame No-slip   = type #22
 2               ! coordinate direction normal to surface
 1   61          ! start, end in i-direction
 1    1          ! start, end in j-direction
 1   81          ! start, end in k-direction
 0               ! flag for order of first derivative bc
11               !*** Exit   = type #11
-1               ! coordinate direction normal to surface
61   61          ! start, end in i-direction
 1   81          ! start, end in j-direction
 1   81          ! start, end in k-direction
 0               ! flag for order of first derivative bc
41               !*** Periodic   = type #41
 3               ! coordinate direction normal to surface
 1   61          ! start, end in i-direction
 1   81          ! start, end in j-direction
 1    1          ! start, end in k-direction
 0               ! flag for order of first derivative bc
92               !*** patched MB #3= type #92
 1               ! coordinate direction normal to surface
 1    1          ! start, end in i-direction
 1   81          ! start, end in j-direction
 1   81          ! start, end in k-direction
 1               ! flag for order of first derivative bc
 3               ! donor mesh
-1               ! coordinate direction normal to surface
61   61          ! donor mesh start, end in i-direction
 1   81          ! donor mesh start, end in j-direction
 1   81          ! donor mesh start, end in k-direction
41               !*** Periodic   = type #41
-3               ! coordinate direction normal to surface
 1   61          ! start, end in i-direction
 1   81          ! start, end in j-direction
81   81          ! start, end in k-direction
 0               ! flag for order of first derivative bc
13               !*** Farfield (dp/dn=0)   = type #13
-2               ! coordinate direction normal to surface
 1   61          ! start, end in i-direction
81   81          ! start, end in j-direction
 1   81          ! start, end in k-direction
 0               ! flag for order of first derivative bc
 1               ! number of boundary surfaces ===> BLK#-5
22               !*** Rel. Frame No-slip   = type #22
 2               ! coordinate direction normal to surface
 1   41          ! start, end in i-direction
 1    1          ! start, end in j-direction
 1   31          ! start, end in k-direction
 0               ! flag for order of first derivative bc
 1               ! number of boundary surfaces ===> BLK#-6
22               !*** Rel. Frame No-slip   = type #22
 2               ! coordinate direction normal to surface
 1   41          ! start, end in i-direction
 1    1          ! start, end in j-direction
 1   31          ! start, end in k-direction
```

```
 0              ! flag for order of first derivative bc
 4              ! number of boundary surfaces ===> BLK#-7
22              !*** Rel. Frame No-slip   = type #22
 2              ! coordinate direction normal to surface
 1   45         ! start, end in i-direction
 1    1         ! start, end in j-direction
 1   31         ! start, end in k-direction
 0              ! flag for order of first derivative bc
92              !*** patched MB #8= type #92
 1              ! coordinate direction normal to surface
 1    1         ! start, end in i-direction
 1   61         ! start, end in j-direction
 1   31         ! start, end in k-direction
 1              ! flag for order of first derivative bc
 8              ! donor mesh
-1              ! coordinate direction normal to surface
45   45         ! donor mesh start, end in i-direction
 1   61         ! donor mesh start, end in j-direction
 1   31         ! donor mesh start, end in k-direction
92              !*** patched MB #16= type #92
 3              ! coordinate direction normal to surface
 1   45         ! start, end in i-direction
 1   61         ! start, end in j-direction
 1    1         ! start, end in k-direction
 1              ! flag for order of first derivative bc
16              ! donor mesh
-3              ! coordinate direction normal to surface
 1   45         ! donor mesh start, end in i-direction
 1   61         ! donor mesh start, end in j-direction
65   65         ! donor mesh start, end in k-direction
92              !*** patched MB #11= type #92
-3              ! coordinate direction normal to surface
 1   45         ! start, end in i-direction
 1   61         ! start, end in j-direction
31   31         ! start, end in k-direction
 1              ! flag for order of first derivative bc
11              ! donor mesh
 1              ! coordinate direction normal to surface
 1    1         ! donor mesh start, end in i-direction
 1   61         ! donor mesh start, end in j-direction
45    1         ! donor mesh start, end in k-direction
 4              ! number of boundary surfaces ===> BLK#-8
22              !*** Rel. Frame No-slip   = type #22
 2              ! coordinate direction normal to surface
 1   45         ! start, end in i-direction
 1    1         ! start, end in j-direction
 1   31         ! start, end in k-direction
 0              ! flag for order of first derivative bc
92              !*** patched MB #7= type #92
-1              ! coordinate direction normal to surface
45   45         ! start, end in i-direction
 1   61         ! start, end in j-direction
 1   31         ! start, end in k-direction
 1              ! flag for order of first derivative bc
 7              ! donor mesh
 1              ! coordinate direction normal to surface
 1    1         ! donor mesh start, end in i-direction
 1   61         ! donor mesh start, end in j-direction
 1   31         ! donor mesh start, end in k-direction
92              !*** patched MB #15= type #92
 3              ! coordinate direction normal to surface
 1   45         ! start, end in i-direction
 1   61         ! start, end in j-direction
 1    1         ! start, end in k-direction
```

```
 1              ! flag for order of first derivative bc
15              ! donor mesh
-3              ! coordinate direction normal to surface
 1   45         ! donor mesh start, end in i-direction
 1   61         ! donor mesh start, end in j-direction
65   65         ! donor mesh start, end in k-direction
92              !*** patched MB #12= type #92
-3              ! coordinate direction normal to surface
 1   45         ! start, end in i-direction
 1   61         ! start, end in j-direction
31   31         ! start, end in k-direction
 1              ! flag for order of first derivative bc
12              ! donor mesh
-1              ! coordinate direction normal to surface
41   41         ! donor mesh start, end in i-direction
 1   61         ! donor mesh start, end in j-direction
 1   45         ! donor mesh start, end in k-direction
 4              ! number of boundary surfaces ===> BLK#-9
22              !*** Rel. Frame No-slip   = type #22
 2              ! coordinate direction normal to surface
 1   45         ! start, end in i-direction
 1    1         ! start, end in j-direction
 1   31         ! start, end in k-direction
 0              ! flag for order of first derivative bc
92              !*** patched MB #10= type #92
-1              ! coordinate direction normal to surface
45   45         ! start, end in i-direction
 1   61         ! start, end in j-direction
 1   31         ! start, end in k-direction
 1              ! flag for order of first derivative bc
10              ! donor mesh
 1              ! coordinate direction normal to surface
 1    1         ! donor mesh start, end in i-direction
 1   61         ! donor mesh start, end in j-direction
 1   31         ! donor mesh start, end in k-direction
92              !*** patched MB #11= type #92
-3              ! coordinate direction normal to surface
 1   45         ! start, end in i-direction
 1   61         ! start, end in j-direction
31   31         ! start, end in k-direction
 1              ! flag for order of first derivative bc
11              ! donor mesh
-1              ! coordinate direction normal to surface
41   41         ! donor mesh start, end in i-direction
 1   61         ! donor mesh start, end in j-direction
 1   45         ! donor mesh start, end in k-direction
92              !*** patched MB #18= type #92
 3              ! coordinate direction normal to surface
 1   45         ! start, end in i-direction
 1   61         ! start, end in j-direction
 1    1         ! start, end in k-direction
 1              ! flag for order of first derivative bc
18              ! donor mesh
-3              ! coordinate direction normal to surface
 1   45         ! donor mesh start, end in i-direction
 1   61         ! donor mesh start, end in j-direction
65   65         ! donor mesh start, end in k-direction
 4              ! number of boundary surfaces ===> BLK#-10
22              !*** Rel. Frame No-slip   = type #22
 2              ! coordinate direction normal to surface
 1   45         ! start, end in i-direction
 1    1         ! start, end in j-direction
 1   31         ! start, end in k-direction
 0              ! flag for order of first derivative bc
```

```
92              !*** patched MB #9= type #92
 1              ! coordinate direction normal to surface
 1    1         ! start, end in i-direction
 1   61         ! start, end in j-direction
 1   31         ! start, end in k-direction
 1              ! flag for order of first derivative bc
 9              ! donor mesh
-1              ! coordinate direction normal to surface
45   45         ! donor mesh start, end in i-direction
 1   61         ! donor mesh start, end in j-direction
 1   31         ! donor mesh start, end in k-direction
92              !*** patched MB #12= type #92
-3              ! coordinate direction normal to surface
 1   45         ! start, end in i-direction
 1   61         ! start, end in j-direction
31   31         ! start, end in k-direction
 1              ! flag for order of first derivative bc
12              ! donor mesh
 1              ! coordinate direction normal to surface
 1    1         ! donor mesh start, end in i-direction
 1   61         ! donor mesh start, end in j-direction
45    1         ! donor mesh start, end in k-direction
92              !*** patched MB #13= type #92
 3              ! coordinate direction normal to surface
 1   45         ! start, end in i-direction
 1   61         ! start, end in j-direction
 1    1         ! start, end in k-direction
 1              ! flag for order of first derivative bc
13              ! donor mesh
-3              ! coordinate direction normal to surface
 1   45         ! donor mesh start, end in i-direction
 1   61         ! donor mesh start, end in j-direction
65   65         ! donor mesh start, end in k-direction
 5              ! number of boundary surfaces ===> BLK#-11
22              !*** Rel. Frame No-slip   = type #22
 2              ! coordinate direction normal to surface
 1   41         ! start, end in i-direction
 1    1         ! start, end in j-direction
 1   45         ! start, end in k-direction
 0              ! flag for order of first derivative bc
92              !*** patched MB #12= type #92
-3              ! coordinate direction normal to surface
 1   25         ! start, end in i-direction
 1   61         ! start, end in j-direction
45   45         ! start, end in k-direction
 1              ! flag for order of first derivative bc
12              ! donor mesh
-3              ! coordinate direction normal to surface
41   17         ! donor mesh start, end in i-direction
 1   61         ! donor mesh start, end in j-direction
45   45         ! donor mesh start, end in k-direction
92              !*** patched MB #12= type #92
-3              ! coordinate direction normal to surface
25   41         ! start, end in i-direction
 1   61         ! start, end in j-direction
45   45         ! start, end in k-direction
 1              ! flag for order of first derivative bc
12              ! donor mesh
-3              ! coordinate direction normal to surface
17    1         ! donor mesh start, end in i-direction
 1   61         ! donor mesh start, end in j-direction
45   45         ! donor mesh start, end in k-direction
92              !*** patched MB #7= type #92
 1              ! coordinate direction normal to surface
```

```
 1    1           ! start, end in i-direction
 1   61           ! start, end in j-direction
 1   45           ! start, end in k-direction
 1                ! flag for order of first derivative bc
 7                ! donor mesh
-3                ! coordinate direction normal to surface
45    1           ! donor mesh start, end in i-direction
 1   61           ! donor mesh start, end in j-direction
31   31           ! donor mesh start, end in k-direction
92                !*** patched MB #9= type #92
-1                ! coordinate direction normal to surface
41   41           ! start, end in i-direction
 1   61           ! start, end in j-direction
 1   45           ! start, end in k-direction
 1                ! flag for order of first derivative bc
 9                ! donor mesh
-3                ! coordinate direction normal to surface
 1   45           ! donor mesh start, end in i-direction
 1   61           ! donor mesh start, end in j-direction
31   31           ! donor mesh start, end in k-direction
 5                ! number of boundary surfaces ===> BLK#-12
22                !*** Rel. Frame No-slip   = type #22
 2                ! coordinate direction normal to surface
 1   41           ! start, end in i-direction
 1    1           ! start, end in j-direction
 1   45           ! start, end in k-direction
 0                ! flag for order of first derivative bc
92                !*** patched MB #11= type #92
-3                ! coordinate direction normal to surface
17   41           ! start, end in i-direction
 1   61           ! start, end in j-direction
45   45           ! start, end in k-direction
 1                ! flag for order of first derivative bc
11                ! donor mesh
-3                ! coordinate direction normal to surface
25    1           ! donor mesh start, end in i-direction
 1   61           ! donor mesh start, end in j-direction
45   45           ! donor mesh start, end in k-direction
92                !*** patched MB #11= type #92
-3                ! coordinate direction normal to surface
 1   17           ! start, end in i-direction
 1   61           ! start, end in j-direction
45   45           ! start, end in k-direction
 1                ! flag for order of first derivative bc
11                ! donor mesh
-3                ! coordinate direction normal to surface
41   25           ! donor mesh start, end in i-direction
 1   61           ! donor mesh start, end in j-direction
45   45           ! donor mesh start, end in k-direction
92                !*** patched MB #8= type #92
-1                ! coordinate direction normal to surface
41   41           ! start, end in i-direction
 1   61           ! start, end in j-direction
 1   45           ! start, end in k-direction
 1                ! flag for order of first derivative bc
 8                ! donor mesh
-3                ! coordinate direction normal to surface
 1   45           ! donor mesh start, end in i-direction
 1   61           ! donor mesh start, end in j-direction
31   31           ! donor mesh start, end in k-direction
92                !*** patched MB #10= type #92
 1                ! coordinate direction normal to surface
 1    1           ! start, end in i-direction
 1   61           ! start, end in j-direction
```

```
 1   45           ! start, end in k-direction
 1                ! flag for order of first derivative bc
10                ! donor mesh
-3                ! coordinate direction normal to surface
45    1           ! donor mesh start, end in i-direction
 1   61           ! donor mesh start, end in j-direction
31   31           ! donor mesh start, end in k-direction
 6                ! number of boundary surfaces ===> BLK#-13
22                !*** Rel. Frame No-slip   = type #22
 2                ! coordinate direction normal to surface
 1   45           ! start, end in i-direction
 1    1           ! start, end in j-direction
51   65           ! start, end in k-direction
 0                ! flag for order of first derivative bc
22                !*** Rel. Frame No-slip   = type #22
 2                ! coordinate direction normal to surface
 1   45           ! start, end in i-direction
 1    1           ! start, end in j-direction
 1   51           ! start, end in k-direction
 0                ! flag for order of first derivative bc
92                !*** patched MB #14= type #92
-1                ! coordinate direction normal to surface
45   45           ! start, end in i-direction
 1   61           ! start, end in j-direction
 1   65           ! start, end in k-direction
 1                ! flag for order of first derivative bc
14                ! donor mesh
 1                ! coordinate direction normal to surface
 1    1           ! donor mesh start, end in i-direction
 1   61           ! donor mesh start, end in j-direction
 1   65           ! donor mesh start, end in k-direction
92                !*** patched MB #10= type #92
-3                ! coordinate direction normal to surface
 1   45           ! start, end in i-direction
 1   61           ! start, end in j-direction
65   65           ! start, end in k-direction
 1                ! flag for order of first derivative bc
10                ! donor mesh
 3                ! coordinate direction normal to surface
 1   45           ! donor mesh start, end in i-direction
 1   61           ! donor mesh start, end in j-direction
 1    1           ! donor mesh start, end in k-direction
92                !*** patched MB #18= type #92
 1                ! coordinate direction normal to surface
 1    1           ! start, end in i-direction
 1   61           ! start, end in j-direction
 1   65           ! start, end in k-direction
 1                ! flag for order of first derivative bc
18                ! donor mesh
-1                ! coordinate direction normal to surface
45   45           ! donor mesh start, end in i-direction
 1   61           ! donor mesh start, end in j-direction
 1   65           ! donor mesh start, end in k-direction
22                !*** Rel. Frame No-slip   = type #22
 3                ! coordinate direction normal to surface
 1   45           ! start, end in i-direction
 1   61           ! start, end in j-direction
 1    1           ! start, end in k-direction
 0                ! flag for order of first derivative bc
 5                ! number of boundary surfaces ===> BLK#-14
22                !*** Rel. Frame No-slip   = type #22
 2                ! coordinate direction normal to surface
 1   41           ! start, end in i-direction
 1    1           ! start, end in j-direction
```

```
51   65           ! start, end in k-direction
 0                ! flag for order of first derivative bc
22                !*** Rel. Frame No-slip   = type #22
 2                ! coordinate direction normal to surface
 1   41           ! start, end in i-direction
 1    1           ! start, end in j-direction
 1   51           ! start, end in k-direction
 0                ! flag for order of first derivative bc
92                !*** patched MB #15= type #92
-1                ! coordinate direction normal to surface
41   41           ! start, end in i-direction
 1   61           ! start, end in j-direction
 1   65           ! start, end in k-direction
 1                ! flag for order of first derivative bc
15                ! donor mesh
 1                ! coordinate direction normal to surface
 1    1           ! donor mesh start, end in i-direction
 1   61           ! donor mesh start, end in j-direction
 1   65           ! donor mesh start, end in k-direction
92                !*** patched MB #13= type #92
 1                ! coordinate direction normal to surface
 1    1           ! start, end in i-direction
 1   61           ! start, end in j-direction
 1   65           ! start, end in k-direction
 1                ! flag for order of first derivative bc
13                ! donor mesh
-1                ! coordinate direction normal to surface
45   45           ! donor mesh start, end in i-direction
 1   61           ! donor mesh start, end in j-direction
 1   65           ! donor mesh start, end in k-direction
22                !*** Rel. Frame No-slip   = type #22
 3                ! coordinate direction normal to surface
 1   41           ! start, end in i-direction
 1   61           ! start, end in j-direction
 1    1           ! start, end in k-direction
 0                ! flag for order of first derivative bc
 6                ! number of boundary surfaces ===> BLK#-15
22                !*** Rel. Frame No-slip   = type #22
 2                ! coordinate direction normal to surface
 1   45           ! start, end in i-direction
 1    1           ! start, end in j-direction
51   65           ! start, end in k-direction
 0                ! flag for order of first derivative bc
22                !*** Rel. Frame No-slip   = type #22
 2                ! coordinate direction normal to surface
 1   45           ! start, end in i-direction
 1    1           ! start, end in j-direction
 1   51           ! start, end in k-direction
 0                ! flag for order of first derivative bc
92                !*** patched MB #16= type #92
-1                ! coordinate direction normal to surface
45   45           ! start, end in i-direction
 1   61           ! start, end in j-direction
 1   65           ! start, end in k-direction
 1                ! flag for order of first derivative bc
16                ! donor mesh
 1                ! coordinate direction normal to surface
 1    1           ! donor mesh start, end in i-direction
 1   61           ! donor mesh start, end in j-direction
 1   65           ! donor mesh start, end in k-direction
92                !*** patched MB #8= type #92
-3                ! coordinate direction normal to surface
 1   45           ! start, end in i-direction
 1   61           ! start, end in j-direction
```

```
65   65          ! start, end in k-direction
 1               ! flag for order of first derivative bc
 8               ! donor mesh
 3               ! coordinate direction normal to surface
 1   45          ! donor mesh start, end in i-direction
 1   61          ! donor mesh start, end in j-direction
 1    1          ! donor mesh start, end in k-direction
92               !*** patched MB #14= type #92
 1               ! coordinate direction normal to surface
 1    1          ! start, end in i-direction
 1   61          ! start, end in j-direction
 1   65          ! start, end in k-direction
 1               ! flag for order of first derivative bc
14               ! donor mesh
-1               ! coordinate direction normal to surface
41   41          ! donor mesh start, end in i-direction
 1   61          ! donor mesh start, end in j-direction
 1   65          ! donor mesh start, end in k-direction
22               !*** Rel. Frame No-slip   = type #22
 3               ! coordinate direction normal to surface
 1   45          ! start, end in i-direction
 1   61          ! start, end in j-direction
 1    1          ! start, end in k-direction
 0               ! flag for order of first derivative bc
 6               ! number of boundary surfaces ===> BLK#-16
22               !*** Rel. Frame No-slip   = type #22
 3               ! coordinate direction normal to surface
 1   45          ! start, end in i-direction
 1   61          ! start, end in j-direction
 1    1          ! start, end in k-direction
 0               ! flag for order of first derivative bc
22               !*** Rel. Frame No-slip   = type #22
 2               ! coordinate direction normal to surface
 1   45          ! start, end in i-direction
 1    1          ! start, end in j-direction
51   65          ! start, end in k-direction
 0               ! flag for order of first derivative bc
22               !*** Rel. Frame No-slip   = type #22
 2               ! coordinate direction normal to surface
 1   45          ! start, end in i-direction
 1    1          ! start, end in j-direction
 1   51          ! start, end in k-direction
 0               ! flag for order of first derivative bc
92               !*** patched MB #15= type #92
 1               ! coordinate direction normal to surface
 1    1          ! start, end in i-direction
 1   61          ! start, end in j-direction
 1   65          ! start, end in k-direction
 1               ! flag for order of first derivative bc
15               ! donor mesh
-1               ! coordinate direction normal to surface
45   45          ! donor mesh start, end in i-direction
 1   61          ! donor mesh start, end in j-direction
 1   65          ! donor mesh start, end in k-direction
92               !*** patched MB #17= type #92
-1               ! coordinate direction normal to surface
45   45          ! start, end in i-direction
 1   61          ! start, end in j-direction
 1   65          ! start, end in k-direction
 1               ! flag for order of first derivative bc
17               ! donor mesh
 1               ! coordinate direction normal to surface
 1    1          ! donor mesh start, end in i-direction
 1   61          ! donor mesh start, end in j-direction
```

```
 1   65           ! donor mesh start, end in k-direction
92                !*** patched MB #7= type #92
-3                ! coordinate direction normal to surface
 1   45           ! start, end in i-direction
 1   61           ! start, end in j-direction
65   65           ! start, end in k-direction
 1                ! flag for order of first derivative bc
 7                ! donor mesh
 3                ! coordinate direction normal to surface
 1   45           ! donor mesh start, end in i-direction
 1   61           ! donor mesh start, end in j-direction
 1    1           ! donor mesh start, end in k-direction
 5                ! number of boundary surfaces ===> BLK#-17
22                !*** Rel. Frame No-slip   = type #22
 3                ! coordinate direction normal to surface
 1   41           ! start, end in i-direction
 1   61           ! start, end in j-direction
 1    1           ! start, end in k-direction
 0                ! flag for order of first derivative bc
22                !*** Rel. Frame No-slip   = type #22
 2                ! coordinate direction normal to surface
 1   41           ! start, end in i-direction
 1    1           ! start, end in j-direction
 1   51           ! start, end in k-direction
 0                ! flag for order of first derivative bc
22                !*** Rel. Frame No-slip   = type #22
 2                ! coordinate direction normal to surface
 1   41           ! start, end in i-direction
 1    1           ! start, end in j-direction
51   65           ! start, end in k-direction
 0                ! flag for order of first derivative bc
92                !*** patched MB #16= type #92
 1                ! coordinate direction normal to surface
 1    1           ! start, end in i-direction
 1   61           ! start, end in j-direction
 1   65           ! start, end in k-direction
 1                ! flag for order of first derivative bc
16                ! donor mesh
-1                ! coordinate direction normal to surface
45   45           ! donor mesh start, end in i-direction
 1   61           ! donor mesh start, end in j-direction
 1   65           ! donor mesh start, end in k-direction
92                !*** patched MB #18= type #92
-1                ! coordinate direction normal to surface
41   41           ! start, end in i-direction
 1   61           ! start, end in j-direction
 1   65           ! start, end in k-direction
 1                ! flag for order of first derivative bc
18                ! donor mesh
 1                ! coordinate direction normal to surface
 1    1           ! donor mesh start, end in i-direction
 1   61           ! donor mesh start, end in j-direction
 1   65           ! donor mesh start, end in k-direction
 6                ! number of boundary surfaces ===> BLK#-18
22                !*** Rel. Frame No-slip   = type #22
 3                ! coordinate direction normal to surface
 1   45           ! start, end in i-direction
 1   61           ! start, end in j-direction
 1    1           ! start, end in k-direction
 0                ! flag for order of first derivative bc
22                !*** Rel. Frame No-slip   = type #22
 2                ! coordinate direction normal to surface
 1   45           ! start, end in i-direction
 1    1           ! start, end in j-direction
```

```
 1   51          ! start, end in k-direction
 0               ! flag for order of first derivative bc
22               !*** Rel. Frame No-slip   = type #22
 2               ! coordinate direction normal to surface
 1   45          ! start, end in i-direction
 1    1          ! start, end in j-direction
51   65          ! start, end in k-direction
 0               ! flag for order of first derivative bc
92               !*** patched MB #17= type #92
 1               ! coordinate direction normal to surface
 1    1          ! start, end in i-direction
 1   61          ! start, end in j-direction
 1   65          ! start, end in k-direction
 1               ! flag for order of first derivative bc
17               ! donor mesh
-1               ! coordinate direction normal to surface
41   41          ! donor mesh start, end in i-direction
 1   61          ! donor mesh start, end in j-direction
 1   65          ! donor mesh start, end in k-direction
92               !*** patched MB #13= type #92
-1               ! coordinate direction normal to surface
45   45          ! start, end in i-direction
 1   61          ! start, end in j-direction
 1   65          ! start, end in k-direction
 1               ! flag for order of first derivative bc
13               ! donor mesh
 1               ! coordinate direction normal to surface
 1    1          ! donor mesh start, end in i-direction
 1   61          ! donor mesh start, end in j-direction
 1   65          ! donor mesh start, end in k-direction
92               !*** patched MB #9= type #92
-3               ! coordinate direction normal to surface
 1   45          ! start, end in i-direction
 1   61          ! start, end in j-direction
65   65          ! start, end in k-direction
 1               ! flag for order of first derivative bc
 9               ! donor mesh
 3               ! coordinate direction normal to surface
 1   45          ! donor mesh start, end in i-direction
 1   61          ! donor mesh start, end in j-direction
 1    1          ! donor mesh start, end in k-direction
```